SMART NANOCOMPOSITES

Volume 2, Number 2

Table of Contents

Nova Science Publishers, Inc.
New York

Smart Nanocomposites

This Journal presents new studies in the fast growing area of smart materials, in particular, composite nanostructured materials. It focuses on the physics and physical chemistry of surfaces, interfaces, thin films and coatings, nanoparticles and other nanostructures, as well as on their new and smart applications. Original approaches in fabrication and applications of nanostructured materials will get special attention. Nanostructured ceramics, alloys, various nanocarbon forms (nanotubes, fullerenes, graphene) and their composites used in sensors (including single molecule sensing) and actuators, artificial metabolism, drug delivery, selective membranes, fuel cells, energy storage, and photovoltaics are just a few examples of new classes of materials and applications that are within the scope of the Journal. It features the results of interdisciplinary research from universities, national labs, and privately owned companies.

The Journal is peer-reviewed with the highest standards and quality of publications. The purpose of this Journal is to bring the most up-to-date advances in nanotechnology together, and to give research groups the opportunity to compare their results with other groups' data. To achieve this, the Journal focuses mostly on practical applications of nanodevices, and on proof of the concept publications. Areas of interest include (but not are limited to): sensors, smart membranes, smart coatings for corrosion protection, aspects of significance to nanorobots: power supplies, nanorobot manipulating devices, and microchips for artificial intelligence. The Journal also deals with safety issues: safety of nanotechnology to the environment, controlling the nanodevices, and other aspects.

Smart Nanocomposites
is published in two issues per year by

Nova Science Publishers, Inc.
400 Oser Avenue, Suite 1600
Hauppauge, New York 11788-3619, U.S.A.
Telephone: (631) 231-7269
Fax: (631) 231-8175
E-mail: main@novapublishers.com
Web: www.novapublishers.com

ISSN: 1949-4823

Subscription Rate per Volume (2011)
Print: $245 Electronic: $245 Combined Print + Electronic: $367

Additional color graphics might be available in the e-version of this journal.

Smart Nanocomposites
Volume 2, Number 2
ISSN: 1949-4823

METAL COMPLEXES OF SOME AZO- AND AZOMETHINE DERIVATIVES OF SULFAMETHOXAZOLE

Fathy A. El-Saied[a*], Rafaat M. Issa[b], and Elsayeda A. Amerah[c]

[a,c] Department of Chemistry, Faulty of Science,
El-menoufia University, Shebin El-Kom, Egypt
[b]Department of Chemistry, Faulty of Science,
Tanta University, Tanta, Egypt

ABSTRACT

The azo ligands of sulfamethoxazole were prepared through coupling the sulfamethoxazole diazonium salt with each of resorcinol, ß-naphthol, salicylaldehyde and acetyl acetone to form $H_2L^{1,}$ HL^2-HL^4 respectively. Different metal complexes of H_2L^1 with $CuCl_2$, $CoCl_2$, $NiCl_2$, $PtCl_2$, $RuCl_3$, $Cr(CO)_6$, and $Mo(CO)_6$ and metal complexes of HL^2 –HL^4 with $CuCl_2$ have been prepared and characterized using variety of analytical, spectral, magnetic and thermal techniques. The ligands were comprised of two compartments, so the study revealed that the prepared complexes except copper complex and the platinum complex were binuclear complexes. The study also showed that each compartment behaved either as a bidentate ligand either as a neutral or monobasic. The results of magnetic moment values and electronic spectra as well as other techniques indicate that all copper complexes and platinum complex exhibit square planar arrangement around the metal ion. The other complexes possess octahedral geometry. The thermal stability of some of the prepared complexes were also studied. The molecular weight of some metal complexes as well as their fragmentations have also been studied by mass spectra measurement.

1. INTRODUCTION

Azo compounds are very important molecules and have attracted much attention in both academic and applied research[1-3]. For example, azo derivatives and their complexes are very important pigments for synthetic leather and vinyl polymers. On the other hand, azo compounds are known to be involved in a number of biological reactions, such as inhibition

* Corresponding author. Email: fathi_elsaied@yahoo.com

of DNA, RNA, and protein synthesis, nitrogen fixation, and carcinogenesis[4]. Furthermore, high-density optical data storage has been a subject of extensive research in the past decade. In general, cyanine dyes, phthalocyanine dyes, and metal-azo complex dyes are used in the recording layer of DVD-R (Digital Versatile Disc –Recordable) discs. It has been reported that the new technology, which employs 405 nm blue-violet diode lasers, requires a new optical recording medium matching 405 nm wavelength laser. In comparison with the dyes themselves, metal azo dyes are more light-stable, allowing easier control to the wavelength by selection of the appropriate azo compounds and the ease with which the absorption band may be tuned by varying the substituents, one of the many applications of azo compounds is the optical data storage. In other words, the thermal substituent groups, and have good thermal stability[5-9] Because of the good thermal properties and suitable absorption band of azo compounds are essential features in relation to their application at high-density optical recording materials.

Metal complexes of sulfa drugs play a vital role in metabolic and toxicological functions in biological systems [10-12] .The studies on metal sulfanilamide compounds have received much attention due to the fact that sulfanilamides were the first effective chemotherapeutic agents to be employed for the prevention and cure of bacterial infections in humans[13] . The sulfanilamides exert their antibacterial action by the competitive inhibition of the enzyme dihydropterase synthetase towards the substrate p-amino benzoate [14]. Several authors have reported the antimicrobial activity of sulfanilamides and their metal complexes[10, 15,16] . The goal of the present article is preparation of metal complexes of some azo- and azomethine derivatives of sulfamethoxazole and elucidation of their chemical structures using variety of analytical , spectral, magnetic and thermal techniques.

2. EXPERIMENTAL

2.1. Chemicals

All reagents used in the present investigation were of highest quality available and used without further purification.

2.2. Preparation of the Azo Dye Ligands

Four ligands H_2L^1, HL^2, HL^3 and HL^4 were prepared by diazotization of sulfamethoxazole with resorcinol H_2L^1, ß-naphthol HL^2, salicylaldehyde HL^3, and acetyl acetone HL^4 in 1:1 mole ratio. The azo products of sulfamethoxazole were prepared through coupling the sulfamethoxazole diazonium salt with each of resorcinol, ß-naphthol, salicylaldehyde and acetyl acetone to form $H_2L^{1,}$ HL^2-H L^4 respectively[17] according to the following method: 2.53g. (0.01 mol.) of sulfamethoxazole were dissolved in 25 ml of distilled water containing 2.5 ml (0.03 mol.) of HCl. The resulting solution was then cooled under stirring to 0.00 $^{\circ}$C. A cold solution containing 0.69g. (0.01mol.) of sodium nitrite $NaNO_2$ was added drop wise to the previous solution with continuous stirring to form the diazonium chloride. This solution was then added to 1.10g. resorcinol (H_2L^1, 1.44g. ß-naphthol (HL^2, 1.22g. (0.262 ml) salicylaldehyde (HL^3) or 1.00g. (0.26 ml) acetyl acetone (HL^4) which were dissolved in 10 ml of water containing 0.4g. of NaOH (0.01mol.) with vigorous stirring to

form the ligands respectively. The colored products, which separated out during the addition, were kept in an ice bath with stirring for 30 minutes. The precipitates were then filtered off, washed several times with distilled water, and finally dried under vacuum over anhydrous $CaCl_2$.

2.3. Preparation of Metal Complexes

The solid metal complexes were prepared by mixing the appropriate amount of the ligand in ethanol with the appropriate metal salt in absolute ethanol in molar ratios 1L: 1M or 1L: 2M.The resulting solutions were heated under reflux for 6 hours; the solid complexes, which separated out on hot, were filtered off, washed several times with ethanol and dried under vacuum over anhydrous $CaCl_2$.

2.4. Instrumentation

Elemental microanalysis for carbon, hydrogen, and nitrogen was determined using a PERKIN-ELMER 2400 Analyzer for CHN at Microanalysis unit, Tanta University, Tanta, Egypt. IR spectra for all ligands and their solid complexes were recorded on a PERKIN-ELMER 1430 Ratio Recording Infrared Spectrophotometer as KBr discs, within the range 4000-200 cm^{-1} at Microanalysis unit, Tanta University, Tanta, Egypt.The ^1H NMR spectra were carried out using N,N-dimethylsulfoxide (DMSO) as a solvent on a Varian Mercury Oxford NMR 300 MHz spectrometer. Tetramethylsilane was used as an internal standard at Cairo University Cairo Egypt. The electronic absorption spectra were recorded using a Shimadzu UV 3101 pc spectrophotometer with a rectangular Quartz cell of dimensions 0.2 x 1 cm**.** Thermogravimetric analyses (TGA) of the solid complexes was recorded using Shimadzu TG-50 Thermogravimetric Analyzer with heating rate 10°C / min under nitrogen atmosphere, in the range 25-800°C. Magnetic susceptibilities of the complexes were measured at room temperature in the polycrystalline state in a borosilicate tube using Johnson Matthey Magnetic Susceptibility Balance. Mass spectra were recorded on a Finnegan MAT 8222 spectrometer operating at 70 eV. Molar conductance measured by using Hanna HI8733 conductivity meter 1999.9 μs temperature coefficient = 1. Magnetic susceptibility was measured and calculated by using the following equation [18]

$$\mu_{eff} = 2.828\ (\chi_n \times T)^{1/2}\ \chi_a = [1.115\ L(R-Ro)]/W\times 10^9\ ,\ \chi_m = \chi_a \times MW\ ,\ \chi_n = \chi_m - D$$

where: χ_a = mass susceptibility, L = sample length in cm, R = tube + sample reading ,R_o = empty tub reading ,W = mass of the sample ,χ_m = molar susceptibility, MW = Molecular weight , χ_n = corrected molar susceptibility D = diamagnetic correction, μ_{eff} = effective magnetic moment, T = room temperature in Kelvin (˚k)

The theoretical effective magnetic moment value calculated using the equation

$\mu_{eff} = [n(n+2)]^{1/2}$, where: μ_{eff} = theoretical effective magnetic moment;
n = the number of the unpaired electrons
Diamagnetic corrections were made using Pascal's constants [19].

3. RESULTS AND DISCUSSIONS

3.1. Structure Investigation and Spectral Studies of Prepared Sulfamethoxazole Ligands (H_2L^1, HL^2 -HL^4)

3.1.1. Elemental Analysis of Sulfamethoxazole Ligands (H_2L^1, HL^2 -HL^4)

The prepared organic ligands were purified by recrystallization from the appropriate solvents. The results of elemental analysis, which are collected in Table 1, confirm the purity of the prepared organic ligands.

3.1.2. IR Spectra of Sulfamethoxazole Azo Dyes (H_2L^1, HL^2 –HL^4)

The IR spectra were recorded in the solid state as potassium bromide discs, within the range 4000-200 cm^{-1}. The assignment of the most diagnostic IR absorption bands were carried out by applying a method similar to that suggested by Looker [20], according to which the spectrum is subdivided into some regions, namely, the 4000-2000, 1800-1500, 1500-1000, 1000-600 and 600-200 cm^{-1}. The bands corresponding to various types of vibrations of the aromatic rings are assigned in light of the results of the studies carried out by Katritziky[21]. The important absorption band frequencies of the organic ligands are recorded in Table 2.

3.1.2.1. Absorption in the 4000-2000 Cm^{-1} Region

In this region, OH, NH and CH stretching vibration bands appear. The infrared spectra show a medium band at 3543 – 3425 cm^{-1} for all ligands that assigned to υ(OH). The weak bands appearing at 3320 – 3145 cm^{-1} corresponds to the stretching vibration of NH group .The two broad bands appearing at 2998 and 2909 cm^{-1} correspond to stretching vibration of aromatic CH.

3.1.2.2. Absorption in the 1800-1500 cm^{-1} Region

This region includes bands corresponding to stretching vibrations of C=N of the ring . The spectra of the ligands show a strong band at 1614 – 1612 cm^{-1} corresponding to υ(C=N) for all ligands . A strong band of υ(C=O) group appears at 1666 and 1679 cm^{-1} of HL^3 and HL^4 respectively.

3.1.2.3. Absorption in the 1500-1000 cm^{-1} Region

This region contains the vibration bands of N=N, SO_2, C-O. The spectra of all ligands show a medium band at 1468-1399 cm^{-1} corresponding to υ(N=N) group. The bands appearing at 1350-1322 and 1167- 1143 cm^{-1} in the spectra of all ligands are corresponding to υSO_2(asy) and, υSO_2(sym) respectively. The band appearing at 1666 and 1679 cm^{-1} in the spectra of HL^3 and HL^4 are corresponding to υ_{C-O}, respectively.

3.1.2.4. Absorption in the 1000-600 cm^{-1} Region

The C-S stretching vibration band appears at 734- 680 cm^{-1} for all ligands . The out of plane deformation frequencies of the aromatic C-H bands are also expected to appear in this region(828cm^{-1}).

Table 1. Color, molar conductivity, molar ratios and elemental analysis of ligands and their metal complexes

No	Compound	Color	Ω_M	Metal salt and molar ratio (L:M)	Elemental analysis %(Calc.)		
					%C	%H	%N
1	H_2L^1	Orange	-	-	51.34(51.34)	3.6(3.7)	14.8(15.00)
2	$[Cu_2H_2L^1Cl_4]$	Brown	15.30	$CuCl_2$ (1:1)	30.9(31.7)	2.0(2.0)	8.7(7.8)
3	$[CuHL^1Cl(H_2O)]$	reddish brown	18.21	$CuCl_2$ (1:2)	38.3(39.2)	2.8(3.1)	10.7(11.4)
4	$[Co_2HL^1Cl_3(H_2O)_5]$	Brown	20.30	$CoCl_2$ (1:2)	27.5(27.9)	3.1(3.3)	8.8(8.2)
5	$[Ni_2HL^1Cl_3(H_2O)_5].3H_2O$	red	19.92	$NiCl_2$ (1:2)	25.1(25.9)	3.6(3.9)	7.1(7.6)
6	$[Ru_2HL^1Cl_5(H_2O)_3]$	brown	15.03	$RuCl_3$ (1:2)	24.3(23.8)	2.5(2.4)	7.4(6.9)
7	$[PtHL^1Cl(H_2O)].H_2O$	Black	17.30	$PtCl_2$ (1:1)	30.6(30.0)	2.6(2.7)	8.6(8.8)
8	$[(Mo)_2(CO)_{12}H_2L^1]$	Brown	15.65	$Mo(CO)_6$ (1:2)	36.6(36.5)	2.1(1.9)	6.8(6.2)
9	$[(Cr)_2(CO)_8H_2L^1]$	reddish brown	10.30	$Cr(CO)_6$ (1:2)	41.1(41.03)	2.0(2.0)	8.3(8.0)
10	HL^2	Pale brown	-	-	58.3(58.8)	3.4(3.9)	13.1(13.7)
11	$[Cu_2L^2Cl_3(H_2O)].3H_2O$	Dark brown	22.3	$CuCl_2$ (1:2)	34.3(33.7)	2.9(3.2)	7.00(7.9)
12	HL^3	Yellow	-	-	52.4(52.8)	3.1(3.6)	14.00(14.5)
13	$[Cu_2L^3Cl_3(H_2O)]$	Dark yellow	17.90	$CuCl_2$ (1:2)	33.00(32.1)	1.9(2.4)	8.6(8.7)
14	HL^4	Pale brown	-	-	49.2(49.5)	4.1(4.4)	15.4(15.4)
15	$[Cu_2L^4Cl_3(H_2O)]$	Pale green	13.7	$CuCl_2$ (1:2)	30.2(29.3)	2.6(2.8)	9.2(9.1)

$\mathbf{\Omega_M}$ = ohm^{-1} cm^2 mol^{-1}.

Table 2. Spectral bands for ligands and their metal complexes and their assignments

No.	Compound	υ(OH)	υ(NH)	υ(C=N)	υ(C=O)	υ(N=N)	υ(SO)	υ(M-O)	υ(M-N)
1	H_2L^1	3543	3320, 3157	1614	-	1411	1341, 1163	-	-
2	$[Cu_2H_2L^1Cl_4]$	3545, 3430	3250, 3170	1614	-	1460	1330, 1115	510	420
3	$[CuHL^1Cl(H_2O)]$	3540, 3460[a]	3280, 3190	1614	-	1468	1340, 1163	520	425
4	$[Co_2HL^1Cl_3(H_2O)_5]$	3540, 3400[a]	3235, 3170	1610	-	1465	1310, 1150	513	410
5	$[Ni_2HL^1Cl_3(H_2O)_5].3H_2O$	3550, 3380[a]	3200, 3165	1615	-	1469	1317, 1150	516	421
6	$[Ru_2HL^1Cl_5(H_2O)_3]$	3520, 3424[a]	3200	1605	-	1485	1325, 1140	520	440
7	$[PtHL^1Cl(H_2O)].H_2O$	3500, 3426[a]	3220	1605	-	1460	1337, 1162	515	460
8	$[(Mo)_2(CO)_{12}H_2L^1]$	3510, 3380	3224	1620	1714	1470	1330, 1137	556	420
9	$[(Cr)_2(CO)_8H_2L^1]$	3530, 3426	3175	1605	1740	1472	1322, 1155	515	422
10	HL^2	3440	3272, 3160	1612	-	1399	1322, 1164	-	-
11	$[Cu_2L^2Cl_3(H_2O)].3H_2O$	3500[a]	3290, 3170	1607	-	1480	1337, 1168	557	425
12	HL^3	3425	3205	1615	1660	1402	1350, 1143	-	-
13	$[Cu_2L^3Cl_3(H_2O)]$	3425[a]	3210	1606	1650	1400	1346, 1177	520	425
14	HL^4	3440	3145	1618[b], 1605	1679	1468	1349, 1167	-	-
15	$[Cu_2L^4Cl_3(H_2O)]$	3462[a]	3282, 3150	1612[b], 1590	1678	1480	1311, 1159	518	408

[a] = υ(OH) of H_2O , [b] = υ(C=C).

3.1.2. Nuclear Magnetic Resonance Spectra

The ^{1}H-NMR spectral of the ligands were recorded in deuterated DMSO as solvent and $CDCl_3$ as internal reference. The assignment of the main signals of these compounds are listed in Table (3).

Table 3. NMR spectra of ligands

Ligand	δNH	δCHO	δOH	δOH (H-bond)	δHC=N	δ H aromatic
H2L1	10.9	-	11.27	15.5	-	7.041-7.246
HL2	10.91	-	11.46	11.49	-	7.047-7.248
HL3	10.91	10.9	-	15.10	-	7.042-8.077
HL4	10.87	-	-	-	-	7.033-7.236

The phenolic OH hydrogens of all ligands appear as a singlet in the range 15.51-11.27 due to the hydrogen bonding between phenolic or enolic hydroxy group with N-atom of azo group in H_2L^1, HL^2 and HL^4 and with the aldehydic oxygen in H L^3 [22]. The presence of this signal in the spectrum of H_2L^1 indicated that the ligand exhibits keto- enol toutomerism. The signal appearing within the range 10.87-10.91 ppm in the spectra of all ligands assigned to NH group. The signals for the aldehyde hydrogens appear at 10.9 in the spectrum of HL^3 . The spectra of ligands also showed multi signals corresponding to the aromatic hydrogen within the range 7.07 -8.077 ppm in the spectra of all ligands.

3.2. Elucidation of Structure of Metal Complexes

3.2.1. Elemental Analysis and Molar Conductivity

The reactions of the ligand H_2L^1 with different metal salts ; $CuCl_2$, $CoCl_2$, $NiCl_2$, $PtCl_2$, $RuCl_3$, $Mo(CO)_6$ and $Cr(CO)_6$, in molar ratios are shown in Table 1and ligands HL^2, HL^3 and HL^4 with $CuCl_2$ in 1:2 (L:M) molar ratio metal complexes are listed in Table 2. The obtained metal complexes are air stable, non-hygroscopic and partially soluble in water and most organic solvents except dimethylformamide (DMF) and dimethylsulphoxide (DMSO), where they are freely soluble. The values of molar conductivities in DMF (10^{-3} M) solutions which are listed in Table 1, indicate that all metal complexes are non-electrolytes[22, 23], evidencing that all anions in metal complexes are directly attached to the metal ion.

3.2.2. Infrared Spectra

Chemical formulas of ligands show that ligands are comprised of two coordination sites (two compartments). The first compartment involves azo nitrogen atom, phenolic oxygen or carbonyl oxygen atom. This site herein and after is referred as A. The second compartment involves, the S=O and C=N which is referred as site B.

The bonding mode of the ligands in the metal complexes has been deduced by comparing the infrared spectra of metal complexes with those of the free ligands . The most diagnostic infrared spectral bands for ligands and their metal complexes and their assignments are listed in Table 2. The data listed in Table 2 showed that, the infrared spectra of metal complexes of ligand H_2L^1 , reveal that the band ascribed to υ(OH) shows a slight shift compared to that of the free ligand , indicates that p-OH group does not participate in coordination. The spectra of complexes 2, 8,and 9 show a band at 3430, 3380 and 3426 cm^{-1} respectively, indicating that the o-OH group is involved in coordination without deprotonation. On the other hand, the infrared spectra of other complexes of ligand H_2L^1 do not show this band, indicating that the coordination took place via the O-phenolic group with the loss of a proton. The spectra of metal complexes of H_2L^1 also reveal that the band characteristic to the azo group shows a shift to a higher frequency compared to that of the free ligand, as a result of its coordination to the metal ions in all metal complexes.

The spectra of complexes of H_2L^1, except complexes 3 and 7 display the υ(SO) bands at lower frequencies compared to that of the free ligand , this could be taken as an evidence for its involvement in coordination via the oxygen atom in all metal complexes of H_2L^1 except, in complexes 3 and 7 is steel free uncoordinated. The band ascribed to υ(C=N) of the ring shows very slight shift upon coordination. Originally hydrogen bonded in the free ligand so, is not greatly affected by coordination. Frequently we can conclude that the C=N group is coordinated in all H_2L^1 complexes except in complexes 3 and 7 it does not take part in coordination. This suggestion is supported because the former complexes are binuclear whereas, complexes 3 and 7 are mononuclear.

The above arguments together with the results of elemental analyses indicate that, the ligand H_2L^1 behaves as a neutral or monobasic bidentate ligand (site A) and a neutral bidentate ligand (site B). Each site binds a metal ion in case of all complexes except 3 and 7 where site A only binds a metal ion. The rest coordinations are satisfied by chloride ions, CO molecules and /or water molecules to complete the coordination number.

The infrared spectrum of complex 11 shows that the band υ(OH) disappeared due to its participation in coordination. The spectrum also displays the band corresponding to υ(N=N) at a higher frequency compared to that of the free ligand, indicating that coordination via the azo group occurred. Moreover, the infrared spectrum of complex 11 shows that the bands characteristic to υ(SO) and υ(C=N) at lower frequencies relative to that of the free ligand. Therefore SO and C=N are involved in coordination to the Cu(II) ion. The infrared spectra of two complexes 8 and 9 show a band at 1714 and 1740 cm-1 respectively, assigned to υ(CO) of carbonyl ligand. The above discussion for results indicate that the ligand HL2 binds two copper(II) ions, one of them coordinated to site A and the other coordinated to site B, the other coordinations are satisfied by chloride ions and water molecules.

The infrared spectrum of bicopper(II) complex of ligand HL3 (13) shows that the band corresponding to υ(OH) disappeared upon coordination as a result of deprotonation upon complexation. The spectra shows also that the bands, due to υ(C=O) and υ(C=N) appear at frequencies lower than that of the free ligand, indicating that the carbonyl oxygen atom and the C=N are coordinated to the copper(II) ion. On the other hand, the band ascribed to υ(N=N) remains at the same position as that of the free ligand, indicating that the azo group does not tack part in coordination. Moreover, the bands corresponding to υ(SO) were observed at lower frequencies compared to that of the free ligand, indicating that the SO is coordinated to the copper(II) ion.

The above arguments prove that the ligand binds two copper(II) ions, one Cu(II) occupied site A ; the C=O and ionized phenolic OH group and the other Cu(II) ion occupied the site B ; the C=N and SO, the rest coordinations were achieved by chloride ions and water molecules.

Ligand HL^4 is comprised of two coordination sites, one of them involves the N=N group and the carbonyl group of β-diketone (site A) and the other site involves , the C=N group and SO (B) ,so the ligand can bind two metal ions to form a binuclear complex. As previously discussed ligand HL^4 undergoes keto-enol toutomerism . The infrared spectrum of Cu(II) complex of ligand HL^4 (15) , shows that the band corresponding to υ(OH) disappears upon complexation, on the other hand, a band at 1612 cm^{-1} appears, assigned to υ(C=C), indicating that the ligand reacts in the enol form as a monobasic via loss of a proton from site A. Moreover, the band corresponding to υ(N=N) is shifted to a lower frequency compared to that of the free ligand. The infrared spectrum of complex 15 reveals that the bands ascribed to υ(C=N) and υ(SO) appear at frequencies lower than that of the free ligand. This indicates that the C=N and S=O are participated in coordination. The above argument proves that ligands are binded to two Cu(II) ions. The first ion is bonded to site A which acts as a mono-negative bidentate, coordinating via the enolic oxygen atom and the azo group. The second ion bonded to site B, which acts as a neutral bidentate, coordinating through the SO and C=N groups.

The presence of water molecules within the coordinated sphere in the hydrated complexes 3, 4, 5, 6, 7, 11, 13 and 15 is supported by the appearance of infrared spectral bands in the ranges 3462- 3380 cm^{-1}, 885 – 827 cm^{-1}, and 695 – 640 cm^{-1}, assigned to OH stretching , H_2O rocking and H_2O wagging, respectively [24]. The spectra of complexes show two new bands at 557 – 510 cm^{-1} and 460 -408 cm^{-1}, assigned to υ(M-O) and υ(M-N), respectively [25].

3.2.3. Magnetic Moments and Electronic Spectral Data for Metal Complexes

The electronic absorption spectral bands as well as the room temperature magnetic moments (μ_{eff} B.M.) per a metal atom of the metal complexes are listed in Table 4.

The magnetic moments for the copper(II) complexes 2, 3, 11, 13and 15 are 1.72, 1.78, 1.8, 1.79 and 1.76 B.M. respectively. The values of magnetic moments of complexes are consistent with the spin only value (1.73 B.M.), correspond to one unpaired electron [26] in a square planar or octahedral geometry [27]. Values also indicate that no exchange interactions occurs between copper ions. The electronic spectra of copper(II) complexes show a broad band within 520 – 510 nm range, which suggests a square planar geometry around the copper(II) ion[28]. Octahedral, tetrahedral and square planar cobalt(II) complexes show magnetic moment values between 4.7 – 5.2, 4.2 – 4.8 and 2.2 – 2.9 B.M., respectively [22, 29-31].

The room temperature magnetic moment value for cobalt (II) complex 4 is 4.93 B.M . This value is indicative for an octahedral geometry around the cobalt(II) ion .The considerably high value ruled out any spin- spin interactions between cobalt(II) ions. The electronic spectrum of cobalt(II) complex shows two weak bands at 630 and 520 nm which may be assigned to $^4A_2g \rightarrow {}^4T_1g$ (P) (υ_3) and $^4T_1g \rightarrow {}^4A_2g$ (υ_2), respectively, which is indicative for octahedral cobalt(II) geometry [32].

The nickel(II) complex was found to be paramagnetic which excludes the possibility of a square planar configuration. The room temperature magnetic moment value of nickel(II) complex 5 is 2.98 B.M.

Table 4. Magnetic moment and solid state electronic spectral bands of metal complexes

No	Complex	μ_{eff} B.M. per metal atom	d – d bands
2	$[Cu_2H_2L^1Cl_4]$	1.72	510 (br)
3	$[CuHL^1Cl(H_2O)]$	1.78	520 (br)
4	$[Co_2HL^1Cl_3(H_2O)_5]$	4.93	630 (w), 520 (br)
5	$[Ni_2HL^1Cl_3(H_2O)_5].3H_2O$	2.98	610, 500 (br)
6	$[Ru_2HL^1Cl_5(H_2O)_3]$	2.30	500 (br)
7	$[PtHL^1Cl(H_2O)].H_2O$	Zero	610(br), 480 (br)
11	$[Cu_2L^2Cl_3(H_2O)].3H_2O$	1.80	510 (br)
13	$[Cu_2L^3Cl_3(H_2O)$	1.79	510 (br)
15	$[Cu_2L^4Cl_3(H_2O)$	1.76	515 (br)

Br = broad, w = weak.

The value is compatible with an octahedral arrangement around the nickel(II) ion The electronic spectrum of nickel(II) complex 5 shows two bands at 610 and 500 nm, assigned to $^3A_2g(F) \rightarrow {}^3T_1g(F)$ (υ_2) and $^3A_2g(F) \rightarrow {}^3T_{1g}(P)$ (υ_3) transitions, respectively in pseudo-octahedral complexes [33, 34] . Ruthenium(III) complex 6 gave a magnetic moment value of 2.30 B.M. This value is compatible with spin only value for Ru(III) complexes. The electronic spectrum of complex 6 shows one band at 500 nm . By taking in consideration that the ligand in case of Ru(III) is considered as a strong ligand , one can assume that this band may be ascribed to $^2T_2g \rightarrow {}^{\mathbf{2}}A_2g$ transition in an octahedral geometry[35].

Platinum(II) complex 7 gave a zero magnetic moment value, which is compatible with a diamagnetic square planar arrangement around the Pt(II) ion. This geometry is supported by the electronic spectrum which shows two bands at 610 and 480 nm , indicative for a square planar complex.

3.2.4. EI-Mass Spectra of Some Metal Complexes

The mass spectra is a given additional structural information about the analyzed species. The molecular ion peak of complexes has been used to confirm the proposed formula. The multi peaks pattern of the mass spectrum gives an impression of the successive degradation of the compound with the series of peaks corresponding to the various fragments and their intensity give an idea of the stability of the fragments.

It has been noted that metal ion complexes containing different ligands usually decompose during spray ionization through the cleavage of the metal ligand bond. This behavior gives a rise to the presence of molecular ion peaks attributed to species as $[H_nL]^+$ are usually present in the mass spectra [36].

Some representative mass spectra of some metal complexes and the pattern of degradation of some complexes were shown in Figs. 1 and 2 and Schemes 1,2 and 3.

The mass spectrum of complex 3 showed molecular ion peak at m/z 490 (5.12 %) amu that is corresponding to [m+] and also show peaks at 408 (5.62 %), 344(0.36 %), 374(22.13 %), 286(5.12 %), 313(0.67%), 109 (100 % base peak), 69.05(19.96 %) and 56.10(1.98%).

The mass spectrum of complex 6 showed molecular ion peak at m/z 807 (23.02 %) amu that is corresponding to [m+] and also gives a series of peaks due to various fragments at 787(0.32 %), 646(41.27 %), 753(42.86 %), 328(52.38 % ligand peak), 253(24.83 %), 224(50.00 %), 116(100.00% base peak), 56(27.78 %).

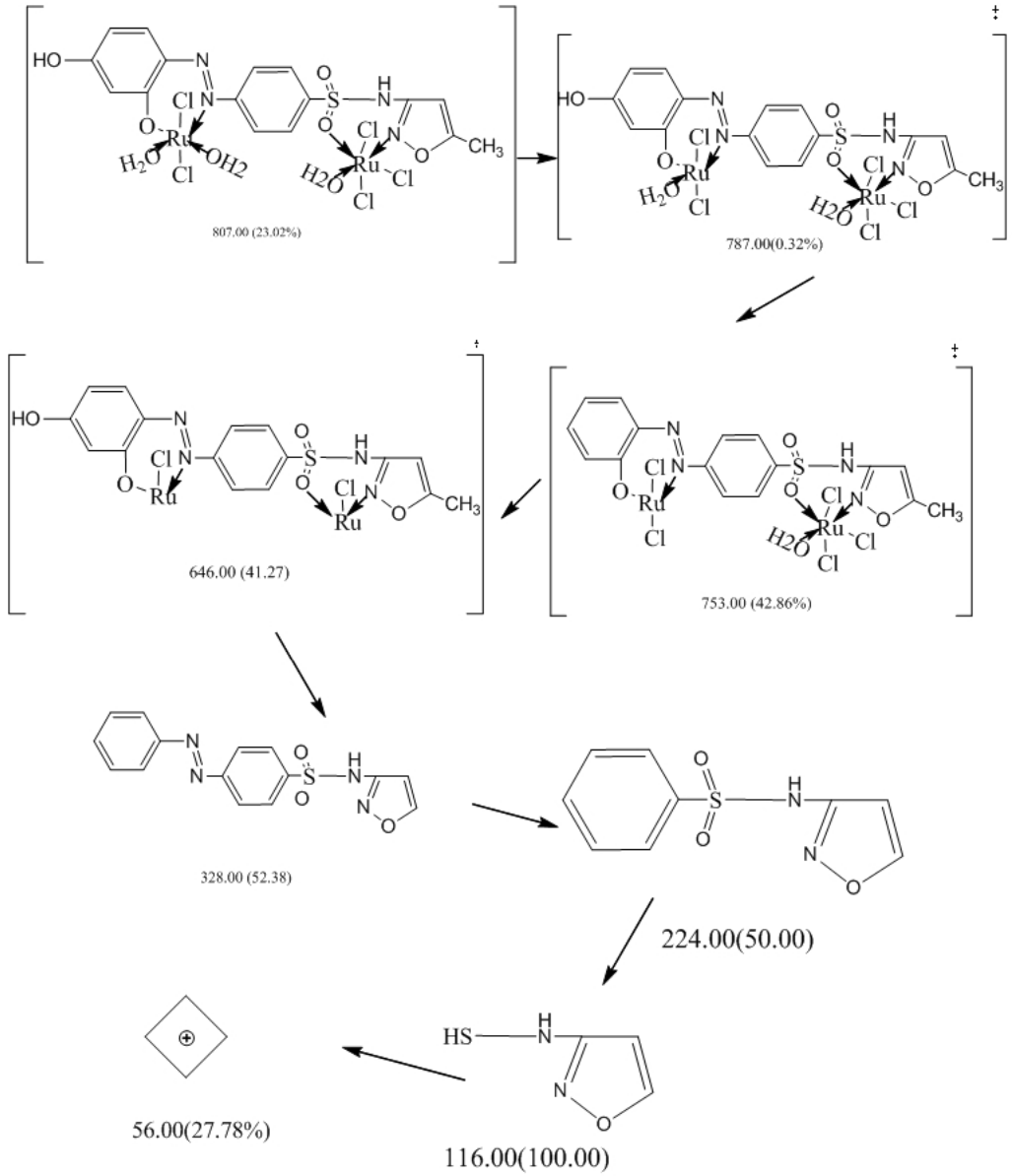

Scheme 1. The proposed fragments of complex 6.

The mass spectrum of complex 7 (Figure 1) showed molecular ion peak at m/z 640(15.24%) amu which corresponding to [m^{++1}] and also showed peaks at 322(23.37 %), 250(8.58 %), 185(56.80 %), 157(15.09 %), 93(23.67 %), 57(100 % base peak).

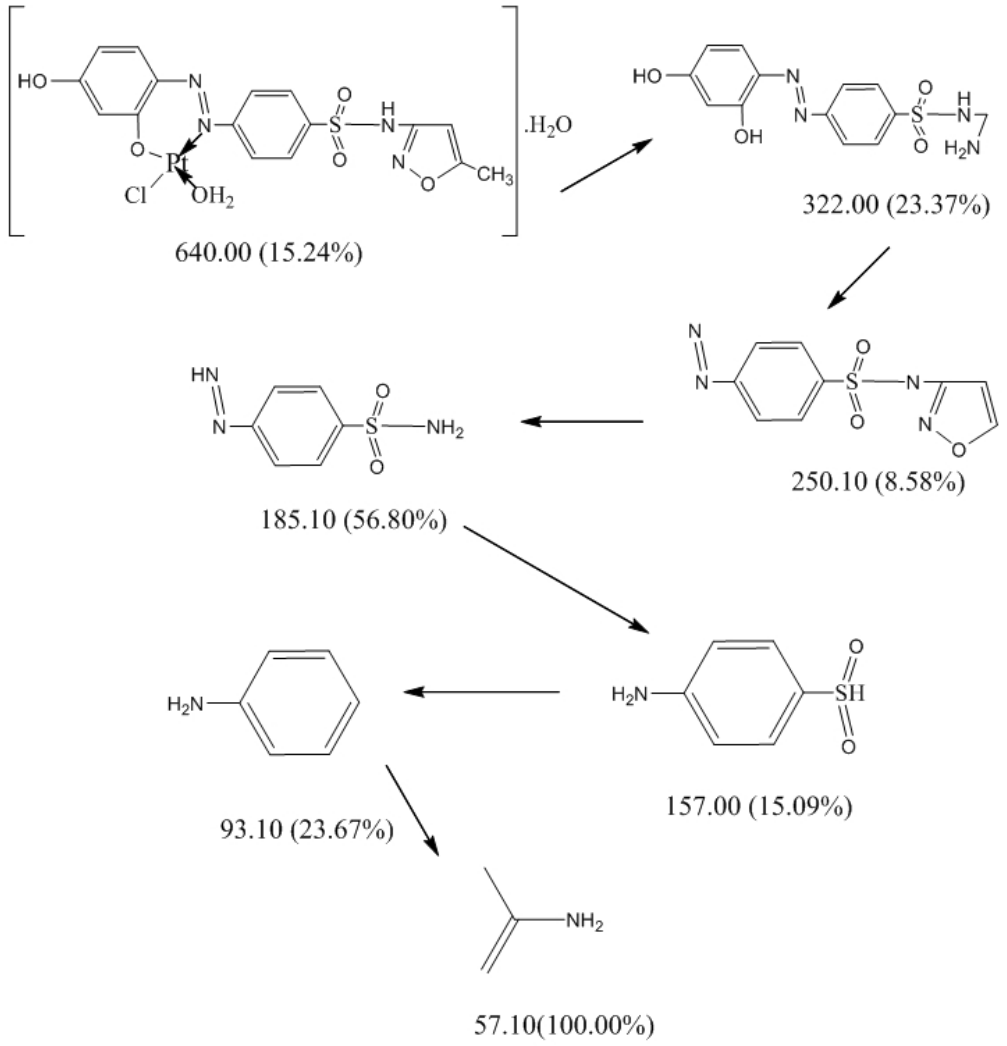

Scheme 2. The proposed fragments of complex 7.

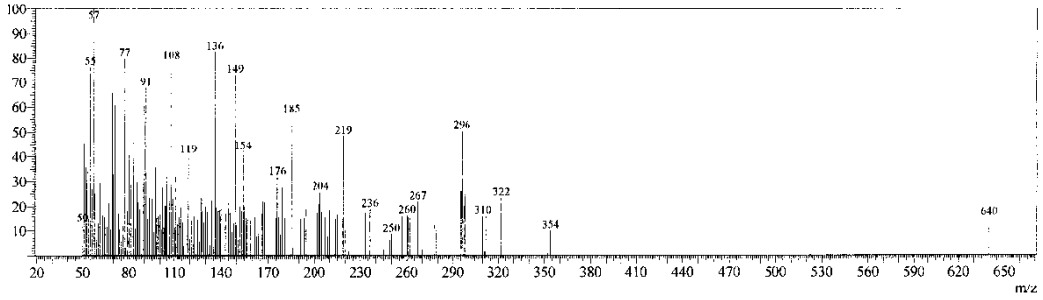

Figure 1. Mass spectrum of complex 7.

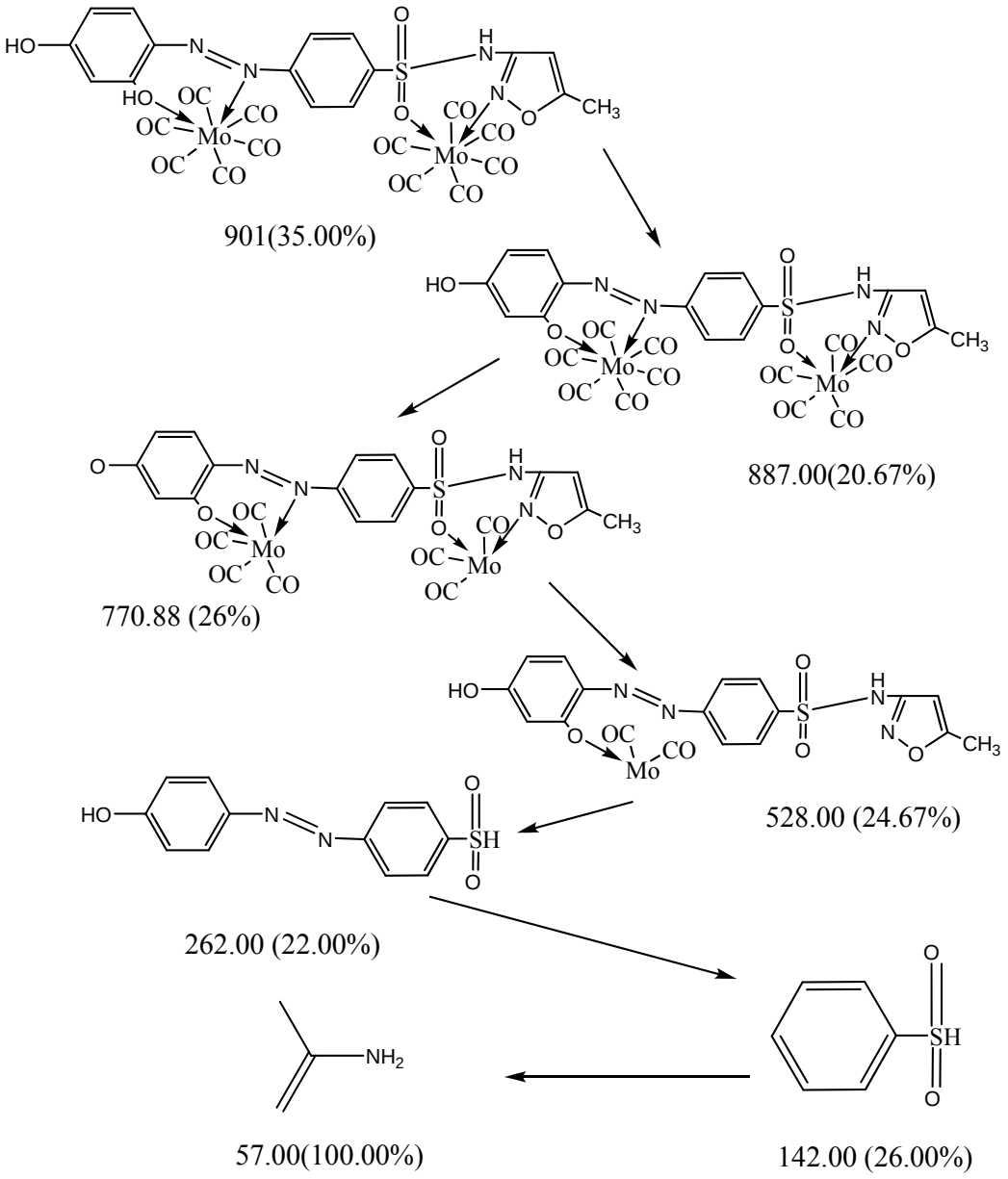

Scheme 3. The proposed fragments of complex 8.

The mass spectrum of complex 8 (Figure 2) showed molecular ion peak at 901(35.00 %) amu corresponding to [m+ -1] and another peaks due to its fragmentation at 887(20.67 %), 770(26 %), 528(24 %), 262(22.00 %) ligand peak , 142(26.00 %), 57(100.00 % base peak). The fragmentation of complex 9 showed ion peak at 702(0.60%) due to its molecular ion peak [m+-2] and also peaks at 645(6.68 %), 575(0.65 %), 278(1.31 %), 138(6.35 %), (109(100% base peak), 69(19.28 %). The fragmentation of complex 11 showed ion peak at 712(22.03%) due to its molecular ion peak [m+-2] and also peaks at 531(23.76 %), 156(27.43 %), 128(27.86 %), 108(36.07 %), (98(19.44 %) 55(100.00% base peak).

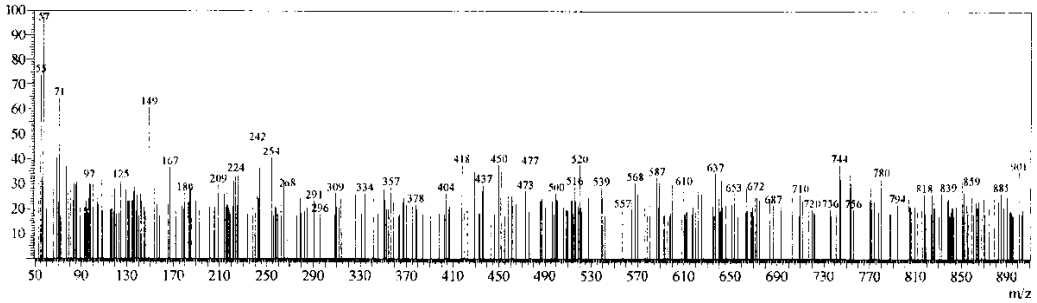

Figure 2. Mass spectrum of complex 8.

THERMAL ANALYSES (TGA)

The TGA results for some of solid metal complexes are depicted in Table 5. The results are in good agreement with the structural formulas shown in Figure 4.

Table 5 concluded that, there is a general pattern for the thermal behaviour of solid metal complexes, whereby, the complexes show mostly four main stages. The first stage is the loss of hydrated water molecules at 33-104 ˚C, followed in a second decomposition stage by the loss of the coordinated water at 104- 155 ˚C , then a third stage occurred which is the loss of coordinated anions (Cl) at 155- 350˚C. Last stage is the loss of organic ligand at 240- 962 ˚C to form finally a stable product which is more likely to be a metal oxide at 550 - 962˚C.

The above results and discussion showed that the investigated complexes have the chemical formulas shown in Figure 3.

Table 5. TGA data of some metal complexes and their assignments

Complex	Temperature(˚C)	Weight loss % Found(calcd)	Species removed or formed
[Ru2(HL1)Cl5(H2O)3]	40-123 125-350 350-550 550	6.4 (6.7) 22.4(22.1)	-3 H2O -6 coordinated Cl loss of ligand formation of oxide
[PtHL1Cl(H2O)].H2O	40-70 122- 272 272- 626 626	2.9 (2.8) 8.8(8.4)	-1 H2O -l(1H2O +Cl) loss of ligand formation of metal oxide
[(Mo)2(CO)12H2L1]	275- 514 555		loss of all ligands Formation of metal oxide
[Cu2L2Cl3 (H2O)].3H2O	33 – 104 104- 155 155-240 240-962 962	7.6 (7.6) 2.6 (2.5) 15.1 (14.9)	-3 H2O -1 H2O (coordinated) -3 coordinated Cl Loss of ligand formation of oxide

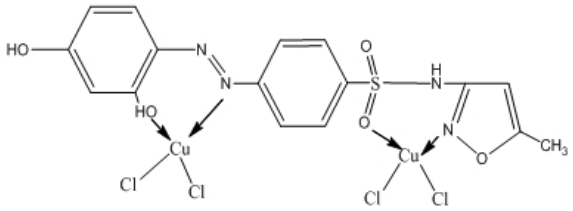

Complex 2

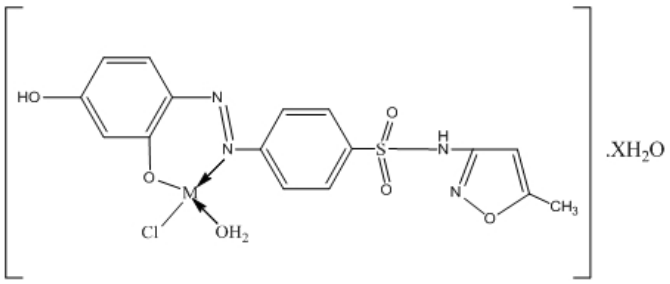

M=Cu(II), X= 0 , complex 3
M= Pt (II), X= 1 , complrx 7

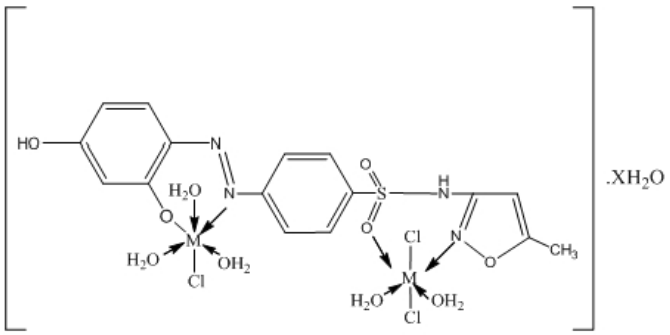

M= Co(II), X= 0, complex 4
M= Ni(II) , X=3, complex 5

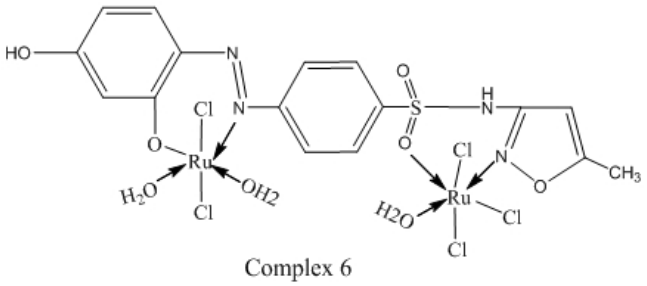

Complex 6

Figure 3. Chemical formulas of metal complexes.

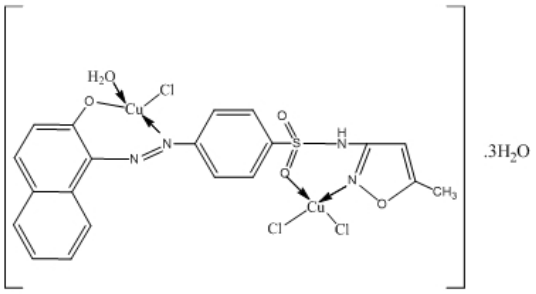

Complex 11

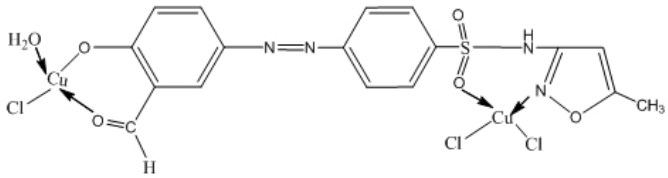

Complex 13

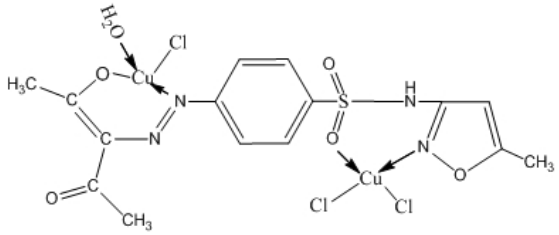

Complex 15

Figure 4. Chemical formulas of metal complexes.

CONCLUSION

Four new azo ligands of sulfamethoxazole and their metal complexes. with $CuCl_2$, $CoCl_2$, $NiCl_2$, $PtCl_2$, $RuCl_3$, $Cr(CO)_6$, and $Mo(CO)_6$ were prepared and characterized. The ligands comprise two compartments, so the study revealed that the prepared complexes, except a copper complex and the platinum complex, are binuclear complexes. The study also showed that each compartment behaved either as a bidentate ligand or as a neutral or monobasic ligand.

The results of magnetic moment values and electronic spectra study as well as other techniques indicate the geometrical shapes of metal complexes. The thermal stability of some of the prepared complexes was also studied. The molecular weight of some metal complexes as well as their fragmentations have also been studied by mass spectra measurements.

REFERENCES

[1] H. Zollinger, Azo and diazo chemistry, *New York: Interscience*: 1961.

[2] H. Zollinger, Colour chemistry, Synthesis, properties, and application of organic dyes, Weinheim; VCH; 1987.

[3] H. Nishihara, Bll. *Chem. Soc*. Japan, 77 (2004) 407.

[4] M. Badea, R. Olar, E. Cristurean, D. Marinescu, A. Emandi, P. Budrugeac, *J. Thermal Analysis and Calorimetry*, 77 (2004) 815.

[5] Y. Geng, D. Gu, F. Gan, *Optical Materials*, 27 (2004) 193.

[6] W. Bin, W. Yi-Qun, G. Dong-Hong, G. Fu-Xi, *Chinese Physics Letters*, 20 (2003) 1596.

[7] H. Fu-Xin, W. Yi-Qun, G.Dong-Hong, G. Fu-Xi, *Chinese Physics Letters*, 20 (2003) 2259.

[8] E. Hamada, T. Fujii, Y. Tomizawa, S. Limura, *Japanese Journal of Applied Physics*, 36 (1997) 593.

[9] Y. Suzuki, Y. Okamoto, Y. Kurose, S. Maeda*, Japanese Journal of Applied Physics*, 38 (1999) 1669.

[10] J.R. Anacona, C.Patino*, J. Coord. Chem*., 62 (2009) 613.

[11] J.R. Anacona, D. Lorono, M.Azocar, R. Atencio, J.Coord. Chem., 62 (2009) 951.

[12] Abu-Husse, W. Linert, 62 (2009) 1388.

[13] Z.H. Chohan, H. Pervez, A. Rauf, K.M. Khan, C.T. Supuran, J. Enzyme Inhib., *Mrd. Chem*. ,19 (2004) 417.

[14] J. Mukta, D. Kumar, R.V. Singh*, Main group Meta Chem*., 26 (2003) 99.

[15] J.J. Plateeuw, *Tropical Med. Int. Health*, 11 (2006) 804.

[16] M.R. Christiane, C.L.M. Paul, B.M. James, Clinical Pharm. *Kinetics*, 12 (2005) 1247.

[17] H.T.S. Bitton; " Hydrogen Ions" 2nd Edit. Chapman Hall, London (1952).

[18] M. Ramadan, I. M. EL-Mehasseb. *Trans. Met. Chem*. 23 (1998) 183.

[19] E. W. Ainscough, A. M. Brodie, A. J. Dobbs, J. D. Ranford, J. M. Waters, *Inorg. Chem. Acta* 267 (1998) 27.

[20] H. Locker; *J. Org. Chem*., 27, 361 (1962).

[21] M. Katritziky; *J. Chem. Soc.,* 3674 (1959).

[22] A.S. El-Tabl, S.A. El-Enein, *J. Coord. Chem*. 57 (4) (2004) 281.

[23] H.M. El-Tabl, F.A. El-Saied, M.I. Ayad, Synth. *React. Inorg. Met*. Org. 32 (7) (2002) 1247.

[24] M. Teotia, J.N. Gurthu, V.B. Rama, *J. Inorg. Nucl*. Chem. 42 (1980) 821.

[25] A.S. El-Tabl, F.A. El-Saied and A.N. Al-Hakimi ,*Transition Met. Chem*. ,32 (2007) 689

[26] K.B. Gudasi, S.A. Patel, R.S. Vadvavi, R.V. Shenoy, M. Nethaji, *Trans. Met. Chem*., 586 (2006) 31.

[27] El-Motaleb, M. Ramada, W. Sawodny, H.F. El-Baradie, M. Gaber*, Trans. Met. Chem*., 211 (1997) 22.

[28] B. P. Lever, Inorganic Electronic Spectroscopy, Second edition*, Elsevier Science Publishing Company*, Amsterdam, 1984.

[29] Labadi, L. Horvath, G. Liptay, *J. Therm. Anal*. Cal. 83, (1) (2006) 247.

[30] Cukurovali, I. Yilmaz, *Trans. Met. Chem*. 31 (2006) 207.

[31] D.X. West, L.K. Pannell, *Trans. Met. Chem*. 14 (1989) 457.

[32] P.K. Singh, D.N. Kumar, Spectrochim. Acta, Part A 64 (2006) 853.
[33] S.A. Sallam, A.S.Orabi, B.A. El-Shetary , A. Lentz , *Trans. Met. Chem*. 27 (2002) 447-453.
[34] S. Yamada, Coord. Chem. Rev., 1 (1966) 415.
[35] G. Venkatachalam, R. Ramesh , Sectrochim. *Acta Part A,* 61 (2005) 2081.
[36] B.K.Singh, P.Mishra, B.S.Garg, *Transition Met. Chem.,* 32, 603 (2007).

Smart Nanocomposites
Volume 2, Number 2
ISSN: 1949-4823

SYNTHESIS AND SPECTROSCOPIC CHARACTERIZATION OF COPPER(II), NICKEL(II) AND COBALT(II) COMPLEXES OF (3,3',4,4')-4,4'-(1,4-PHENYLENEBIS(AZAN-1-YL-1-YLIDENE)) BIS(3-(HYDROXYIMINO)PENTAN-2-ONE)

Abdou S. El-Tabl*[1], Ahmed M. A. El-Seidy[2], Mohamad. M. E. Shakdofa[2,3] , and Alaa El-Deen A. I. Hamdy[1]

[1]Department of chemistry, Faculty of science,
El-Menoufia University, Shebin El-Kom, Egypt
[2]Inorganic Chemistry Department,
National Research Center, Cairo, Egypt
[3]Department of Chemistry, Faculty of Science and Arts, Khulais,
King Abdulaziz University, Saudi Arabia

ABSTRACT

Copper(II), nicke(II) and cobalt(II) complexes of of (3,3',4,4')-4,4'-(1,4-phenylenebis(azan-1-yl-1-ylidene))bis(3-(hydroxyimino)pentan-2-one) have been prepared by direct and template methods. The ligand and its complexes have been characterized by elemental analyses, spectroscopic technique as IR, UV. Vis., ESR, magnetic moment and conductivity measurements. The molar conductivity values of the complexes in DMF are commensurate with their non-electrolytic nature. The spectral data showed that the ligand act as neutral tetradentate or dibasic tetradentate ligand bonded to the metal ions throughall C=N and protonated or deprotonated C=N-O groups forming octahedral geometry around the metal ions. The ESR spectra of copper(II) complexes **(9), (10) and (13)** show $\mathbf{g_{\|}}$-values (2.274, 2.282, 2.256) which commensurate with considerable covalent bond character with a d_{x2-y2} ground state.

Keywords: 3-(hydroxyimino)pentane-2,4-dione, synthesis, spectroscopic studies, metal complexes

* Corresponding Author E-mail: asaeltabl@yahoo.com

1. INTRODUCTION

Oxime metal chelates are biologically active and are reported to possess semiconducting properties [1]. Derivatives of monoaminoglyoxime, heterocyclic and macrocyclicoximes and their metal complexes have been described [2]. Metal complexes of oxime ligands have antibacterial and fungal activities [3-4]. Also oximes compounds such as butane-2,3-dionethiosemicarbazone oximehas potential antioxidant and toxic activities [5]. Nickel(II) complexes of 3-(2-amino-ethylimino)-butan-2-one oxime, 3-(2-amino-propylimino)butan-2-one oxime] and 3-[2-(3-hydroxy-1-methyl-but-2-enyli-deneamino)-1-methyl-ethylimino]-butan-2-one oxime have been prepared and characterized by analytical, spectroscopic and x-ray single crystal [6]. oximes have been widely used as very efficient complexing agents in analytical chemistry for isolation, separation and extraction of different metal ions [7-12]. A number of review articles have been reported dealing with the coordination chemistry of oximes [13] which has received great attention during the last 20 years for a variety of reasons including (i) the ability of the oxidation states of metals (ii) the development of bioinorganic models (iii) the design of selective receptors for Ca(II) and Ba(II) ions (iv) the development of new oxygen activation catalysis (v) the mechanistic study of corrosion inhibition on iron surfaces. All these reasons stimulated our interest in study metal complexes of oxime compounds. The aim of this article is the synthesis and characterization of copper(II), nickel(II) and cobalt(II)complexes of (3,3',4,4')-4,4'-(1,4-phenylenebis(azan-1-yl-1-ylidene))bis(3-(hydroxyimino)pentan-2-one).

2. EXPERIMENTAL

All complexes were put in oven for 4 h. at 45^{O}C. All chemicals and solvents were reagent grade commercial material and used as received. Elemental analyses for (C, H, N, Cl) were determined at the Analytical Unit of Cairo University, Egypt. Standard analytical methods were used to determine the metal ion content [14-17]. IR spectra of the ligand and its metal complexes were measured using KBr discs with a Jasco FT/IR 300E Fourier transform infrared spectrophotometer covering the range 400-4000 cm^{-1} and in the 500-100 cm^{-1} region using polyethylene-sandwiched Nujol mulls on a Perkin Elmer FT-IR 1650 spectrophotometer. Electronic absorption spectra in the 200-900 nm regions were recorded on a Perkin-Elmer 550 spectrophotometer. Magnetic susceptibilities were measured at 25^{o}C by the Gouy method using mercuric tetrathiocyanato-cobaltate(II) as the magnetic susceptibility standard. The magnetic moments were calculated from the equation:

$$\mu_{eff.} = 2.84\sqrt{\chi_M^{corr} . T} .$$

Diamagnetic corrections were estimated from Pascal's constant [18]. Molar conductance was measured on a Tacussel type CD_6NG conductivity bridge using 10^{-3} M DMF solutions. The resistance measured in ohms and the molar conductivities were calculated according to the equation:

$$(= (V \times K \times g)/(Mw \times "(")$$

where Λ is molar conductivity (ohm^{-1} cm2 mol^{-1}); V, volume of the complex solution (mL); K, cell constant 0.92 cm^{-1}; Mw, molecular weight of the complex; g, weight of the complex; and Ω, resistance measured in ohms. TLC was used to confirm the purity of the prepared compounds.

2.1. Preparation of the Ligand

(3,3',4,4')-4,4'-(1,4-phenylene bis(azan-1-yl-1-ylidene))bis(3-(hydroxyimino)pentan-2-one)was prepared by the published method [19]. The hot (75 ^{o}C) ethanolic solution (30 mL) of *p*-phenylenediamine (0.037 mol.) was added dropwise to the hot (75 ^{o}C) ethanolic solution (50 mL) of (hydroxyimino)pentane-2,4-dione (0.077 mol). The reaction solution was refluxed for 2 hours and left to cool to precipitate, filtered off, washed with warm ethanolic and dried. The ligand was crystallized from ethanol (m.p. 213^{o}C).^{1}H NMR (300 MHz, DMSO): δ = 13.9 (s, 2OH, H(23), H(24)7.10 (d, 4H, aromatic, H(2, 3, 5, 6), 2.1, (s, 6H, 2CH_3(H(15), H(22), 2.7, (s, 6H, 2CH_3, H(12), H(19).

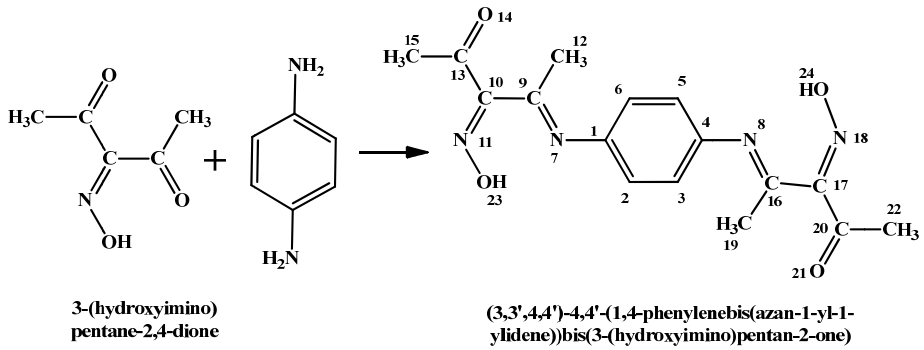

Figure 1. Preparation of the ligand.

2.2. Preparation of Complexes2, 6, 7, 9, 12 and 13

A filtered ethanol solution (100 cm^{3}, 6.1 X 10^{-3}mol) of $Ni(CH_3COO)_2.4H_2O$, $NiCl_2.6H_2O$, $Ni(NO_3)_2.6H_2O$, $Cu(CH_3COO)_2.H_2O$, $Cu(NO_3)_2.3H_2O$ $CuCl_2.2H_2O$ was added to an ethanol (100 cm^{3}) suspension of equimolar concentration of the ligand to form complex **2**, **6**, **7**, **9, 12,** and **13** respectively. The reaction solution was warmed while stirring for 3 hours. The prepared complex was filtered off, washed several times with ethanol and dried under vacuum in presence of P_2O_5.

2.3. Preparation of Complex 3

Complex **3** was prepared by adding water solution (100 cm^{3}) of $Ni(CH_3COO)_2.4H_2O$ (6.1 X 10^{-3}mol) to water (100 cm^{3}) suspension of equimolar concentration of the ligand. The

reaction solution was warmed while stirring for 3 hours. The prepared complex was filtered off, washed several times with water and dried under vacuum in presence of P_2O_5.

2.3.1. Reactions of Complex 3

a) With Ethanol

The ethanol suspension of complex **3** (6.1 X 10^{-3}mol) in hot (70^oC) ethanol (100 cm^3) was refluxed for 5 h. The formed complex was filtered off, washed with warm ethanol and dried under vacuum in presence of P_2O_5. The prepare complex was identified as complex **2**.

b) With $NiCl_2.6H_2O$ and $Ni(NO_3)_2.6H_2O$

$NiC1_2.6H_2O$ or $Ni(NO_3)_2.6H_2O$ethanolic solution (8.4 X 10^{-3}mol, 70 cm^3) was added dropwise while stirring to a suspension of an equimolar concentration of complex **3** in ethanol (50 cm^3) to form complex **4** or **5**, respectively.

The reaction solution was refluxed for 2 hours and the formed complex was filtered off, washed several times with warm ethanol and dried under vacuum in presence of P_2O5.

2.4. Reactions of Complex 6

a) With Sodium Acetate in Water

The aqueous solution (50 cm^3) of $CH_3COONa.3H_2O$ (14.7 X 10^{-3} mol.) was added, while stirring to an aqueous (50 cm^3) suspension of complex **6** (7.3 X 10^{-3}mol.).

The reaction solution was warmed for 3 h and the formed complex **8** was filtered off, washed several times with water and dried.

b) With Piperidine in Ethanol:

The reaction of complex **6** with piperidine (1:5 molar ratio) was carried out as described above in the reaction with sodium acetate and water to produce complex **8.**

2.5. Reactions of Complex 12

a) With Sodium Acetate in Water

The aqueous solution (50 cm^3) of $NaCH_3COO.3H_2O$ (1.1 X 10^{-2}mol) was added while stirring to an aqueous (50 cm^3) suspension of complex **12** (2.1 X 10^{-3} mol). The reaction solution was warmed for 3 h.

The formed complex was filtered off, washed with warm water and dried. The produced complex was identified as complex **9**.

2.6. Preparation of Complex 10

A filtered mixed solution of ethanol and water in ratio 1:10(100 cm^3, 6.1 X 10^{-3}mol) of $Cu(CH_3COO)_2.H_2O$was added to an (100 cm^3) suspension of the ligand in molar ratio (5M:1L) in the same solution.

The reaction solution was warmed while stirring for 3 hours. The prepared complex was filtered off, washed several times with ethanol and dried under vacuum in presence of P_2O_5.

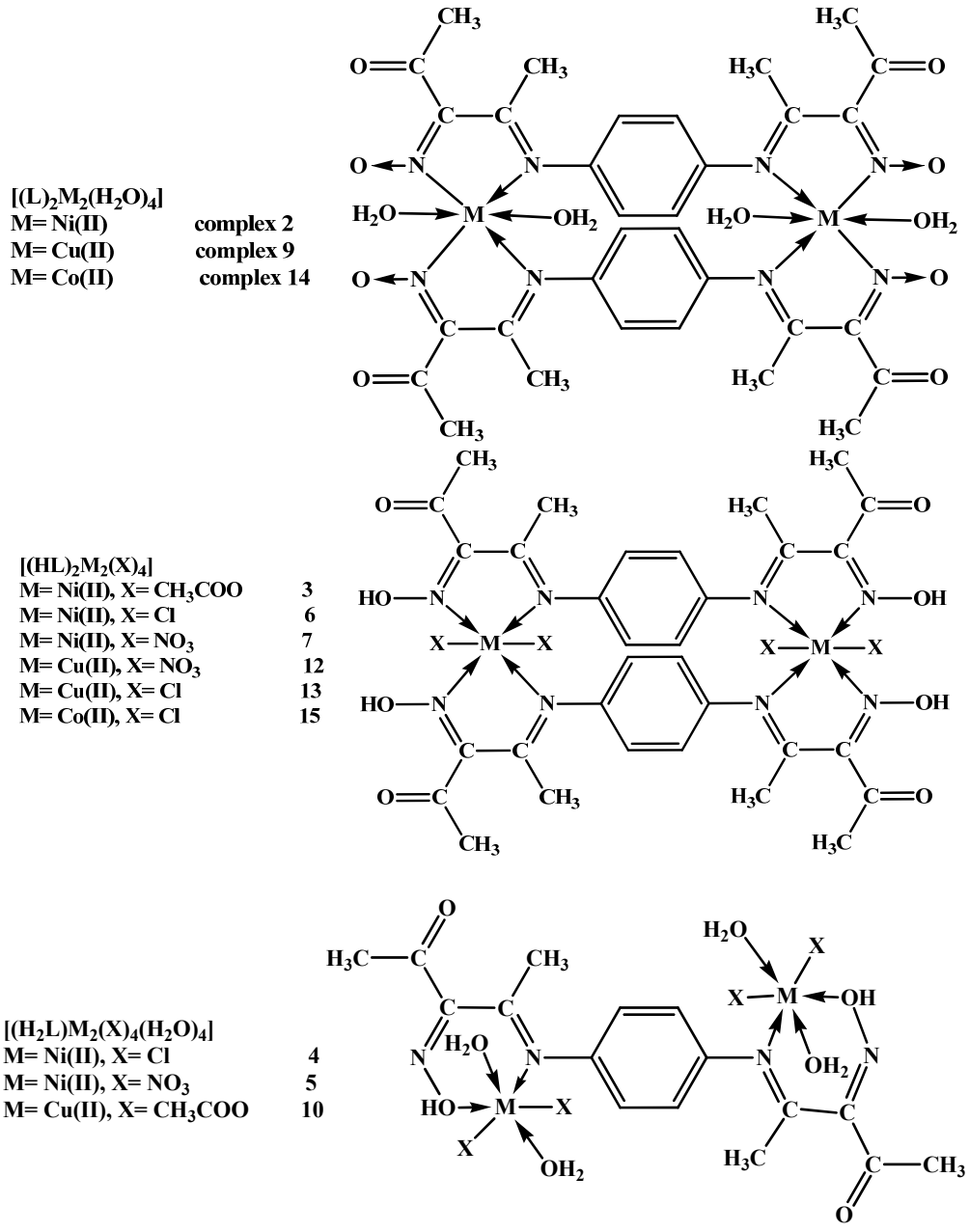

Figure 2. (Continued).

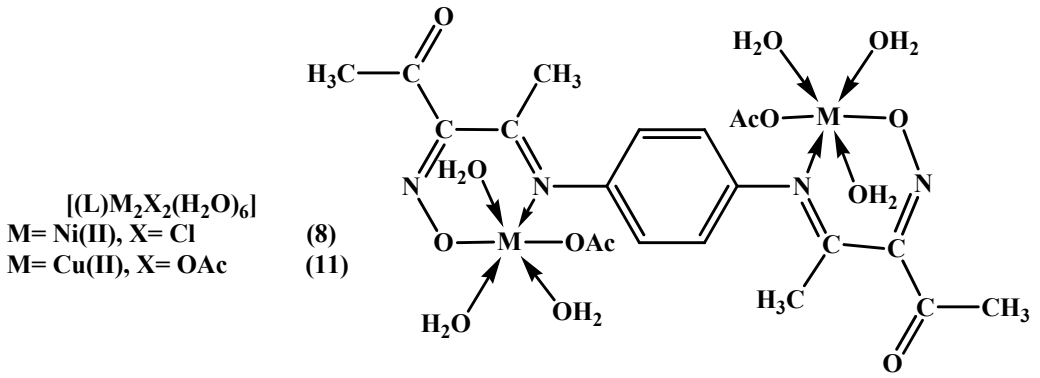

Figure 2. The proposed structures of metal complexes.

2.6.1. Reaction of Complex 10

a) With Ethanol

The ethanol suspension of complex **10** (3.2 X 10^{-3}mol, 100 cm^3) was refluxed for 5 hours. The formed complex **11** was filtered off, washed with warm ethanol and dried.

2.7. Preparation of Complex Cobalt Complexes

2.7.1. Preparation Cobalt Complex 14

A filtered ethanol solution (100 cm^3, 6.1 X 10^{-3}mol) of $Co(CH_3COO)_2.4H_2O$was added to an ethanol (100 cm^3) suspension of equimolar concentration of the ligand to form complex **2 14** respectively. The reaction solution was warmed while stirring for 3 hours. The prepared complex was filtered off, washed several times with ethanol and dried under vacuum in presence of P_2O_5. The same complex is by the reaction of the ligand with $Co(CH_3COO)_2.4H_2O$, $CoCl_2.6H_2O$or $Co(NO_3)_2.6H_2O$ in water

2.7.2. Preparation of Complex 15

A filtered ethanol solution (100 cm^3, 6.1 X 10^{-3}mol) of $CoCl_2.6H_2O$was added to an ethanol (100 cm^3) suspension of equimolar concentration of the ligand to form complex **15**. The reaction solution was warmed while stirring for 3 hours. The prepared complex was filtered off, washed several times with ethanol and dried under vacuum in presence of P_2O_5.

2.8. Template Reactions

1. The Reaction of 3-(Hydroxyimino)Pentane-2,4-Dione with P-Phenylenediamine in the Presence of $Ni(CH_3COO)_2.4H_2O$,$Nic1_2.6H_2O$, $Cu(CH_3COO)_2.H_2O$ Or $Co(CH_3COO)_2.4H_2O$ (2:1:1 Molar Ratio) in Ethanol:

The ethanolic solution (50 cm^3, 15.4 X 10^{-3} mol.) of $Ni(CH_3COO)_2.4H_2O$, $NiC1_2.6H_2O$ $Cu(CH_3COO)_2.H_2O$ or $Co(CH_3COO)_2.4H_2O$was added while stirring to that (50 cm^3) containing an equimolar concentration of *p*-phenylenediamine in the same solvent. The solution of (hydroxyimino)pentane-2,4-dione (30.1 X 10^{-3} mol.) in ethanol was added to the warned solution of Ni(II) - *p*-phenylenediamine complex. The stirred reaction solution was

refluxed for 2 h, washed several times with warm ethanol and dried. This complex was identified as complex **2, 4, 7** and **14** respectively.

3. RESULT AND DISCUSSION

All the prepared compounds are colored, non-hygroscopic, crystalline solid and stable at room temperature. The complexes are insoluble in non-polar solvents but soluble in polar coordinating solvents such as DMSO and DMF. Elemental analyses, physical data, Table 1, and spectral data, Tables 2 and 3 are compatible with the proposed structures shown in Chart 1. To date, no diffractable crystals have been grown. The elemental analysis showed that, the molar ratio of ligand : metal was either 2:2 (in cases of complexes 2, 3, 6, 7, 9 and 12-15) or 1:2 (in cases of complexes 2, 4, 5, 8 and 10-11)

3.1. Conductivity Measurements

The molar conductance values of the complexes in DMF (10^{-3} M), lie in the 12-23.2 Ω^{-1} $mol^{-1}cm^2$ range, Table 1, indicating that, all the complexes are not electrolytes. These confirmed that the anion is coordinated to metal ion [20]. The considerably high values of molar conductance of some complexes may be due to the partial solvolysis by DMSO. These data are agreeable with Greenwood el al. studies. They have suggested 50-70 Ω-1cm2mol-1 as the range for 1:1 electrolyte in DMSO [21].

3.2. IR Spectra

The IR spectral data for the ligand (H_2L, 1) and its metal complexes are presented in Table 2.The IR spectrum of the ligand showed bands at 3250cm^{-1} may be due to υ(OH) groups [22]. The spectrum shows bands in the 1692-1682 and 1643-1618 cm^{-1} ranges were assigned to υ(C=O) andυ(C=N) groups, respectively [23,24]. The spectra of solid complexes are compared with those of the ligand in order to know the mode of bonding. The spectra showed that, the ligand behaved either as:

1. Neutral tetradentate ligand, coordinating through all C=N groups (complexes 3, 6-7, **12-13** and **15),** the mode of coordination was suggested by the following evidence: i) the bands due C=N groups were shifted to lower wave number with decreasing their intensities indicating their coordination to the central metal [25-28], ii) the bands due to the carbonyl and hydroxyl moieties were found almost at its original position indicating they are not involved in coordination [29], iii) the bands due to υ(N-O) were slightly shifted to lower wave umber indicating a slight decrease in the double bond character iv) the appearance of new bands in the 550-625 cm^{-1} range which further supports the coordination of the o nitrogen of the C=N group [30].
2. Bibasic tetradentate ligand, coordinating through all C=N groups (complexes 2, 9 and **14**),the mode of coordination was suggested by the following evidence: i) the bands due C=N groups were shifted to lower wave number with decreasing their

intensities indicating their coordination to the central metal [25-28], ii) the bands due to the carbonyl groups were found almost at its original position indicating they are not involved in coordination [29], iii) the disappearance of the bands due to hydroxyl group. iv) the bands due to υ(N-O) were shifted to lower wave umber indicating a decrease in the double bond character v) the simultaneous appearance of new bands in the 545-635 cm^{-1} region are due to the ν(M–N) and ν(M←N) vibrations respectively

3. Bibasic tetradentate ligand, coordinating through C=N and deprotonated oxime groups (complexes **8** and **11**), the mode of coordination was suggested by the following evidence: i) on set of υ(C=N) bands were shifted to higher wave number indicating the presence of ring strain and the coordination to the adjacent oxygen, while the other set is shifted to lower wave number indicating their involvement in coordination to the central metal [25-28], ii) the bands due to the carbonyl groups were found almost at its original position indicating they are not involved in coordination [29], iii) the disappearance of the bands due to hydroxyl group. iv) the bands due to υ(N-O) were shifted to lower wave umber indicating a decrease in the double bond character v) the appearance of new bands in the 610-630, 660-670 range assigned the ν(M←N) and ν(M—O) bond [31,32].
4. Neutral tetradentate ligand, coordinating through C=N and hydroxyl groups (complexes **4, 5** and **10**),the mode of coordination was suggested by the following evidence: i) on set of υ(C=N) bands were shifted to higher wave number indicating the presence of ring strain and the coordination to the adjacent oxygen, while the other set is shifted to lower wave number indicating their involvement in coordination to the central metal [25-28], ii) the bands due to the carbonyl groups were found almost at its original position indicating they are not involved in coordination [29], iii) the bands corresponding to the hydroxyl were shifted down field indicating their involvement in coordination to the central metal, iv) the bands due to υ(N-O) were shifted to higher wave umber indicating an increase in the double bond character v) the appearance of new bands in the 595-630, 660-677 cm^{-1} range assigned theν(M←N) and ν(M←O) bond [26-27].

The appearance of a new band in the 330-365 cm^{-1}range may be assigned to ν(M-Cl) in the chloro complexes (4), (6), (8), (13) and (15) [33]. Extensive IR spectral studies reported on metal acetocomplexes indicated that the acetate ligand may coordinate to the central metal in either a monodentate, bidentate or bridging manner [34]. The $\nu_{asym.}(CO_2)$ and $\nu_{sym.}(CO_2)$ of the free acetate ions are found at 1560 and 1416 cm^{-1}, respectively. In monodentate coordination ν(C=O) is found at higher energy than $\nu_{asym.}(CO_2)$ and ν(C-O) is lower than $\nu_{sym.}(CO_2)$. As a result, the separation between the two ν(CO) bands is much larger in monodentate complexes than the free ion [35].The opposite trend is observed in bidentate aceto coordination; the separation between ν(CO) is smaller than for the free ion. For bridging acetate with both oxygen atoms coordinated as in copper(ll) acetate, however, the two ν(CO) bands are close to the free ion values [36].

Table 1. Elemental analyses and physical properties of the ligand (H_4L) and its metal complexes

No.	Ligand\ complexes		M. Wt	$\Omega^{-1}mol^{-1}$ cm^2	Found (Calc.) %			
					C	H	N	M
1	H_2L $C_{16}H_{18}N_4O_4$	Yellow	330.3	-	57.88(58.2)	5.21(5.5)	17.40(17.0)	-
2	$L_2Ni_2(H_2O)_4$ $C_{32}H_{40}N_8Ni_2O_{12}$	Brown	846.1	14	45.30(45.4)	4.56(4.8)	12.91(13.2)	13.64(13.9)
3	$(H_2L)_2Ni_2(OC(O)CH_3)_4$ $C_{40}H_{48}N_8Ni_2O_{16}$	Dark brown	1014.2	18	47.21(47.4)	4.71(4.8)	10.89(11.1)	11.23(11.6)
4	$H_2LNi_2Cl_4(H_2O)_4$ $C_{16}H_{26}Cl_4N_4Ni_2O_8$	Brown	661.6	15	28.90(29.1)	4.01(4.0)	8.81(8.5)	17.52(17.7)
5	$H_2LNi_2(NO_2)_4(H_2O)_4$ $C_{16}H_{26}N_8Ni_2O_{16}$	Dark brown	703.8	19	27.10(27.3)	3.75(3.7)	14.67(15.9)	16.61(16.7)
6	$(H_2L)_2Ni_2Cl_4$ $C_{32}H_{40}Cl_4N_8Ni_2O_{10}$	Green	955.9	20	39.95(40.2)	4.31(4.2)	11.56(11.7)	12.04(12.3)
7	$(H_2L)_2Ni_2(NO_2)_4$ $C_{32}H_{36}N_{12}Ni_2O_{16}$	Grey	962.1	18	39.66(40.0)	3.68(3.8)	17.62(17.5)	11.80(12.2)
8	$LNi_2Cl_2(H_2O)_6$ $C_{16}H_{28}Cl_2N_4Ni_2O_{10}$	Brown	624.7	21	30.56(30.8)	4.45(4.5)	8.78(9.0)	18.45(18.8)
9	$L_2Cu_2(H_2O)_4$ $C_{32}H_{40}Cu_2N_8O_{12}$	Grey	855.8	12	44.56(44.9)	4.59(4.7)	13.01(13.1)	14.60(14.9)
10	$H_2LCu_2(OC(O)CH_3)_4(H_2O)_4$ $C_{24}H_{38}Cu_2N_4O_{16}$	Brown	765.7	20	37.46(37.7)	5.1(5.0)	7.012(7.3)	16.40(16.6)
11	$LCu_2(OC(O)CH_3)_2(H_2O)_6$ $C_{20}H_{34}Cu_2N_4O_{14}$	Deep brown	681.6	18	35.00(35.2)	4.82(5.0)	8.31(8.2)	18.52(18.7)
12	$(H_2L)_2Cu_2(NO_2)_4$ $C_{32}H_{36}Cu_2N_{12}O_{16}$	brown	971.8	19	39.39(39.6)	3.50(3.7)	17.01(17.3)	12.79(13.1)
13	$(H_2L)_2Cu_2Cl_4$ $C_{32}H_{36}Cl_4Cu_2N_8O_8$	Violet	929.6	23	41.01(41.4)	3.58(3.9)	12.035(12.1)	13.61(13.7)
14	$L_2Co_2(H_2O)_4$ $C_{32}H_{40}N_8Co_2O_{12}$	Red	846.57	9	45.65(45.40)	4.92(4.76)	13.51(13.24)	13.54(13.92)
15	$(H_2L)_2Co_2Cl_4$ $C_{32}H_{36}Cl_4Cu_2N_8O_8$	Brown	920.36	25	42.00(41.76)	4.05(3.94)	12.11(12.18)	12.58(12.81)

$\Omega^{-1}mol^{-1}cm^2$ in 10^{-3} M DMF

Table 2. IR spectra (assignments) of the ligand and its metal complexes

NO.	υ(H_2O)	υ(OH)	υ(C=O)	υ(C=N)	υ(N-O)	υ(M-N)	υ(M-O)	υ(M-Cl)
1	-	3250br	1690s,1682s	1643s,1618s	1022s, 1008s			
2	3435br	-	1692s,1680s	1633s,1610s	1160s	545m,612m		
3	-	3257br	1689s,1681s	1629s,1607s	1018s	625m		
4	3442br	3260br	1693s,1684s	1626s,1619s	975s,969s	605m	670m	330m
5	3450br	3225br	1690s,1684s	1621s,1618s	981s,974s	595m	660m	
6	-	3232br	1691s,1685s	1627s,1610s	1010s	572m		345m
7	-	3262br	1693s,1681s	1631s,1609s	1014s	565m		
8	3441br	-	1691s,1683s	1630s,1625s	979s,966s	610m	670m	325m
9	3455br	-	1692s,1682s	1634s,1606s	1151s	585m,635m		
10	3440br	3224br	1691s,1680s	1634s,1620s	974s,964s	630m	677m	
11	3444br	-	1692s,1681s	1634s,1605s	970s,962s	630m	660	
12	-	3261br	1693s,1683s	1637s,1609s	1014s	645m		
13	-	3263br	1691s,1683s	1630s,1603s	1019s	640m		355m
14	3470br		1700s,1679s	1624s,1600s	1169s	565m,610		
15	--	3300br	1695s,1680s	1632s,1611s	990,970	550m		365m

b=broad, s=strong, m=medium, w=week

The acetato group in complexes **(3) (10)** and **(11)** acted as a monodentate ligand and this is supported by the appearance of two new bands in the ranges 1572-1582 and 1365-1371 cm^{-1}, which may be attributed to $\nu_{asym.}(COO^-)$ and $\nu_{sym.}(COO^-)$, respectively. Further, the complex exhibits δ(COO) at 765 cm^{-1} which is considered diagnostic for monodentate acetates [34].

The separation value (Δ) between $\nu_{asym}(COO^-)$ and $\nu_{sym.}(COO^-)$ in these complexes were more than 200 cm^{-1} (205-217 cm^{-1}) suggesting the coordination of carboxylate group in a monodentate fashion [35].

The spectrum of nitrato complexes **(5), (7),** and **(12)** show bands in 1448-1440 ($\tilde{o}_1$),1034-1029 ($\tilde{o}_2$), 1372-1367 ($\tilde{o}_4$) and 730-715 ($\tilde{o}_5$) regions with$\tilde{o}_1$–$\tilde{o}_4$ separation in the 81-88 cm^{-1}range, characteristic of mono-dentate nitrato group [37].

The broad bands in the 3470-3435 cm^{-1} region are due to coordinated water or water of crystallization. The bands for water of crystallization are different from those of coordinated water; the latter has a band in the 600-400 cm^{-1} region.

The presence of water molecules within the coordination sphere in the hydrated complexes **(2),(4-5)**,(**8-11)**and (**14)**were supported by the presence of bands at 3475-3435 cm^{-1}, 1602-1595 cm^{-1}, 930-953 cm^{-1} and 627-635 cm^{-1} due to OH stretching, HOH deformation, H_2O rocking and H_2O wagging, respectively [38].

3.3. Electronic Spectra

Nickel(II) complexes **(2-8)** showed bands in 480-515, 600-620 and 865-895 nm ranges respectively, which are attributable to $^3A_{2g}(F)\rightarrow{}^3T_{1g}(P)$ (ν_3), $^3A_{2g}(F)\rightarrow{}^3T_{1g}(F)$ (ν_2) and $^3A_{2g}(F)\rightarrow{}^3T_{2g}(F)$ (ν_1) transitions indicating octahedral nickel(II) complexes [39,40].

Copper(II) complexes **(9-13)** showed bands in the 570-600 and 620-655 nm range, which were assigned to $^2B_1\rightarrow{}^2E$ and $^2B_1\rightarrow{}^2B_2$ transitions indicating a distorted octahedral structure [41,42].

Cobalt(II) complexes **(14-15)** showed bands in the 945-965 633-670 and 490-525nm range, which were assigned to $^4T_{1g}(F)\rightarrow{}^4T_{2g}(F)$, $^4T_{1g}(F)\rightarrow{}^4A_{2g}(F)$, and $^4T_{1g}(F)\rightarrow{}^4T_{2g}(P)$ transitions respectively, indicating a distorted octahedral structure [43,44].

3.4. Magnetic Moments

The solid nickel(II) complexes show magnetic moment values at room temperature in the 2.58-2.85 B.M. range(Table 3). These values are considered to be in the normal range that usually observed in case of six coordinate nickel(II) species which contain two unpaired electrons. The solid copper(II) complexes show magnetic moment values at room temperature in the 1.65-1.70 B.M. range (Table 3) which are consistent with the presence of one unpaired electron in copper(II) complexes. The magnetic moment of complexes were lower than the spin-only value, implying an operation of spin-exchange interactions taking place between metal ions [29,45,46]. The magnetic moment values for solid cobalt(II) complexes at room temperature were in the range 3.77- 3.59 B.M. (Table 3) which are consistent with the presence of three unpaired electron in cobalt(II) complexes. which is smaller than the calculated value for two Co(II) ions in octahedral geometries and this may be due to anti-ferromagnetism between the two ion-centers [29,45,46].

Table 3. UV-Vis. spectra of the ligand, (H_4L) and its metal complexes

No.	Compounds	$\lambda_{max,}$ nm	μ_{eff} (B.M)
1	H_2L	250, 298	-
2	$L_2Ni_2(H_2O)_4$	250,308,405,495,590,880	2.6
3	$(H_2L)_2Ni_2(OC(O)CH_3)_4$	260,310,415,495,590,865	2.65
4	$H_2LNi_2Cl_4(H_2O)_4$	295,310,400,495,590,870	2.58
5	$H_2LNi_2(NO_2)_4(H_2O)_4$	260,303,410,495,590,890	2.75
6	$(H_2L)_2Ni_2Cl_4$	260,305,335,415,520,600,875	2.85
7	$(H_2L)_2Ni_2(NO_2)_4$	255,295,340,405,490,590,890	2.75
8	$LNi_2Cl_2(H_2O)_6$	260,305,420,460,600,895	2.69
9	$L_2Cu_2(H_2O)_4$	255,315,410,570, 635	1.65
10	$H_2LCu_2(OC(O)CH_3)_4(H_2O)_4$	250,308,415,600, 650	1.70
11	$LCu_2(OC(O)CH_3)_2(H_2O)_6$	250,308,400,560, 620	1.71
12	$(H_2L)_2Cu_2(NO_2)_4$	245,308,395,580, 645	1.66
13	$(H_2L)_2Cu_2Cl_4$	250,308,405,575,640	1.65
14	$L_2Co_2(H_2O)_4$	255, 300,415,	3.87
15	$(H_2L)_2Co_2Cl_4$	260, 315,395,	3.77

3.5. Electron Spin Resonanace

The ESR spectra of the solid copper(II) complexes **(11)** and **(12)** at room temperature exhibit signals at high field, which is isotropic due to the tumbling motion of the molecules. The g_{iso}values of the complexes are 2.055, and 2.104 respectively [47,48]. The ESR spectra of solid copper(II) complexes **(9), (10)** and **(13)** at room temperature is characteristic to d^9 configuration and having an axial symmetry type of a $d_{(x2-y2)}$ ground state which is the most common for copper(II) complexes [49,50]. The g values are $g_{\|}$= 2.274, 2.282, 2.250 $g_{\perp}$= 2.057, 2.064, 2.052 with g_{iso}= 2.109, 2.117, 2.107 respectively suggest elongated tetragonal octahedral geometry [51].The trend of g-values show $g_{\|}<g_{\perp}<g_{e(2.0023)}$ confirmed the tetragonal distortion around the copper(II) ion **(9), (10)** and **(13)** corresponding to elongation the four fold symmetry axis z [47]. In addition, exchange coupling interactions between the copper(II) ion is explained by Hathaway expression $G = (g_{\perp}((-2)(g_{\perp}(-2)$. If G < 4.0 the exchange interactions is negligible. If the value of G<4.0 a considerable exchange coupling is present in the solid complex. which is typically as in the case of complexes **(9), (10)** and **(13)** (G= 3.8, 3.4, 3.5) confirmed tetragonal octahedral structure [52,53]. Kivelson and Neiman showed that, for ionic environment $g_{\|}$ is ≥ 2.3 but for covalent environment $g_{\|}$< 2.3. The $g_{\|}$-values for complexes **(9), (10)** and **(13)** are 2.274, 2.282, 2.250 respectively; consequentially the

environment is considerably covalent [52,53].The values of $\mathbf{g_{\|}/A_{\|}}$ quotient in the range (105–135 cm^{-1}) are expected for copper complexes within perfectly square based geometry and those higher than 150 cm^{-1} for tetrahedrally distorted complexes. The values for the complexes under investigation are 150.81, 152.96 and 158.63 which indicated that, all complexes are associated with a tetragonally distorted field around the copper(II) [54-56].

CONCLUSION

Copper(II), nicke(II) and cobalt(II) complexes of of (3,3',4,4')-4,4'-(1,4-phenylenebis(azan-1-yl-1-ylidene))bis(3-(hydroxyimino)pentan-2-one) have been prepared by direct and template methods. The prepared compounds have been synthesized and identified by elemental analyses, molar conductivities, spectral (UV-Vis, IR, ^{1}H NMR, ^{13}C NMR, mass) as well as magnetic moment measurements technique. The analytical data showed that, the complexes are formed in molar ratio (2Ligand:2Metal) or (1Ligand:2Metal). The spectral data showed that the ligand behaves as neutral tetradentate or dibasic tetradentate ligand bonded to the metal ions through all C=N and protonated or deprotonated oximato groups (C=N-O). The electronic spectra (UV-Vis) magnetic moment measurements showed that the complexes have octahedral geometry. The ESR spectra of solid copper(II) complexes (9), (10) and (13) is characteristic to d^9 configuration and having an axial symmetry type of a d_{x2-y2} ground state with a covalent bond character. The ESR confirmed that the copper complexes have tetragonally distorted octahedral geometry.

REFERENCES

[1] Thomas, T.W.; Underhill, A.E. *Chem. Soc. Rev.* 1972, *1*, 99.

[2] Pekacar, A.I.; Ozcan, E. *Macromolecular Reports A* 1995, *32*, 1161.

[3] EI-Tabl, A.S.; Plass, W.; Buchholz, A.; Shakdofa, M.M.E. *J. Chemical Research* 2009, 582.

[4] Plass, W.; EI-Tabl, A.S.; Buchholz, A. *J. Coord. Chem.* 2009, *62*, 358.

[5] Puntel, G.O.; de Carvalho, N.R.; Gubert, P.; Palma, A.S.; Corte, C.L.D.; Âvila, D.S.; Pereira, M.E.; Carratu, V.S.; Bresolin, L.; da Rocha, J.B.T.; Soares, F.A.A. *Chemico-Biological Interactions* 2009, *177*, 153.

[6] Maity, D.; Chattopadhyay, S.; Ghosh, A.; Drew, M.G.B.; Mukhopadhyay, G. *Polyhedron* 2009, *28*, 812.

[7] Jeffery, G.H.; Bassett, J.; Mendham, J.; Dennney, R.C. (Eds.), *Vogel's Textbook of Quantitative Chemical Analysis*, 5th Ed., Longman Group UK Limited, 1989.

[8] Ray, M.S.; Mukhopadhyay, G.; Bhattacharya, R.; Chaudhuri, S.; Righi, L.; Bocelli, G.; Ghosh, A. *Polyhedron* 2003, *22*, 617.

[9] Chattopadhyay, S.; Ray, M.S.; Chaudhuri, S.; Mukhopadhyay, G.; Bocelli, G.; Cantoni, A.; Ghosh, A. *Inorg. Chim. Acta* 2006, *359,* 1367.

[10] Ray, M.S.; Ghosh, A.; Bhattacharya, R.; Mukhopadhyay, G.; Drew, M.G.B.; Ribas, J. *Dalton Trans.* 2004, 252.

[11] Ray, M.S.; Mukhopadhyay, G.; Drew, M.G.B.; Lu, T.-H.; Chaudhuri, S.; Ghosh, A. *Inorg. Chem. Commun.* 2003, *6*, 961.

[12] Ray, M.S.; Ghosh, A.; Chaudhuri, S.; Drew, M.G.B.; Ribas, J. *Eur. J. Inorg. Chem.* 2004, *15*, 3110.
[13] Seleem, H.S.; El-Inany, G.A.; Mousa, M.; Hanafy, F.I. *Spectrochim. Acta Part A* 2010, *75*, 1446.
[14] Svehla, G. "Vogel's textbook of macro and semi micro Quantitative inorganic analysis" fifth Ed. Longman Inc. New York 1979.
[15] Welcher, F.J. "The Analytical Use of EDTA" Van Norstrand, USA, 1958.
[16] Vogel, A.I. "A Text Book of Quantitative Inorganic Analysis" 4th ed., Longmans, London, 1978.
[17] Holzbecher, Z.; Divis, L.; Kral, M.; Sucha, L.; Vracil, F. "Handbook of Organic Reagents in Inorganic Analysis" Wiley, Chichester, 1976.
[18] Lewis, L.; Wilkins, R.G. "Modern Coordination Chemistry" Interscience, New York, P. 1960, 403.
[19] M. M Ali and F. A. El-said, J. Inorg. Nucl. Chem., 43, 287(1981).
[20] Geaey, W. J.; *Coord. Chem. Rev.,* 1970, *7*, 81.
[21] Greenwood, N. N.; Straughan, B. P.; Wilson, A. E. J. Chem. Soc. A, 1968, 2209.
[22] Tas, E.; Ulusoy, M.; Guler, M.; Yilmaz, L.; *Trans. Met. Chem.,* 2004*, 29*, 180.
[23] El-Behery, M.; El-Twigry, H. *Spectrochim. Acta Part A* 2007, *66*, 28.
[24] El-Tabl, A.S.; *Trans. Met. Chem.,* 1997, *22*, 400.
[25] Nakatamato, K. "Infrared Spectra of Inorganic and Coordination Compounds" 2nd Edit., Wiley Inc. New York, 1967.
[26] El-Wahab, Z.H.A.; Mashaly, M.M.; Salman, A.A.; El-Shetary, B.A.; Faheim, A.A. *Spectrochim. Acta Part A* 2004, *60,* 2861.
[27] El-Tabl, A.S.; Imam, S.M. *Trans. Met. Chem.,* 1997, *22*, 259.
[28] Youssef, N.S.; El-Zahany, E.; El-Seidy, A.M.A.; Caselli, A.; Cenini, S. *J. Mol. Catal. A: Chem.* 2009, 308, 159.
[29] Cukurovali, A.; Yilmaz, I.; Kirbag, S. *Trans. Met. Chem.,* 2006, 31, 207.
[30] Tossidis, A.; Bolos, C.A. *Inorg. Chim. Acta* 1986, 112, 93.
[31] Murukan, B.; Mohanan, K.; *Trans. Met. Chem.* 2006, *31*, 441.
[32] Patel, R.N.; Gundla,V.L.N.; Patel, D.K. *Polyhedron,* 2008, *27*, 1054.
[33] Nakarnota, K. "Infrared and Raman Spectra of Inorganic and coordination compounds", Wiley Interscience, New York, 1986.
[34] Boghaei, D.M.; Gharagozlou, M. *Spectrochim. Acta part A,* 2007, *67*, 944.
[35] El-Shazly, R.M.; Al-Hazmi, G.A.A.; Ghazy, S.E.; El-Shahawi, M.S.; El-Asmy, A.A. *Spectrochim. Acta Part A,* 2005, *61*, 243.
[36] Shauib, N.M.; Elassar, A.-Z.A.; El-Dissouky A. *Spectrochim. Acta Part A,* 2006, *63*, 714.
[37] Teotia, M.P.;Gurtu J.N.;Rama, V.B. *J. Inorg. Nucl. Chern*.,1980, 42, 821-831.
[38] Gudasi, K.B.; Patil, M.S.; Vadavi, R.S.; Shenoy, R.V.; Patil, S.A.; Nethaji, M. *Trans. Met. Chem.,* 2006, *31*, 580.
[39] Thakkar, N.V.; Bootwala, S. Z. *Indian J. Chem.,* 1995*, 34A*, 370.
[40] Lever, A.B.P. "*Inorganic Electronic Spectroscopy*" 2nd edn, Elsevier, Amsterdam, 1984.
[41] El-Tabl, A.S.; El-Enein, S.A. *J. Coord. Chem.* 2004*, 57*, 281.
[42] Mondal, N.; Dey, D.K.; Mitra, S.; Malik, K.M.A. *Polyhedron* 2000, *19*, 2707.
[43] Mohamed, G.G.; El-Gamel, N.E.A. *Spectrochim. Acta, Part A* 2004, *60*, 3141.

[44] Youssef, N.S.; El-Zahany E.; El-Seidy, A.M.A. *Phosphorus, Sulfur Silicon Relat. Elem.* 2010, *185*, 785.
[45] Singh, K.; Barwa, M.S.; Tyagi, P. *Eur. J. Med. Chem.* 2006, *41,* 147.
[46] Chandra, S.; Gupta, L.K. *Spectrochim. Acta Part A* 2005, *61*, 1181.
[47] Gudasi, K.B.; Vadavi, R.S.;S henoy, R.V.; Patil, S.A.; Nethaji, M. *Trans. Met. Chem.* 2006, *31*, 374.
[48] El-Tabl, A.S. *Bull. Korean Chem. Soc.* 2004, *25,* 1757.
[49] Hathaway, B.J.; Billing, D.E. *Coord. Chem. Rev.* 1970, *5*, 143.
[50] El-Tabl, A.S. *Trans. Met. Chem.* 2002, *27*, 166.
[51] El-Tabl, A.S. *Trans. Met. Chem.* 1998, *23*, 63.
[52] Ray, R.K.; Kauffman, G.B. *Inorg. Chim. Acta* 1990, *174*, 237.
[53] Ray, R.K.; Kauffman, G.B. *Inorg. Chim.Acta* 1990, *174*, 257.
[54] Sakaguchi, U.; Addison, A. W. *J. Chem. Soc., Dalton Trans.* 1979, 600.
[55] Massacesi, M.; Ponticelii, G.; Devoto, G.; Micera G.; Piu, P. *Trans. Met. Chem.* 1984, *9*, 362.
[56] El-Tabl, A.S.; Shakdofa, M.M.E.; El-Seidy, A.M.A. *J. Korean Chem. Soc.* 2011, *55*, 603.

Smart Nanocomposites
Volume 2, Number 2
ISSN: 1949-4823

SYNTHESIS AND SPECTROSCOPIC CHARACTERIZATION OF NICKEL(II), COBALT(II) AND COPPER(II) COMPLEXES OF DIOXIME LIGANDS

Abdou S. El-Tabl[1*], Mohamed M. E. Shakdofa[2,3], and Ahmed M. A. El-Seidy[2]

[1]Department of Chemistry, Faculty of Science,
Menoufia University, Shebin El-Kom, Egypt
[2]Inorganic Chemistry Department,
National Research Center, Cairo, Egypt
[3]Department of Chemistry, Faculty of Science and Arts,
Khulais, King Abdulaziz University, Saudi Arabia

ABSTRACT

Nickel(II), cobalt(II) and copper(II) complexes of dibasic ligands with two oxime groups have been synthesized and characterized by elemental analyses, molar conductance, magnetic moments, IR, UV-Vis. spectra, DTA, mass spectra, ^{1}H- and ^{13}C-NMR and ESR measurements. IR spectra showed that, the ligands behaved as dibasic ligands. Ni(II), d^8 complex was exposed to ^{60}Co-γ rays at 77 K using a 0.2217 M. rad. H^{-1} Vicrad source to give Ni(I), d^9, with a d_{x2-y2} ground state. Annealing the complex above 77 K led to the formation of a low spin Ni(III), d^7 system with d_{z2} orbital. However, copper(II) complexes showed an axial type symmetry with a d_{x2-y2} ground state. The suggested structures of the ligands and their metal complexes are in accordance with analytical, spectral and magnetic moment data.

Keywords: Oxime, nickel(II), cobalt(II), copper(II), isonitrosoacetylacetone, ^{60}Co-γ-rays on metal complexes, Ni(I)

INTRODUCTION

During the last decade, metal complexes containing oxime group have received much attention [1,2], due to their biological activity mainly because of the need to gain insight into

* E-mail: asaeltabl@yahoo.com

the electron transfer pathway in biological systems [3,4] and to obtain useful information concerning the design of molecule-based magnets [5]. Metal complexes of oxime ligands have been examined as compounds with columnar stacking, which is thought to be the reason for their semiconducting properties [6], and as model compounds which mimic bio-functions such as the reduction of vitamin B12 [7]. Metal complexes of multifunctional triaminoxime have been prepared and spectrally characterized. The ligand and its metal complexes showed significant biological activity [8]. Also, metal complexes of Benzedrine diacetyloxime and its metal complexes were described [9]. Transition metal complexes of either α-dioxime [10] or vicinal oxime-imine ligands [11] have revealed several interesting aspects. One is related to the ability of the oximato group to coordinate to the metal ion through either the oximino-oxygen or the oximino-nitrogen atoms. The bioactivity indicated by oximes and their metal complexes was related to the coordination mode of the oxime sites [12,13] as well as to the bridging capacity of the coordinated oximato group to transition metal ion [14]. The aim of this paper is to prepare and characterize Ni(II), Co(II) and Cu(II) complexes of 4,4'-(propane-1,3-diylbis(azan-1-yl-1-ylidene)) bis(3-(hydroxyimino)pentan-2-one) and 4,4'-(butane-1,4-diylbis (azan-1-yl-1-ylidene))bis (3-(hydr-oxylimino) pentan-2-one) and to investigate the ESR and spectral data in connection with their structures. This kind of investigation seems to be important for the structural estimation of various other metal complexes and the metal binding sites of various metaloenzymes [15].

EXPERIMENTAL

Chemicals used were of reagent grade and were used without further purification. The elemental analysis for C, H and N were determined at the analytical unit of Cairo University, Egypt**.** Standard analytical methods were used to determine the metal ion content [16]. The IR spectra of the ligand and complexes were measured using KBr discs on a Perken Elmer 681 spectrophotometer. The Uv-Visble spectra in the 200-900 nm regions were recorded on a Perkin-Elmer 550 spectrophotometer. ^{1}H- and ^{13}C-NMR spectra were recorded on Brucker AM 300-NMR spectrometers. Chemical shifts (ppm) are reported relative to TMS. The mass spectra of the complexes were recorded on micro-mass 16B mass spectrometer. Magnetic susceptibilities were measured at 25^{o}C by the Gouy method using mercuric tetrathiocyanato-cobaltate(II) as the magnetic susceptibility standard. Diamagnetic corrections were estimated from Pascal's constant [17]. All ESR measurements throughout (77-300 K) were carried out using a Varian E-109 X-band spectrometer (Leicester University, England).. Samples were irradiated in a Vickrad ^{60}Co-source at room or 77 K. dose rate of about 0.22 M rad h-1. TLC was used to test the purity of the compounds.

1.1. Preparation of Ni(II), Co(II) and Cu(II) Complexes of 4,4'-(Propane-1,3-Diylbis(Azan-1-Yl-1-Ylidene))Bis(3-(Hydroxyimino)Pentan-2-One) (1, 2 and 3)

Many attempts were made to prepare the Schiff-base 4,4'-(propane-1,3-diylbis(azan-1-yl-1-ylidene))bis(3-(hydroxyimino)pentan-2-one) but unfortunately, this was unsuccessful. However, the metal complexes (1, 2 and 3) were prepared by template method. The methanol

solution of Ni(II) acetate tetrahydrate, Co(II) acetate tetrahydrate or Cu(II) acetate monohydrate (19.3 X 10^{-3} mol, 50 cm^3) was added while stirring to a solution (50 cm^3) containing an equimolar concentration of the methanol solution of 1,3-diaminopropane. The solution of isonitrosoacetylacetone (5.0 g, 38.7 X 10^{-3} mol.) in ethanol was added to the warmed solution of metal acetate and 1,3-diaminopropane. The stirred reaction solution was refluxed for 2 hours and the complexes formed was filtered off, washed several times with warm ethanol and dried under vacuum in presence of P_2O_5. The analytical, Table 1 and spectral data Tables 2 and 3 are compatible with the suggested structures. The structure was formulated as shown in Figure 1.

[M(L^1)X]
complex (1):M= Ni(II), X=none
complex (2):M= Co(II), X=H_2O
complex (3):M= Cu(II), X=none

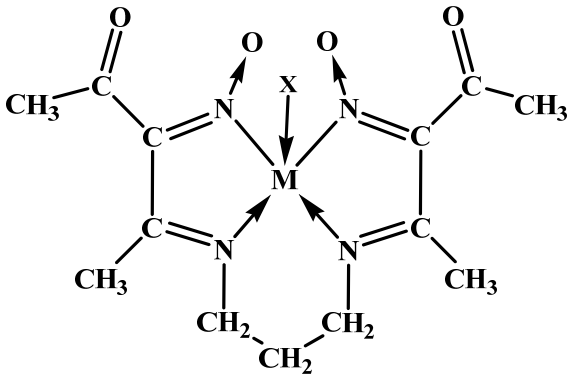

Figure 1. Structure representation of the Ni(II), Co(II) and Cu(II) complexes of 4,4'-(propane-1,3-diylbis(azan-1-yl-1-ylidene))bis(3-(hydroxyimino)pentan-2-one.

1.2. Preparation of 4,4'-(Butane-1,4-Diylbis(Azan-1-Yl-1-Ylidene))Bis (3-(Hydroxyimino)Penta N-2-One) Ligand (H_2L^2) (4)

The ligand, **4** was prepared by the published method form the 2:1 molar ratio reaction of 3-(hydroxyimino)pentane-2,4-dione with 1,4-diaminobutane [18]. The ethanolic solution of 1,4 diaminobutane (2.3 ml, 0.033 mol, 30 cm^3) was added dropwise to a solution of 3-(hydroxyimino) pentane-2,4-dione (6.0 g, 0.047 mol, 50 cm^3) in the same solvent. The reaction solution was refluxed for 2 hours and left to cool to precipitate the ligand. The precipitate was filtered off, washed with warm ethanol and dried. The ligand was crystallized from ethanol (m.p.= 210^oC).

1.3. Preparation of Ni(II), Co(II) And Cu(II) of 4,4'-(Butane-1,4-Diylbis(Azan-1-Yl-1-Ylidene)) Bis(3-(Hydroxyimino)Pentan-2-One) (5, 6 And 7)

a) Normal Method

An aqueous solution of $(CH_3CO_2)_2Ni.4H_2O$, (0.83 g 0.003 mol, 100 cm^3), $(CH_3CO_2)_2Co.4H_2O$ (0.83 g. 3.2 X 10^{-3} mol, 100 cm^3) or $(CH_3CO_2)_2Cu.H_2O$ (0.61 g, 0.5 X 10^{-2} mol, 100 cm^3) were added to the suspension of the equimolar concentration of the ligand in the same solvent (100 cm^3). The reaction mixture was warmed while stirring for 3 hours.

The prepared complexes were filtered off, washed several times with water and dried under vacuum in presence of P_2O_5.

Table 1. Analytical and some physical Characteristics for the compounds

No.	Compound	Color	M. Wt.	Calcd (Found)		Yeild		
				C	H	N	M	(%)
1	$[Ni(L^1)]$	Red	353.0	44.53(44.23)	5.61(5.14)	16.21(15.86)	16.82(16.63)	62
2	$[Co(L^1)(H_2O)]$	Orange	371.3	42.31(42.06)	5.51(5.39)	14.80(15.08)	16.00(15.87)	59
3	$[Cu(L^1)]$	Brown	357.0	41.87(41.58)	5.41(5.32)	14.72(14.91)	16.53(16.80)	56
4	H_2L^2	Yellow	310.4	54.31(54.18)	6.92(7.11)	17.95(18.04)	-	87
5	$[Ni(L^2)]$	Green	367.0	45.81(45.74)	5.49(5.54)	15.27(15.35)	15.99(15.89)	72
6	$[Co(L^2)(H_2O)]$	Orange	407.9	43.26(43.67)	5.12(5.23)	14.23(14.54)	14.95(15.29)	68
7	$[Cu(L^2)(H_2O)_2]$	Green	385.3	37.52(37.90)	4.70(4.54)	12.25(12.62)	14.48(14.26)	67

Table 2. IR spectral assignment for the compounds (in cm^{-1})

No.	**Compound**	**υ(OH)**	**υ(OH)**	**υ(C=O)**	**υ(C=N)**	**$\upsilon(C=N)_{N\text{-}Coord}$**	**υ(N-O)**	**υ(M-L)**
1	$[Ni(L^1)]$	-	-	1650s	1608s	1570m	1163s	660m
2	$[Co(L^1)(H_2O)]$	3450 br	-	1675s,1660s, 1655s	1585s, 1570m	1535m,1520m	1183m, 1175m	680m
3	$[Cu(L^1)]$	-	-	1660s	1618s	1570m	1165s	630m
4	H_2L^2	-	2700-2100br	1690s,1668s, 1660s	1640s	-	1063s, 1025m	-
5	$[Ni(L^2)]$	-	-	1665s	1615s	1580s	1168s	655m
6	$[Co(L^2)(H_2O)]$	3440 br	-	1665s	1583s	1535m,1520m	1187m, 1175m	675m
7	$[Cu(L^2)(H_2O)_2]$	3455 br	-	1670s	1616s	1565m,1551m	1155m, 1148m	650m

The same nickel(II) complex was obtained when the reaction was carried out in water / ethanol (9:1). The same cobalt(II) complex was obtained when the reaction was carried out in ethanol.

b) Template Method

The methanol solution of Ni(II) acetate tetrahydrate, Co(II) acetate tetrahydrate or Cu(II) acetate monohydrate (1.9×10^{-2} mol, 50 cm^3) was added while stirring to the ethanol solution (50 cm^3) containing an equimolar concentration of 1,4-diaminobutane. The solution of 3-(hydroxyimino) pentane-2,4-dione (5.0 g, 3.8×10^{-2} mol) in ethanol was added to the warmed solution of the metal(II) and the 1,4-diamine. The stirred reaction was refluxed for 2 hours. The complexes produced were filtered off, washed several times with warm ethanol and dried. These complexes were identified as complexes **5, 6, 7** and comparing their elemental analyses, electronic and vibrational spectra with those of complexes **5, 6, 7** which prepared by normal method.

Table 3. The Uv-Visble spectra and magnetic moments for the compounds

No.	Ligand / Complexes	Nujol mull[a]	$CHCl_3$[a]	μ_{eff}(B.M.)
1	$[Ni(L^1)]$	507, 464, 335	498, 460, 342	-
2	$[Co(L^1)(H_2O)]$	535, 460, 402	510, 420, 345	2.12
3	$[Cu(L^1)]$	495, 455, 370	420, 330	1.53
4	H_2L^2	Ethanol 320 ($\varepsilon = 1.8 \times 10^3$ mol cm^{-1})		-
5	$[Ni(L^2)(H_2O)_2]$	510, 450	505, 440	-
6	$[Co(L^2)(H_2O)]$	535, 508, 490, 410	515, 455, 335	2.4
7	$[Cu(L^2)(H_2O)_2]$	590, 485, 390	420, 330	1.6

[a] in cm^{-1}.

RESULTS AND DISCUSSION

2.1. Characterization of Ni(II), Co(II) and Cu(II) Complexes of 4,4'-(Propane-1,3-Diylbis(Azan-1-Yl-1-Ylidene))Bis(3-(Hydroxyimino) Pentan-2-One

a) Nickel(II) Complex (1)

The IR spectrum of Ni(II) complex **(1)** revealed the presence of υ(C=O) at 1650 $cm^{-1,}$ this vibration is located in the 1670-1630 cm^{-1} region of the carbonyl group attached to a five-membered chelate ring in the vicinal oxime-imino complexes of Ni(II) [11,13,19]. It is suggested, therefore, that the chelate rings in complex **(1)** is of five-membered type which requires the oximato group to be coordinated to the metal ion through the oximino nitrogen. The observed υ(N-O) in this complex is located at a higher frequency (1163 cm^{-1}) as compared to that of the isonitroso O-bonded ligand [11,20]. This accords with the suggested structure of complex **(1)** since coordination by the oximino nitrogen will produce an N-O bond with a greater double- bond character and consequently a higher υ(N-O) than is the case with oximino-oxygen coordination of less double-bond character for the N-O bond and a lower υ(N-O). The coordination of the imino-nitrogen is shown at (1608 cm^{-1}). The lower frequency band at 1570 cm^{-1} is associated with υ(C=N) of the N-coordination oximato groups. The location of this band is identical with that reported for the Ni(II) complexes of camphorquinone dioxime ligand [10]. The absence of other υ(C=N) bands in this region suggests that both oximato groups have the same N-coordination mode. The presence of a single band at 1163 cm^{-1} is compatible with this conclusion. The complex found to be diamagnetic which is in agreement with square-planar geometry [21]. The electronic spectrum of this complex displays three bands at 507, 464 and 335 nm. These spectral bands may be assigned to the transition $A_1 \leftarrow B_1$, $A_1+B_2 \leftarrow B_1$ and $B_2 \leftarrow B_1$ respectively, in a square-planar geometry [22]. The Ni(II) complex **(1)** is diamagnetic,d^8, hence ESR spectroscopy has

not been applied to the study of its electronic structure. In order to overcome this, the complex was exposed to ionizing radiation to form electron-gain and electron-loss species amenable to be studded by ESR spectroscopy. The Ni(II) complex **(1)** was studied as a frozen solution in CD_3OD+D_2O (10%) in liquid nitrogen in the form of small beads. The sample was exposed to ^{60}Co γ-rays at 77K using a 0.2217 M.rad.h^{-1} Vicrad source for periods up to 3 h. Addition of an electron to the d^8 electronic configuration of the Ni(II) ion resulted in the formation of a d^9, Ni(II) complex. The only signal detected from the spectrum is the $g_{\|}$ feature in the low field region as shown in Figure 2, $g_{\|}$ =2.15 (Figure 2-A).

In addition, free radical signal of the solvent was observed at ≈2.0. The sample was annealed above 77 K by decanting the liquid nitrogen from the Dewar flask and continuously monitoring the ESR spectra. Whenever significant changes were observed, the sample was recooled to 77 K for studying.

The analysis of the spectrum at 77K showed a shift of $g_{\|}$ (A) to 2.137 (B) and new features were observed (C) and (D). The species (C) was not identified. The ESR values of the new feature (D) showed axial symmetry with $g_{\perp} > g_{\|} > 2.0$, and the value of g considerably greater than 2.0. This observation is consistent with the existence of a low-spin Ni(III), d^7, system with the unpaired electron in the d_{z2} orbital [23-26]. The g-values are $g_{\|}$ (=2.05) and $g_{\perp}$ (=2.10) as shown in Figure 2. The Ni(III) species was formed by the reaction of Ni(II) complex **(1)** with solvent radicals, e.g.

$$(Ni^{2+})L + {}^{\cdot}OH \rightarrow (Ni^{3+})L + {}^{-}OH$$

$$(Ni^{2+})L + R^{\cdot} \rightarrow (R)^{-} (Ni^{3+})L$$

The ESR spectrum of a polycrystalline sample of the same complex was recorded at room temperature and at 77K after exposure to ^{60}Co γ-rays from a Vickrad source at a dose rate of ca. 0.2217 M rad h^{-1} for periods up to ca. 4h. It exhibited an axial symmetry with $g_{\|} > g_{\perp} > 2.0$, the signal intensity observed was weekend. However, at 77K the ESR spectrum it showed an axial symmetry type with the following ESR parameters $g_{\perp}$ (=2.042), $g_{\|}$ (=2.15) as shown in Figure 3. The values $g_{\|} > g_{\perp} > 2.04$ suggested a d_{x2-y2} ground state, characteristics of an essentially square-planar geometry.

These complexes were remarkable that, the geometry was not affected by the oxidation-reduction processes and one can obtain planar complexes containing the nickel ion with different oxidation states.

The mass spectra of the Ni(II) complex is consistent with the proposed structure. The suggested mechanism of the fragmentation of this complex is shown in Figure 4.

The ^{1}H-NMR spectrum of the Ni(II) complex **(1)** consists of six distinct regions with resonances attributable to different groups. A sharp singlet resonance at 2.27 ppm corresponds to the protons of methyl groups in the acetyl groups and those at 2.38 and 2.52 ppm are due to the protons of methyl groups attached to imino-groups.

The two methylene groups adjacent to imino-nitrogen groups give rise to peaks at 3.25 and 3.47 ppm showing a spin triplet (coupling with (C-CH_2-C).

The resonance due to methylene group protons (C-CH_2-C) of the propyl arm appears at 2.07 ppm as a multiplet (coupling with methylene groups-attached to imino-nitrogen groups)

[27]. The ^{13}C-NMR spectrum contains thirteen lines of comparable intensities, six between 150 and 200 ppm and the remaining seven in the aliphatic region between 10 and 60 ppm.

These facts permit the conclusion that the complex has thirteen types of carbon nuclei. The presence of four single CH_3 lines indicate the non-equivalence of four methyl groups and also three CH_2 lines indicate non-equivalence of three methylene groups.

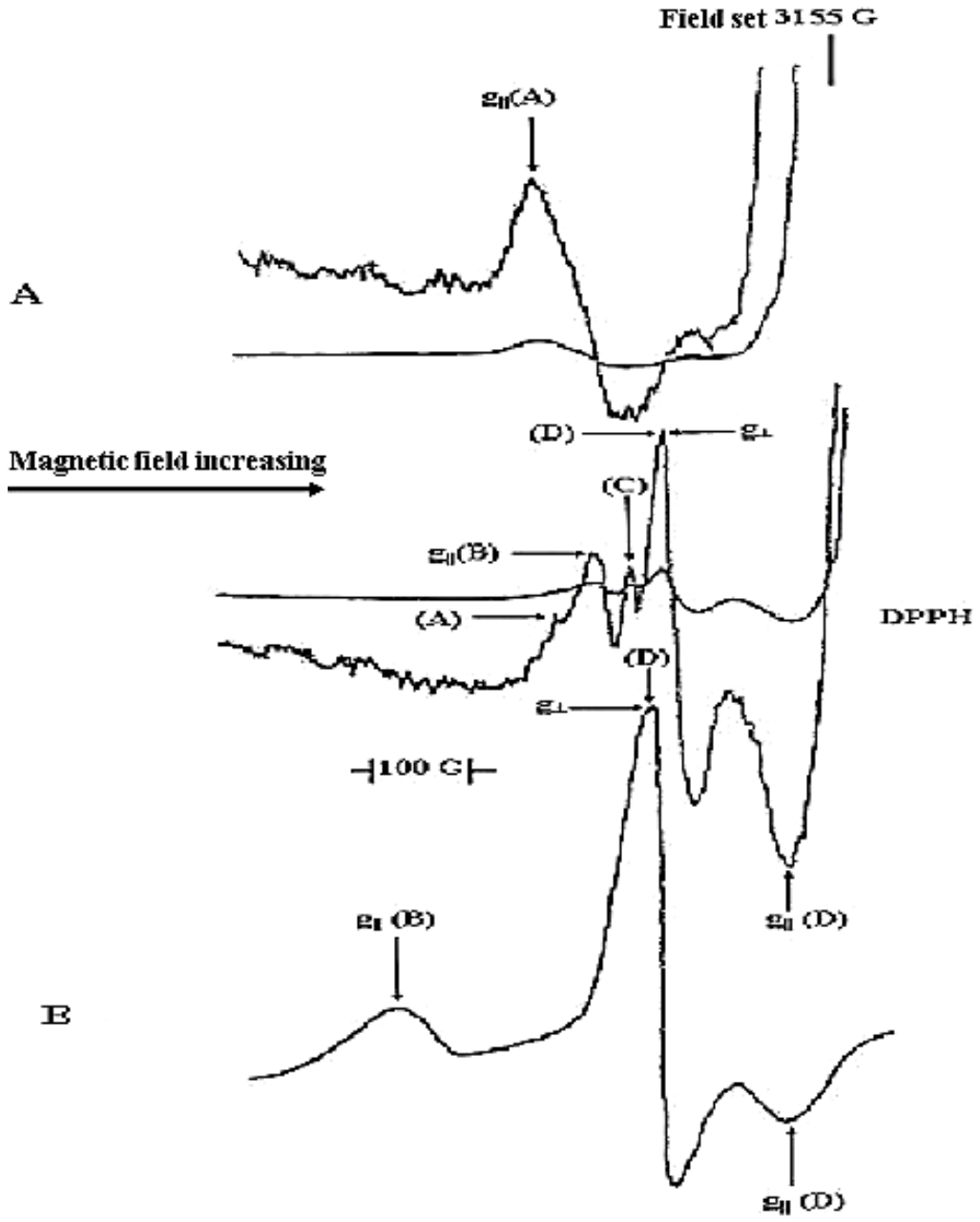

Figure 2. (A) The ESR spectrum of the Ni(II) complex (1) in CD_3OD +D_2O(10%) at 77 k (B) Simulated spectrum of the Ni(II) complex (1).

The peaks at 18.11 and 20.48 ppm are assigned to the methyl of the acetyl groups and those at 28.27 and 28.45 ppm to the methyl groups adjacent to imino-nitrogen groups.

Three peaks at 32.2, 47.55 and 50.81 ppm were observed for two methylene groups adjacent to the nitrogen atoms of the imino-groups CH_2—N=C and the methylene group C-CH_2-C of the propyl arm respectively. Peaks at 152.91 and 152.97 ppm very close to each other correspond to the carbon of imino-nitrogen groups. Carbon atoms of the carbonyl groups give rise to peaks at 157.08 and 176.28 ppm [28].

The other two features at 191.96 and 198.44 ppm could arise from the carbon atoms of the oxime groups. For the monomer species, seven lines were expected corresponding to the carbon nuclei, but thirteen lines were observed. This means that, the complex could exist in a dimeric form.

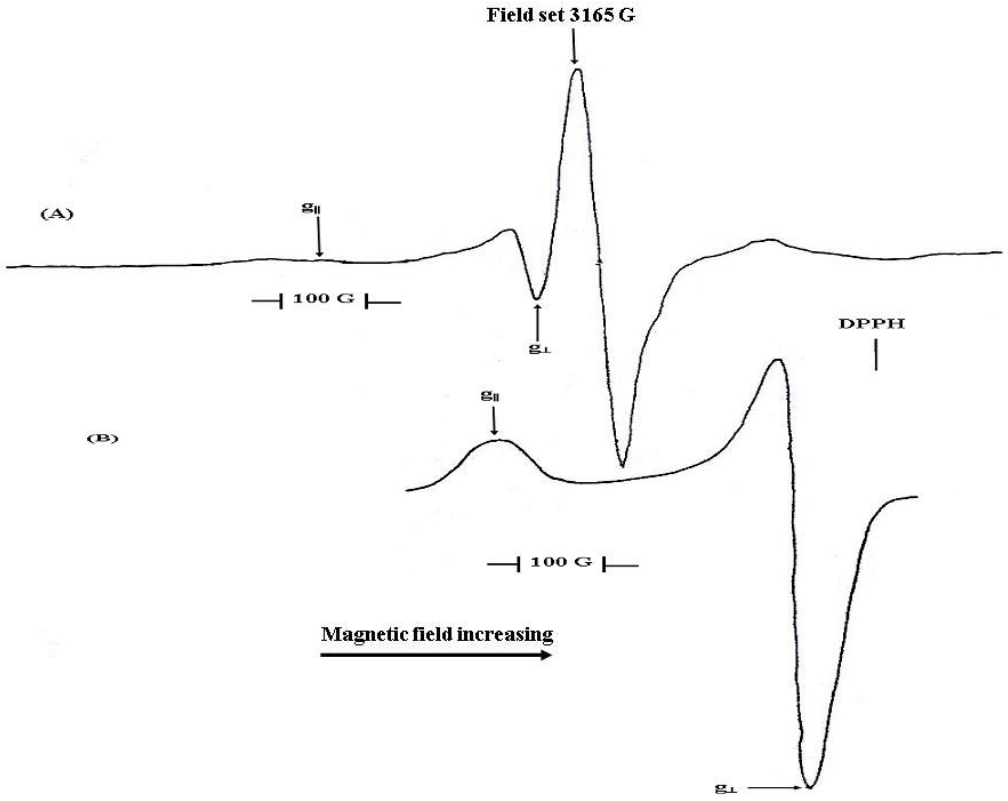

Figure 3. (A). the ESR spectrum of the polycrystalline Ni complex (1) at 77 k (B) Simulated spectrum of the Ni(II) complex (1).

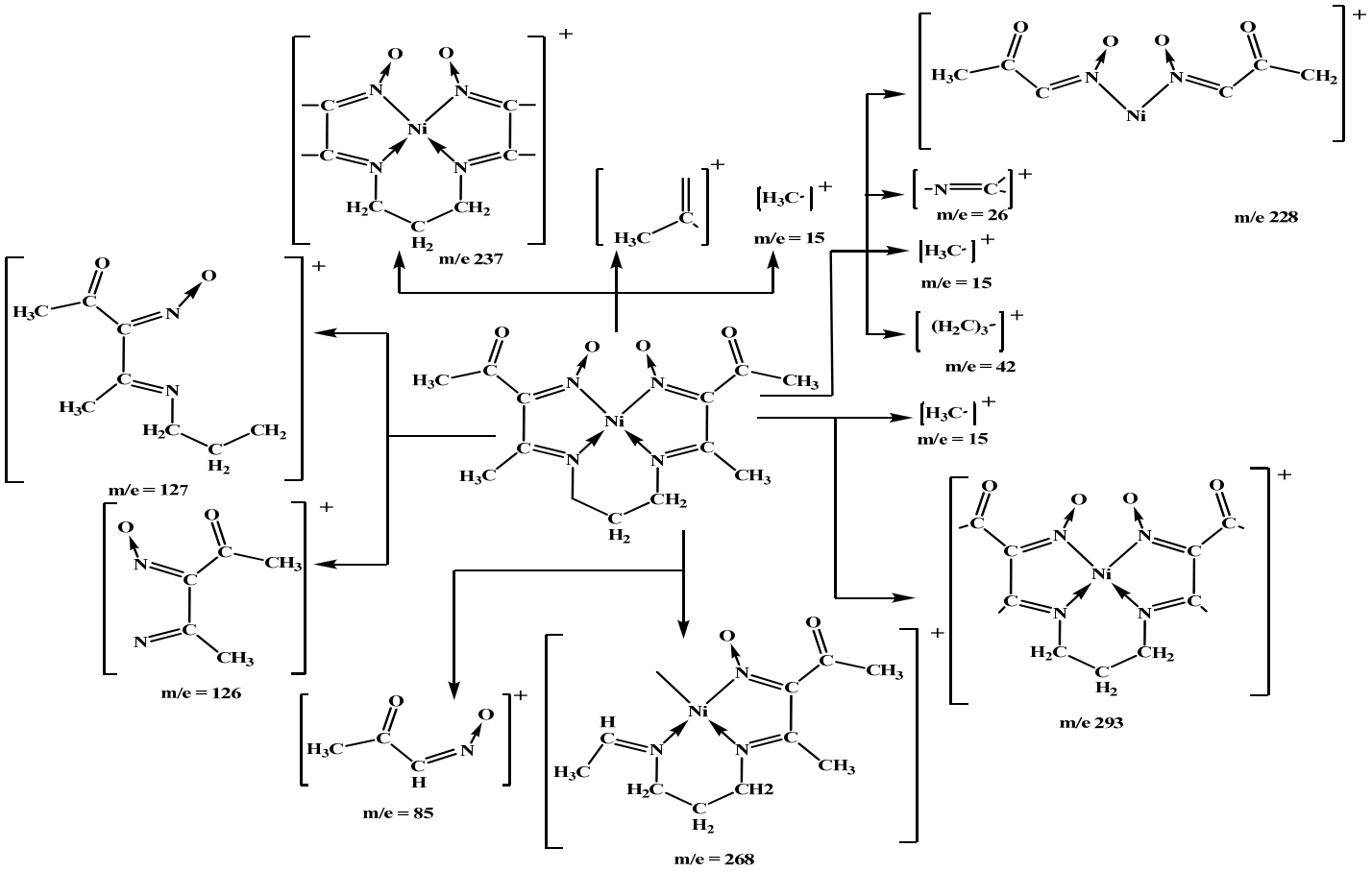

Figure 4. The Suggested mechanism of the fragmentation of Ni(II) complex 1.

b) Cobalt(II) Complex (2)

The suggested structure of Co(II) complex (2) is based on the presence of carbonyl groups in the 1675-1630 cm^{-1} region which was tentatively associated with N-coordination of the oximato group in complexes of vicinal oxime-imine ligands [29,30]. Moreover, the presence of υ(N-O) at higher frequency (1175 and 1183 cm^{-1}). This band is in agreement with N-coordination of the oximato group, since N-coordination by this group would produce an N-O bond with higher double bond character (higher-υ(N-O) vibration) than the N-O bond of the O-coordination oximato group (lower υ(N-O) ,two υ(C=N)) bands at 1535 and 1520 cm^{-1} were assigned to the two non-equivalent N-coordination oximato groups.

The latter vibration was not observed from IR spectrum of the complex in chloroform solution which became identical. The υ(C=N) of the imino-nitrogen coordination appeared at 1585 cm^{-1}. The five-membered chelate ring in this complex appears to be stabilized by the hydrogen bonding of the oxime group with the coordinated water molecule. The broad υ(O-H) at 3650-3150 cm^{-1} provides evidence for this [31]. The splitting of the υ(N-O) to two bands indicates non-equivalence of the N-O bond. This could be interpreted in terms of H-bonding of the water molecule to one oxygen atom of the N-coordinated oxime leaving the other oxygen unsatisfied. The splitting of υ(C=O) in the solid state to several bands is consistent with the steric crowding condition which is a consequence of molecule association. However, in chloroform, sharp single band at 1675 cm^{-1} was observed.

This complex could be square pyramidal in the chloroform solution and molecular association takes place in the solid state [30] as shown in figure 1. The magnetic moment of this complex was found to be 2.12 B.M. indicating low-spin cobalt(II). The low magnetic moment of this complex may be due to molecular association in the solid state [30] and spin-spin interaction is operative.

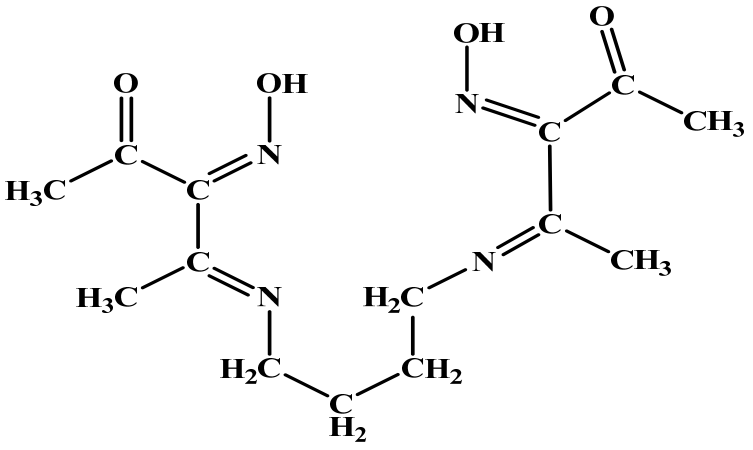

H_2L^2

4,4'-(butane-1,4-diylbis(azan-1-yl-1-ylidene))bis(3-(hydroxyimino)pentan-2-one)

Figure 5. Structure representation of the ligand (4) (H_2L^2).

The electronic spectrum of this complex in chloroform shows bands at 510, 420 and 345 nm. These features are similar to penta-coordinated of Co(II) which correspond to $^1A_2 \leftarrow {}^1A_1$, $^1E_2 \leftarrow {}^1A_1$ and $^1E \leftarrow {}^1A_1$, whereas, in the solid state, the molecular association lowers the symmetries and explain the splitting of ^1E energy level.

Attempts were made to study the ESR spectrum of this complex in different solvents as frozen solutions at different temperatures, but no ESR spectra were observed at 77K or above. This could be due to the formation of a dimeric species in solution [32]. Also in the case of the polycrystalline form at room temperature and 77K, no ESR spectra were observed. The broad band at 3450 cm^{-1} was due to coordinated water or water of crystallization. The presence of water molecules within the coordination sphere in this complex were supported by the presence of bands at 3450 cm^{-1}, 1608 cm^{-1}, 950 cm^{-1} and 630 cm^{-1} due to OH stretching, HOH deformation, H_2O rocking and H_2O wagging, respectively [33].

c) Copper(II) Complex 3

The suggested structure of Cu(II) complex **(3)** showed that the N-atom of oximato groups are coordinated to the Cu(II) ion. N-coordination of both of the oximato groups is proven by the presence of υ(N—O) at 1165 cm^{-1} whereas the higher frequency band at 1618 cm^{-1} is assigned to the υ(C=N) of the coordinated imino-nitrogen. These assignments are consistent with those reported for the Cu(II) complexes of the dioximato ligands like dimethylglyoxime [34] and cyclohexanedione dioxime [35]. The presence of a broad band in the 3650-3560 cm^{-1} is due to uncoordinated water molecules [31]. The carbonyl band υ(C=O) of this complex was located at a lower frequency (1660 cm^{-1}) to that in complex **(1)**. This means, the oximato group must be coordinated to the metal ion through the oximino nitrogen. The magnetic moment of this complex in the solid state is 1.53 B.M. which is observed to be lower than the spin-only value for copper indicating spin-exchange interactions take place in the solid state [36]. The ESR spectrum of this complex in methanol at 77K is axial with a d_{x2-y2} ground state. The electronic spectrum of this complex shows three absorption bands at 495,455 and 370 nm due to the transition $^2A_1 \leftarrow {}^2B_1$, $^2B_2 \leftarrow {}^2B_1$ and $^2E \leftarrow {}^2B_1$ respectively [37]. These transitions suggested a distorted square planar structure in the solid state. The water dissociation or the axial distortion in chloroform stabilizes the d_z^2, d_{xy} and d_{yz} and explain the disappearance of the band at 495 nm. The position of the peaks observed from the nujol mull spectra are not identical with those observed from the chloroform solution spectra. Accordingly, it suggested that all these observed bands from the spectra of the metal complexes are related to change of the structure due to the solvolysis.

2.2. Characterization of 4,4'-(Butane-1,4-Diylbis(Azan-1-Yl-1-Ylidene))Bis(3-(Hydroxyimino) Pentan-2-One) (H_2L^2) And Its Ni(II), Co(II) and Cu(II) Complexes (5), (6) and (7)

The IR spectrum of the ligand (H_2L^2) showed the presence of two υ(O-H) bands illustrated the presence of two types of hydrogen bonded oxime groups which could be intra- and inter-molecular hydrogen bonding to the basic imino-nitrogen as well as the oximino-nitrogen which is consistent with earlier findings for other dioxime Schiff-base ligand [38]. Thus, the higher frequency band (3500-3100 cm^{-1}) is associated with a weaker hydrogen bonding compared with the lower frequency band (2700-2100 cm^{-1}) of the relatively stronger

hydrogen bonding. The υ(C=O) band of the ligand (H_2L^2) appears at (1690 cm^{-1}) which in metal complexes is split (1690-1850 cm^{-1}) in a trosoacetylacetone and its derivatives [39,40] and more significantly to the related Schiff-base N,N-ethylene bis-isonitroso-acetylacetoneimine and its complexes [13,29,38]. It is deduced, therefore, that the carbonyl groups of the ligand (H_2L^2) are involved in neither the hydrogen bond formation in the ligand nor the coordination to the metal ion in complexes (5), (6) and (7). The υ(C=N) vibrations (oximes and imine υ(C=N) types) are located at 1655 and 1640 cm^{-1}. Two strong bands at 1063 and 1025 cm^{-1} are assigned to υ (N-O). The υ $(C=N)_{oxime}$ and υ(N-O) vibrations [38]. The splitting of the υ(N-O) vibration to two bands is consistent with the presence of two υ(O-H) bands and confirms the conclusion regarding the presence of two non-equivalent hydrogen bonds formations whereby the intra-molecular type should be stronger than the intermolecular type. The electronic spectrum of the ligand (H_2L^2) in ethanol shows absorption at 320 nm ($\epsilon=1.8\times10^3$ mol cm^{-1}) ascribed to inter-ligand electronic transitions.

The IR spectrum of Ni(II) complex **5** showed the shift of the υ(C=N) band to lower frequency at 1615 cm^{-1} due to the coordination to the metal ion. The band at 1580 cm^{-1} is associated with υ(C=N) of the N-coordinated oximato groups. The location of this band is identical with that reported [13]. The absence of the band characteristic to other υ(C=N) groups in this region suggests that both oximato groups have the same N-coordination mode; this is implied by υ(N-O) band at 1168 cm^{-1}. The presence of a single band in this region is compatible with the conclusion derived from the υ(C=N) band, that both oximato groups are N-coordinated to the Ni(II) ion. The υ(C=O) of this complex was located at 1665 cm^{-1}. This vibration is located in the region of the carbonyl group attached to a five-membered chelated ring in the vicinal oxime-imino complexes of the Ni(II) ion [13]. This complex found to be diamagnetic indicating square planar geometry [42]. The electronic spectrum of this complex exhibits three bands at 510 and 450 Characteristic of square planar diamagnetic Ni(II) complexes (Figure 6) [41].

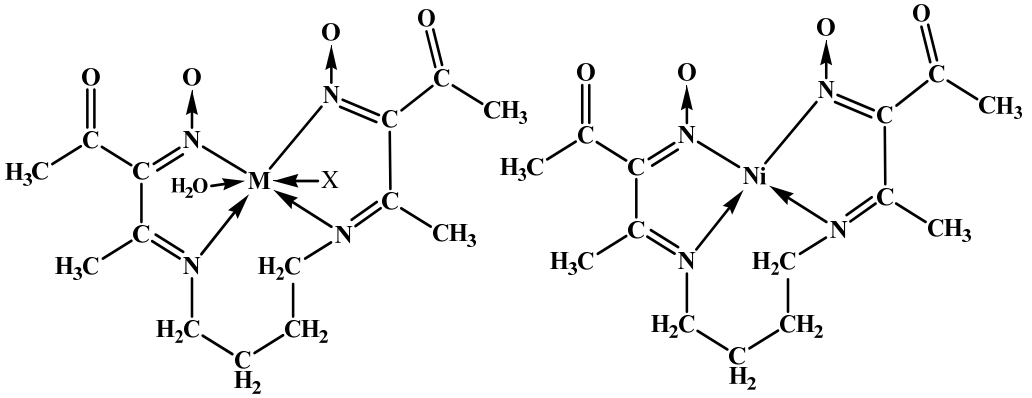

Figure 6. Structure representation of the Ni(II), Co(II) and Cu(II) complexes of 4,4'-(butane-1,4-diylbis(azan-1-yl-1-ylidene))bis(3-(hydroxyimino)pentan-2-one).

The Ni(II) complex **(5)** is diamagnetic hence no ESR spectrum is possible for this complex. In order to generate Ni(I) d^9, the powdered sample was exposed to ^{60}CO γ-rays at 77K using a 0.221 M $radh^{-1}$ vicrad source for periods up to 3h. The complex gives rise to an ESR spectrum with both $g_{\|}$(2.17) and $g_{\perp}$ (2.03) features as shown in Figure 7. This is characteristic of the Ni(I), d^9, system with d_{x2-y2} ground state [26,42,43]. The ESR spectrum of the frozen solution in CD_3OD+ D_2O (10%) was recorded at 77K in the form of small beads after irradiation with ^{60}Co γ-rays for 3h. at 77K. this gave a spectrum similar to that for the powder state. Also, a free radical signal was observed at g ≅ 2.0, and a broad signal was detected in the high field region. The latter could be from impurities of metals having d^1 configuration, but this seems unlikely. The sample was annealed above 77 K by decanting the liquid nitrogen from the Dewar flask and continuously monitoring the spectrum, however, no significant change was observed. If the d^8 species is a dimmer, then probably the d^9 species is a d^8-d^9 mixed valence species. Due to the absence of detectable hyperfine splitting for, low abundant Ni^{63}. It is impossible to differentiate between the two.

The IR spectrum of complex (6) is identical to that of complex **(2)**. The suggested structure of this complex is based on:

1. The υ(O-H) is broad indicating H-bonding of the water molecule with the O-atom of the N-coordinated oximato groups.
2. Two υ(C=N) bands at 1535 and 1520 cm^{-1} were assigned to the two in-equivalent N-coordinated oximato groups.
3. The υ(C=N) the imino nitrogen coordination appeared at 1583 $cm\text{-}^{1}$.
4. The υ(N-O) is split to two bands at 1187 and 1175 cm^{-1}, indicating non-equivalent of the N-O bond. This could be interpreted in terms of H-bonding of a water molecule to one oxygen atom of the N-coordinated oxime leaving the other oxygen unsatisfied or due to the dimerization.
5. The dimeric structure is compatible with the vibrational evidence regarding presence of two υ(C=N) for the N-coordinated oximato groups. The magnetic moment of this complex was found to be 2.40 B.M. indicating spin-spin interaction of the spin Co(II).

The electronic spectrum of the complex in chloroform was different from that of the nujol mull spectrum. Therefore, the complex could be square pyramidal in the chloroform solution and molecular association takes place in the solid state [30]. The complex shows a rich spectrum in chloroform with different bands at 535, 508, 490 and 410 nm, respectively. These bands may be due to the following transitions $^1A_2 \leftarrow {}^1A_1$, $^1E_2 \leftarrow {}^1A_1$, $^1E_2 \leftarrow {}^1A_1$. These absorptions are consistent with a distorted tetragonal structure of Co(II) which gives rise to four transitions. Attempts were made to study this complex in different solvents as frozen solutions or in polycrystalline form at different temperatures, unfortunately, no ESR spectra were observed. This could be due to the formation of a dimeric species.

The IR spectrum of complex (**7**) showed that, the N-coordination of both oximato groups are proven by the presence of υ(N-O) at 1155 and 1148 cm^{-1} whereas the higher frequency 1616 cm^{-1} is assigned the υ(C=N) of the coordinated imino-nitrogen. These assignments are consistent with those reported for Cu(II) complexes of the dioximato ligands [34,35].

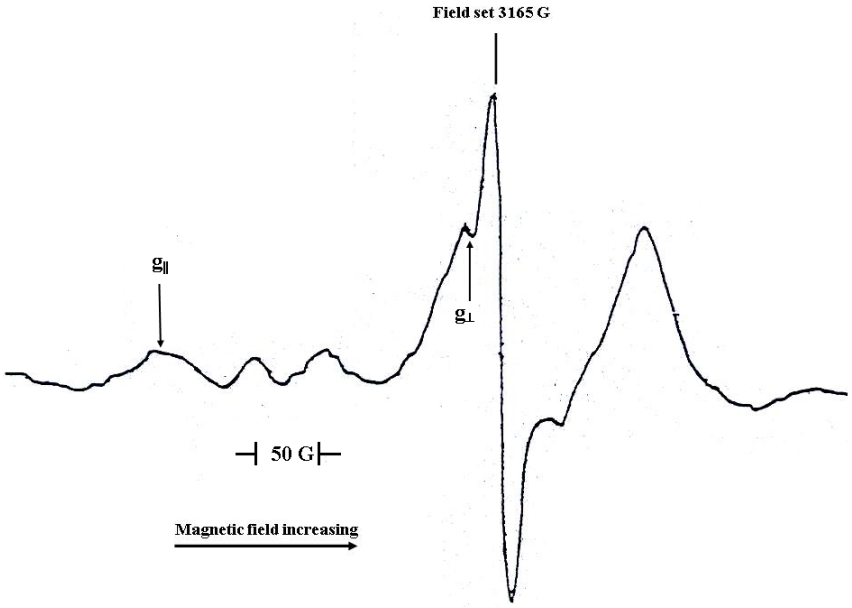

Figure 7. The ESR spectrum of the polycrystalline Ni(II) complex (5) at 77 k.

The observed bands at 1565 and 1551 cm^{-1} were assigned to N-coordination of the oximato groups. The splitting of υ(N-O) bands in this case could be explained by the hydrogen bonding formation of the oxygen atom of the oximato group in the coordinated water molecule (3670-3120 cm^{-1}, broad). The presence of two water molecules in the structure of complex **(7)** which are lattice components seem to be for crystal formation. The υ(C=O) of this complex appeared at 1670 cm^{-1}.

This can be assigned to the carbonyl group attached to the five membered ring in the vicinal oxime-imino complex of Cu(II) [13]. The mass spectrum data of this complex showed that, it could exist in a dimeric form. The electronic spectrum of this complex display absorption transitions indicating distorted octahedral structure [9].

This complex shows 1.6 B.M. confirming spin-spin coupling is present between the two copper(II) ions. The ESR spectra of solid or solution state shows very broad signal. The broad band in 3440-3455 cm^{-1} range was due to coordinated water or water of crystallization. The presence of water molecules within the coordination sphere in complexes **6-7** were supported by the presence of bands in the 3440-3455 cm^{-1}, 1600-1615 cm^{-1}, 930-955 cm^{-1} and 610-640 cm^{-1} ranges due to OH stretching, HOH deformation, H_2O rocking and H_2O wagging, respectively [33].

CONCLUSION

The Nickel(II), cobalt(II) and copper(II) of 4,4'-(propane-1,3-diylbis(azan-1-yl-1-ylidene))bis(3-(hydroxyimino)pentan-2-one) and of 4,4'-(butane-1,4-diylbis(azan-1-yl-1-ylidene))bis(3-(hydroxyimino)penta n-2-one) have been synthesized and characterized by elemental analyses, molar conductance, magnetic moments, IR, UV-Vis. spectra, DTA, mass spectra, ^{1}H- and ^{13}C-NMR and ESR measurements. IR spectra showed that, the ligands

behaved as dibasic ligands. Ni(II), d^8 complex was exposed to ^{60}Co-γ rays at 77 K using a 0.2217 M. rad. H^{-1} Vicrad source to give Ni(I), d^9, with a d_{x2-y2} ground state. Annealing the complex above 77 K led to the formation of a low spin Ni(III), d^7 system with d_{z2} orbital. However, copper(II) complexes showed an axial type symmetry with a d_{x2-y2} ground state. The suggested structures of the ligands and their metal complexes are in accordance with analytical, spectral and magnetic moment data

REFERENCES

[1] Yilmaz, A.; Taner, B.; Deveci, P.; Obali, AY.; Arslan, U.; Şahin, E.; Uçan, H.I.; Özcan, E., "Novel bioactive vic-dioxime ligand containing piperazine moiety: Synthesis, X-ray crystallographic studies, 2D NMR applications and complexation with Ni(II)" *Polyhedron*, 29, (2010). 2991-2998.

[2] El-Tabl A.S., "Synthetic and spectroscopic investigations of some transition metal complexes of hydroxy-oxime ligand" *J. Chem. Res.,* (2004) 19-24.

[3] Colak, A.; Terzi, Ü.; Col, M.; Karaoglu, Ş.A.; Karaböcek, S.; Küçükdumlu, A.; Ayaz, F.A., "DNA binding, antioxidant and antimicrobial activities of homo- and heteronuclear copper(II) and nickel(II) complexes with new oxime-type ligands" *Eur. J. Med. Chem.,* 45, (2010) 5169-5175.

[4] Wey, S.P.; Ibrahim, A.M.; Green, A.M.; Fanwiek, P.E., "Synthesis and crystal structure of a copper(II) complex with a tetradentate dithiadioxime ligand" Polyhedron, 14, (1995) 1097-1100.

[5] Zhuang, Z. J.; Okawa, H.; Matsumoto, N.; Sakiyama, H.; Kida, S., "Ferromagnetic oximate-bridged complexes of chromium(III)–copper(II) and of chromium(III)–copper(II)–chromium(III)" *J. Chem. Soc. Dalton Trans.,* (1991) 497-500.

[6] Thomas, T.W.; Underhill, A.E., "Metal–metal interactions in transition-metal complexes containing infinite chains of metal atoms" *Chem. Soc. Rev.,* 1, (1972) 99-120.

[7] Oguchi, K.; Sanui, K.; Ogata, N., "Relationship between electron sensitivity and chemical structures of polymers as electron beam resist. VII: Electron sensitivity of vinyl polymers containing pendant 1,3-dioxolan groups" *Polymer Eng. Sci.,* 30, (1990) 449-452.

[8] Plass, W.; El-tabl, A.S.; Pohlmann, A., "Synthesis, characterization and biological activity of triaminoxime and its metal complexes" *J. Coord. Chem.,* 62, (2009) 358-372.

[9] El-Tabl, A.S., "Synthesis and physico-chemical studies on cobalt(II), nickel(II) and copper(II) complexes of benzidine diacetyloxime" *Trans. Met. Chem.,* 27, (2002) 166-170.

[10] Ma, M.S.; Angelici, R.J., "Novel transition-metal complexes of camphorquinone dioxime ligands" *Inorg. Chem.,* 19, (1980) 363-370.

[11] Lacey, M.J.; Shannon, J.S.; Macdonald, C.G., "Factors influencing the chelate linkage isomerism of some oxime complexes of nickel(II)" *J. Chem. Soc. Dalton Trans.,* (1974) 1215-1217.

[12] Kukushkin, V.Y.; Tudeta, D.; Pombeiro, A.J., "Hydroxamic and aminohydroxamic acids and their complexes with metal ions" *Coord. Chem. Rev.,* 114, (1992) 169-200.

[13] Baghlaf, A.O.; Aly, M.M.; Ganji, N.S,. "Diagnostic features for the linkage isomerism of the oximato group: Characterization of some Cu(II), Co(II) and U(VI) complexes of a dioxime schiff-base ligand" *Polyhedron,* 6, (1987) 205-211.

[14] Coacio, E.; Dominguez-vera, J.M.; Escure, A.; Klinga, M.; Kivekas, R.; Romerosa, A., "A mixed-bridged Cu_3 cluster with an isosceles-triangular array of copper(II) ions: synthesis, crystal structure and magnetic properties" *J. Chem. Soc. Dalton Trans.,* (1995) 343-348.

[15] Peisach, J.; Blumberg W.E., "Electron Spin resonance of metal complexes, Ed. By T.F.Yen, Plenum press, New York 1969 PP. 71.

[16] Svehla, G., "Vogel's textbook of macro and semi micro Quantitative inorganic analysis" 5th Ed. Longman Inc. New York 1979.

[17] Lewis, L.; Wilkins, R.G., "Modern coordination chemistry" Interscience, New York; 1960.

[18] Aly, M.M.; El-Said, F.A., "The characterization of some square planar Ni(II) complexes of N,N′-ethylenebis (isonitrosoacetylacetoneimine)" *J. Inorg. Nucl, Chem.,* 43, (1981) 287-292.

[19] Bose, K.S.; Sharma, B.C.; Patel, C.C., "Ambidentate coordination of isonitrosoacetylacetone imines in their nickel(II) and palladium(II) complexes" *Inorg. Chem.,* 12, (1973) 120-123.

[20] Sreekantan, A.; Dixit, N.S.; Patel, C.C., "Mixed ligand cobalt(III) complexes of tetradentate N,N′-ethylenebis(acetylacetonimine) and flexidentate isonitroso-β-diketones and isonitrosomonoketones" *J. Inorg. Nucl. Chem.,* 42, (1980) 483-487.

[21] Cotton, F.A.; Wilkinson, G.; "*Advanced inorganic chemistry*" John Wiley and Sons; 1980.

[22] Hayter, R.G.; Humiec, F.S., "Square-Planar-Tetrahedral Isomerism of Nickel Halide Complexes of Diphenylalkylphosphines" *Inorg. Chem.,* 4, (1965) 1701-1706.

[23] Lovecchio, F.V.; Gore, E.S.; Busch, D.H., "Oxidation and reduction behavior of macrocyclic complexes of nickel. Electrochemical and electron spin resonance studies" *J. Am. Chem. Soc.,* 10, (1974) 3109-3118.

[24] Porter, G.B.; Houten, J.V., "Evidence of a chromium(II) intermediate in the photolysis of tris(2,2'-bipyridyl)chromium(III) in dimethylformamide" *Inorg. Chem.,* 19, (1980) 2903-2907.

[25] Haines, R.I.; McAuley, A., "Synthesis and reactions of nickel(iii) complexes" *Coord. Chem. Rev.,* 39, (1981) 77-119.

[26] McAuley, A.; Subramanian, S., "Synthesis, structure, and reactivity of the nickel(II) complex of 7-aza-1,4-dithiacyclononane" *Inorg. Chem.,* 29, (1990) 2830-2837.

[27] Brand, J.C.D.; Eglinton, G., "Application of spectroscopy to organic chemistry" 1965.

[28] Wehrli, F.W.; Wirthlin, T., "Interpretation of carbon-^{13}-NMR spectra" 1978.

[29] Aly, M.M.; Baghlaf, A.O.; Ganji, N.S., "Linkage isomerism of the oximato group: The characterization of some mono- and binuclear square planar nickel(II) complexes of vicinal oxime-imine ligands" *Polyhedron*, 4, (1985) 1301-1309.

[30] Aly, M.M., "Size and stability of chelate rings in coordination compounds of cobalt(II), manganese(II), iron(III) and palladium(II) with vicinal oxime-imine ligands" *Trans. Met. Chem.,* 15, (1990) 99-105.

[31] Fleming, I.; Williams, D.H., "*Spectroscopic methods in organic chemistry*" 1966.

[32] Teotia, M.; Gurtu, N.; Rama, V.B., "Dimeric 5-and 6-coordinate complexes of tri and tetradentate ligands" *J. Inorg. Nucl. Chern.,* 42, (1980) 821-831.

[33] Hoffman, B.M.; Diemente, D.L.; Basolo, F., "Electron paramagnetic resonance studies of some cobalt(II) Schiff base compounds and their monomeric oxygen adducts" *J. Am. Chem, Soc.,* 92, (1970) 61-65.

[34] Bigatto, A.; Costa, G.; Galasso, V.; Alti, G., "Infra-red spectra and normal vibrations of bis-dimethylglyoximates of transition metals" *Spectrochim. Acta,* 26, (1970) 1939-1949.

[35] Blinc, R.; Hadzi, D., "Infrared spectra and hydrogen bonding in the nickel–dimethylglyoxime and related complexes" *J. Chem. Soc.,* (1958) 4536-4540.

[36] Nickles, D.E.; Powers, M.J.; Urbach, F.L., "Copper(II) complexes with tetradentate bis(pyridyl)-dithioether and bis(pyridyl)-diamine ligands. Effect of thioether donors on the electronic absorption spectra, redox behavior, and EPR parameters of copper(II) complexes" *Inorg. Chem.,* 22, (1983) 3210-3217.

[37] Lever, A.B.P., "Inorganic electronic spectroscopy" Elsevier New York, 1968.

[38] Satpathy, S.; Sahoo, B., "Diacetylazine-dioximato metal chelates of Cu(II) and Ni(II); Their i.r. spectra and magnetic properties" *J. Inorg. Nucl. Chem.,* 33, (1971) 1313-1317.

[39] Bose, K.S.; Patel, C.C., "Nitrosation of N,N′-ethylenebis-(acetylacetoneimine) complexes of copper (II) and nickel(II) and characterization of the products" *J. Inorg. Nucl. Chem.,* 33, (1971) 2947-2952.

[40] Lacey, M.J.; Macdonald, C.G.; Shannon, J.S.; Collin, P.J., "Two modes of chelation in Bis(4-iminopentane-2,3-dione 3-oximato)nickel(II)" *Aust. J. Chem.,* 23, (1970) 2279-2286.

[41] Amirnasr, M.; Schenk, K. J.; Meghdadi, S.; Morshedi, M., "Synthesis, characterization and X-ray crystal structures of [Ni(Me-sal)$_2$dpt] and [Ni(Me-sal)dpt]Cl" *Polyhedron* 25, (2006) 671-677.

[42] Hathaway, B.J.; Billing, T.E., "The electronic properties and stereochemistry of mono-nuclear complexes of the copper(II) ion" *Coord. Chem. Rev.,* 5, (1970) 143-207.

[43] El-Dissouky, A.; Abou-Sakkina, M.M.; El-Kersh, M.; El-Sonabaat, A.Z., "Metal chelates of heterocyclic Nitrogen containing ketones. XV. Five-coordinate nickel(II) and copper(II) complexes with a sulphur-nitrogen tridentate schiff base" *Trans. Met. Chem.,* 9, (1984) 372-376.

Smart Nanocomposites
Volume 2, Number 2
ISSN: 1949-4823

SYNTHESIS AND CYTOTOXIC ACTIVITY ON MCF-7 CELL LINE OF SOME TRANSITION METAL COMPLEXES OF SCHIFF BASE LIGANDS DERIVED FROM 2-AMINOMETHYLBENZIMIDAZOLE AND 4,6-DIACETYLRESORCINOL

Nabil S. Youssef[1*], Ahmed M. A. El-Seidy[1.], Shadia A. Galal[2], Eman A. El-Zahany[1], Khaled H. Hegab[1,3], A. S. Barakat[4] and Sayed A. Drweesh[1]

[1]Inorganic Chemistry Department, National Research Centre, Giza, Egypt
[2]Department of Chemistry of Natural and Microbial Products,
Division of Pharmaceutical and Drug Industries,
National Research Centre, Cairo, Egypt
[3]Inorganic Chemistry Department, Faculty of Science, Zagazig University
[4]Chemistry Department, Faculty of Science, Gazan University, Gazan. KSA

ABSTRACT

Novel metal complexes of 1-(5-(1-(((1H-benzo[d]imidazol-2-yl)methyl)imino)ethyl)-2,4-dihydroxyphenyl)ethanone, H_3L^1, 3-((E)-(1-(5-((E)-1-(((1H-benzo[d]imidazol-2-yl)methyl)imino)ethyl)-2,4-dihydroxyphenyl)ethylidene)amino)-2-thioxothiazolidin-4-one, H_3L^2 and 4,6-bis((E)-1-(((1H-benzo[d]imidazol-2-yl)methyl)imino)ethyl)benzene-1,3-diol, H_4L^3 with $Ag^{(I)}$, $Cu^{(II)}$, $Fe^{(III)}$, $Ru^{(III)}$, $Pt^{(II)}$, VO^{II}, $Ni^{(II)}$ have been prepared and characterized using physico-chemical and spectroscopic methods. The molar conductance data revealed that all complexes are non-electrolytes except complex 6, which behaved as a 1:1 electrolyte. IR data showed that H_3L^1 behaved as neutral tridentate ligand except in case of complex 2, in which it behaved as neutral pentadentate ligand. Ligands H_3L^2 and H_4L^3 behaved as neutral hexadentate ligands. The spectral data and magnetic measurements of the complexes indicated that, the geometries are either square planar, square pyramidal or octahedral.

The Copper complexes 3 and 15 showed a remarkable smaller value of IC50 than that of the Tamoxifen which would provide a new potential antitumor drug that deserves more attention.

* Corresponding authors at: Inorganic Chemistry Department, National Research Centre, Dokki, 12622, Cairo, Egypt. Tel.: 002-01095105802. E-mail address: nabilyoussef@hotmail.com (N. S. Youssef), ahmedmaee2@gmail.com(A. M. A. El-Seidy).

Keywords: Benzimidazole, Diacetylresorcinol, Schiff bases, Transition metal complexes, Cytotoxic activity, human breast cancer cell line (MCF-7)

INTRODUCTION

Schiff base transition metal complexes have been of great interest for many years since they are becoming increasingly important as biochemical, analytical and antimicrobial reagents. [1] Many Schiff base transition metal complexes are reported to have anticancer and antimicrobial activities. [2-4].

It was reported that some drugs have greater activity when administered as metal complexes than that as free organic compounds. [5].

Hence, Schiff base transition metal complexes may be an untapped reservoir for drugs. There are ca. 30 derivatives of 2-aminobenzimidazole registered in the world as drugs, which exhibit diverse pharmacological activities, e.g. antiparasitic, antifungal, antiviral and antiallergic. [6].

The structures, syntheses and pharmacological properties of these compounds have been presented in recently published reviews. [7] 2-Aminobenzimidazole derivatives active against herpes simplex virus (HSV), human cyclomegalovirus (HCMV) and HIV were also described and patented. [8, 9]

A group of complex compounds of 2-aminobenzimidazole derivatives with some metals, such as cobalt, zinc and copper, showed also antifungal and antibacterial activity while complexes with ruthenium [10] were cytotoxic in vitro against SKW-8 cells (human T-lymphoma). Cancer is thought to reflect a multi-step process, resulting from an accumulation of inherited and/or acquired defects in genes involved in the positive or negative regulation of cell proliferation and survival. [11] Breast cancer has been defined as an abnormal division or proliferation of epithelial cell in lactiferous duct or lobe, and can be classified into ductal carcinoma and lobular carcinoma. [12]

The main target of present work is to study the coordination behavior of the benzimidazole ligands H_3L^1, H_3L^2 and H_4L^3 that incorporate many binding sites towards $Ag^{(I)}$, $Cu^{(II)}$, $Fe^{(III)}$, $Ru^{(III)}$, $Pt^{(II)}$, VO^{II}, $Ni^{(II)}$ ions. The structures of the ligands and their metal complexes were elucidated by elemental analysis, IR, ^{1}H NMR, ^{13}C NMR, UV-Vis, mass spectra, conductivity and magnetic susceptibility measurements at room temperature. The biological activity of the present organic ligands and their metal complexes are also reported. The remarkable smaller value of IC50 of complexes 3 and 15, than that of the Tamoxifen would provide a new potential antitumor drug that deserves more attention.

EXPERIMENTAL

1.1. The Preparation of 2-Aminomethylbenzimidazoledihydrochloride and 4,6-Diacetylresorcinol

Followed the procedure described before in literature. [13]

1.2. The Preparation of Platinum (II) Compounds

A stock $[PtCl_4]^{2-}$ solution was prepared by dissolving $PtCl_2$ (2.66 g, 10 mmol) in conc. HCl (till dissolve) under reflux, the turbidity of the undissolved material is then removed by filteration. The solution is then neutralized with Na_2CO_3 and diluting with distilled water up to 250 mL (pH 6.0-6.5) to yield a solution of 0.04 M $[PtCl_4]^{2-}$. [14].

1.3. Physical Measurements

The ligands and their metal complexes were analyzed for C, H, N and S contents at the Microanalytical Laboratory, Faculty of Science, Cairo University, Egypt. Analytical and physical data of the ligands H_3L^1, H_3L^2 and H_4L^3 and their metal complexes are reported in (Table 1).

The metal ion contents of the complexes were also determined by the previously reported methods. [15-17] IR spectra of the ligands and their metal complexes were measured using KBr discs with a Jasco FT/IR 300E Fourier transform infrared spectrophotometer covering the range 400-4000 cm^{-1} and in the 500-100 cm^{-1} region using polyethylene-sandwiched Nujol mulls on a Perkin Elmer FT-IR 1650 spectrophotometer. ^1H and ^{13}CNMR spectra were obtained on Brucker Avance 300-DRX or Avance 400-DRX spectrometers. Chemical shifts (ppm) are reported relative to TMS. The electronic spectra of the ligands and their complexes were obtained in Nujol mulls using a Shimadzu UV–240 UV-Visible recording spectrophotometer.

Molar conductivities of the metal complexes in DMSO (10^{-3} M) were measured using a dip cell and a Bibby conductimeter MC1 at room temperature. The resistance measured in ohms and the molar conductivities were calculated according to the equation: $\Lambda = V \times K \times Mw/g \times \Omega$, molar conductivity ($ohm^{-1}\ cm^2\ mol^{-1}$); V, volume of the complex solution (mL); K, cell constant 0.92 cm^{-1}; Mw, molecular weight of the complex; g, weight of the complex; and Ω, resistance measured in ohms. Magnetic moments at 298 K were determined using the Gouy method with $Hg[Co(SCN)_4]$ as calibrant. Mass spectra of the solid ligands was recorded using JEUL JMS-AX-500 mass spectrometer.

1.4. Synthesis of the Schiff Bases

1.4.1. Synthesis of H_3L^1 and H_4L^3

The methanol solution (50 mL) of 2-Aminomethylbenzimidazoledihydrochloride (2.21 gm, 10.0 mmole in case of H_3L^1 or 4.42 gm, 20.0 mmole in case of H_4L^3) was neutralized by NaOH and then filtrated to remove the sodium chloride precipitate. The filterate was then added to the hot (65°C) solution of diacetylresorcinol (1.94 gm, 10.0 mmol) in MeOH (20 mL).

The reaction mixture was refluxed for 6 h. and then left to cool. The formed yellow precipitate is filtered off, washed several times by methanol and dried under vacuum over anhydrous $CaCl_2$, Scheme 1.

Table 1. Analytical and some physical data of the ligands H_3L^1, H_3L^2, H_3L^4 and their metal complexes

No.	Ligands/Complexes	Color	FW	Yield (%)	Anal./found (calc.) (%)					Molar conductance [1]
					C	H	N	S	M	
1	H_3L^1, $C_{18}H_{17}N_3O_3$	yellow	323.4	74	66.8(66.9)	5.2(5.3)	12.9(13.0)	-	-	-
2	$H_3L^1Ag_2(NO_3)_2.H_2O$, $C_{18}H_{19}Ag_2N_5O_{10}$	yellow	681.1	71	31.5(31.7)	3.0(2.8)	10.4(10.3)	-	31.5(31.7)	18
3	$H_3L^1Cu(OC(O)CH_3)_2.H_2O$, $C_{22}H_{25}CuN_3O_8$	brown	523.0	81	50.5(50.5)	4.9(4.8)	8.2(8.0)	-	12.0(12.2)	12
4	$H_3L^1FeCl_3$, $C_{18}H_{17}Cl_3FeN_3O_3$	brown	485.6	79	44.4(44.5)	3.6(3.5)	8.9(8.7)	-	11.3(11.5)	20
5	$H_3L^1RuCl_3$, $C_{18}H_{17}Cl_3N_3O_3Ru$	brown	530.8	72	40.5(40.7)	3.3(3.2)	8.1(7.9)	-	18.8(19.0)	35
6	$[H_3L^1PtCl].Cl$, $C_{18}H_{17}Cl_2N_3O_3Pt$	yellow	589.3	80	36.7(36.7)	3.0(2.9)	7.2(7.1)	-	33.2(33.1)	89
7	H_3L^2, $C_{21}H_{19}N_5O_3S_2$	yellow	453.5	72	55.5(55.6)	4.2(4.2)	15.3(15.4)	14.0(14.1)	-	-
8	$H_3L^2Ag_2(NO_3)_2$, $C_{21}H_{19}Ag_2N_7O_9S_2$	yellow	793.3	69	31.9(31.8)	2.5(2.4)	12.5(12.4)	7.9(8.1)	27.0(27.2)	10
9	$H_3L^2Cu_2(OC(O)CH_3)_4$, $C_{29}H_{31}Cu_2N_5O_{11}S_2$	brown	816.8	81	42.4(42.6)	3.9(3.8)	8.9(8.6)	8.0(7.9)	15.4(15.6)	19
10	$H_3L^2(VO)_2(OSO_3)_2$, $C_{21}H_{19}N_5O_{13}S_4V_2$	brown	779.5	71	32.2(32.4)	2.8(2.5)	9.0(9.0)	16.4(16.5)	13.0(13.1)	28
11	$H_3L^2Ni_2(OC(O)CH_3)_4.(H_2O)_2$, $C_{29}H_{35}N_5Ni_2O_{13}S_2$	Reddish brown	843.1	76	41.1(41.3)	4.3(4.2)	8.5(8.3)	7.5(7.6)	14.0(13.9)	25
12	$H_3L^2Ru_2Cl_6$, $C_{21}H_{19}Cl_6N_5O_3Ru_2S_2$	brown	868.4	71	28.9(29.0)	2.5(2.2)	8.2(8.1)	7.3(7.4)	23.1(23.3)	35
13	H_4L^3, $C_{26}H_{24}N_6O_2$	yellow	452.5	70	69.0(69.0)	5.5(5.4)	18.7(18.6)	-	-	-
14	$H_4L^3Ag_2(NO_3)_2$, $C_{26}H_{24}Ag_2N_8O_8$	yellow	792.3	67	39.2(39.4)	3.2(3.1)	14.3(14.1)	-	27.0(27.2)	18
15	$H_4L^3Cu_2(OC(O)CH_3)_4.(H_2O)_2$, $C_{34}H_{40}Cu_2N_6O_{12}$	brown	851.8	74	47.6(47.9)	4.9(4.7)	10.1(9.9)	-	14.8(14.9)	22

[1] $\Lambda m(\Omega^{-1}cm^2mol^{-1})$.

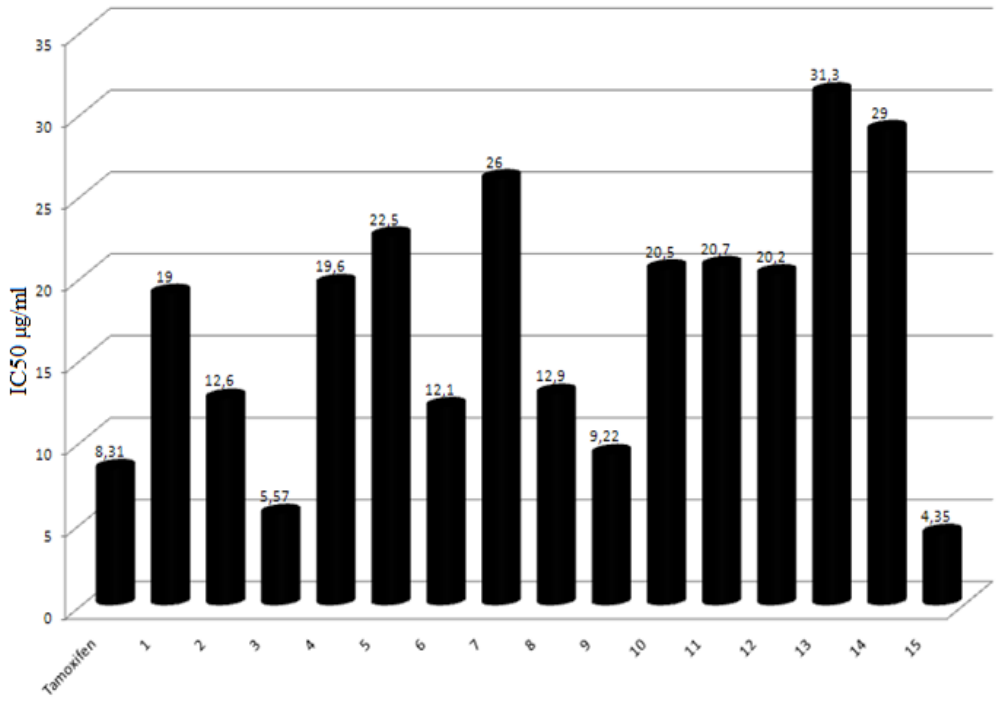

Scheme 1. Schematic representation for the formation of the Schiff base ligands H_3L^1, H_3L^2 and H_4L^3 and their numbering.

1.4.2. Synthesis of H_3L^2:

The methanol solution (10 mL) of N-aminorhodanine (1.48 gm, 10.0 mmol) was added to the solution of H_3L^1 (3.23 gm, 10 mmol) in methanol (40 mL).

The reaction mixture was stirred under reflux at 90 C^o for 10 h. then the solvent volume is reduced to half by evaporation under reduced pressure.

The precipitate was filtered off, washed several times with methanol and dried under vacuum over anhydrous $CaCl_2$.

1.4.3. Synthesis of the Metal Complexes

The metal complexes of the ligands were prepared by mixing a hot (70 ^oC) methanol solution of the metal salt with the required amount of methanol solution of the ligand to form 1:1 or 2:1 M/L (metal/ligand) complexes. The reaction mixture was then refluxed for a time depending on the transition metal salt used. The precipitates formed were filtered off, washed with methanol, then with diethyl ether and dried under vacuum at 50 ^oC for 5 h.

1.5. Cytotoxicity Assays

The cell culture cytotoxicity assays were carried out as described previously, [18] at the National Cancer Institute, Cairo University, Cairo, Egypt.

RESULTS AND DISCUSSION

Elemental Analysis

The elemental and physical data of the ligands H_3L^1, H_3L^2 and H_4L^3 and their complexes (Table 1) showed that the stoichiometry of the complexes obtained is either 1:1 or 2:1 M/L (metal:ligand).

Mass Spectra of the Ligands

The mass spectra of the Schiff bases H_3L^1, H_3L^2 and H_4L^3 revealed the molecular ion peaks at m/e 323, 453 and 452 which is coincident with the formulae weights 323.3, 453.5 and 452.5 respectively, for these compounds and supports the identity of their structures.

Conductivity Measurements

All metal complexes are stable in air and insoluble in common organic solvents but soluble in DMSO. The molar conductivities of the complexes in DMSO (10^{-3} M) are listed in Table 1. Only complex **6** behaved as a 1:1 electrolyte. [19] The rest of the complexes show a non-electrolyte nature. [3].

Infrared Spectra

The infrared spectra of the ligands showed broad bands centered in the 3434-3430 and 3267-3233 cm^{-1} ranges corresponds to $NH_{benzimidazole}$ and hydroxyl groups, respectively. The sharp band located in the 1620-1630 cm^{-1} range corresponds to $C=N_{benzimidazole}$ while the other imine bands were found in the 1663-1635 cm^{-1} range. The bands due to C=O were found as strong bands at 1653 and 1731 cm^{-1} in the spectra of 1 and 7, respectively. The thio-ketone band was found at 1100 cm^{-1} in spectrum of the ligand H_3L^2. [4]

The IR data for the Schiff bases H_3L^1, H_3L^2 and H_4L^3 and their complexes are listed in (Table 2). The IR spectra of the complexes are compared with those of the free ligand in order to determine the coordination sites that may be involved in chelation.

In all complexes of H_3L^1, except complex 2, the ligand behaved as neutral tridentate ligand coordinating through both imine groups and one hydroxyl group. These complexes showed a shift to lower wave number with decreasing intensity of the bands of both imine's and the appearance of new band in the 3212-3185 region corresponding to the coordinated hydroxyl group. [20-23] The other hydroxyl, carbonyl and amino groups almost retained their original positions indicating they were not involved in coordination. The appearance of two bands due to υ(C–O)'s, one almost at its original position while the other was shifted to higher wave number further supports the coordination of only one of the two phenolic oxygen to the central metal. [22] In case of complex 2, H_3L^1 behaved as neutral pentadentate ligand coordinating through all imine's and hydroxyl's groups and also through the carbonyl group.

Table 2. IR frequencies of the bands (cm^{-1}) of ligand H_3L^1, H_3L^2, H_3L^4 and their Metal Complexes and their assignments

No.	Ligands/Complexes	ν(H_2O)	ν(OH)	ν(NH)	ν(C=O)	ν(C=N) and	ν(C=S)	ν(C-O)	ν_s(Coo), ν_{as}(Coo^-),(Δ), ν(NO_3), ν(SO_4) ν(NO_3), SO_4
1	H_3L^1	-	3235br	3434br	1653s	1646s, 1626s	-	1239m	-
2	$H_3L^1Ag_2(NO_3)_2.H_2O$	3530br	3185br	3435br	1631s	1630s, 1610s	-	1245m	1457, 1369, 1035, 703
3	$H_3L^1Cu(OC(O)CH_3)_2.H_2O$	3500br	3234br, 3195br	3437br	1650s	1639s, 1608s	-	1255m, 1239sh	1579, 1363, 216
4	$H_3L^1FeCl_3$	-	3235br, 3205br	3433br	1654s	1636s, 1614s	-	1252m, 1240m	-
5	$H_3L^1RuCl_3$	-	3233br, 3202br	3432br	1652s	1633s, 1609s	-	1258m, 1238m	-
6	$[H_3L^1PtCl].Cl$	-	3234sh, 3212br	3434br	1656	1630s, 1613s	-	1248m, 1237m	-
7	H_3L^2	-	3267br	3433br	1731s	1663s, 1635v.s, 1620sh	1100m	1245m	-
8	$H_3L^2Ag_2.(NO_3)_2$	-	3252br	3433br	1695 w	1651s, 1628s, 1612s	1104m	1263m	1458, 1370, 1030, 709
9	$H_3L^2Cu_2(OC(O)CH_3)_4$	-	3248sh	3435br	1714 w	1654s, 1630s, 1609s	1102m	1269m	1543, 1314, 229
10	$H_3L^2(VO)_2.(OSO_3)_2$	-	3238br	3434br	1718 w	1655s, 1628s, 1613sh	1099m	1264m	1135s, 1040s, 968m, 650s, 600s
11	$H_3L^2Ni_2(OC(O)CH_3)_4.(H_2O)_2$	3490br	3242br	3433br	1708 w	1653s, 1629s, 1610sh	1100m	1259m	1590, 1377, 213

Table 2. (Continued)

12	$H_3L^2Ru_2Cl_6$	-	3248br	3433br	1710 w	1655s, 1628s, 1607s	1102m	1255m	-
13	H_4L^3	-	3233br	3430br	-	1650s, 1630s	-	1245m	-
14	$H_4L^3Ag_2(NO_3)_2$	-	3216br	3430br	-	1635s, 1619s	-	1258m	1455, 1367, 1028, 699
15	$H_4L^3Cu_2(OC(O)CH_3)_4.(H_2O)_2$	3480br	3218br	3430br	-	1637, 1615s	-	1263m	1588, 1384, 204

The bands of all of these groups were shifted to lower wave number with decreasing their intensities indicating they were involved in coordination to the central metal. [20-23] The band of the amino group almost retained its original position indicating it was not involved in coordination. The band of υ(C–O)'s appeared as a single band at higher wave number, which more supports the coordination of both phenolic oxygen to the central metal. [22]

In case of ligand H_3L^2 complexes, the ligand behaved as neutral hexadentate ligand and coordinated through the imine's, hydroxyl's and carbonyl groups. The IR data of these complexes showed a shift to lower wave number in the bands of these groups along with a decrease in their intensities, indicating they were involved in coordination. [20-23]

The band of υ(C–O)'s was shifted to higher wave number which more supports the coordination of both phenolic oxygen to the central metal. [22] The bands of the amino and thioketone groups almost retained their original positions indicating they were not involved in coordination. [20-23]

Ligand H_4L^3 behaved as neutral hexadentate ligand coordinating through all imines and hydroxyl groups. All of these complexes showed a shift to lower wave number with decreasing intensity of the bands of all imine's and hydroxyl's groups indicating they are involved in coordination to the central metal, [20-23] while the band of the amino group almost retained its original positions indicating it was not involved in coordination.

The new bands in spectra of all complexes in the 430-470 and 510-561 cm^{-1} regions were assigned to υ(M–N) and υ(M–O) vibrations, respectively. [24, 25]

Extensive IR spectral studies reported on metal acetato complexes [26] indicated that the acetate ligand may coordinate to the central metal in either a monodentate, bidentate or bridging manner. The $\nu_{asym.}(COO^-)$ and $\nu_{sym.}(COO^-)$ of the free acetate ions are found at 1560 cm^{-1} and 1416 cm^{-1}, respectively. In monodentate coordination ν(C=O) is found at higher energy than $\nu_{asym.}(CO_2)$ and ν(C-O) is lower than $\nu_{sym.}(CO_2)$. As a result, the separation between the two ν(CO) bands is much larger in monodentate complexes than the free ion. [27] The opposite trend is observed in bidentate acetato coordination; the separation between ν(CO) is smaller than for the free ion. For bridging acetate with both oxygens coordinated as in copper(ll) acetate, however, the two ν(CO) bands are close to the free ion values. [28, 29] The acetato group in complexes 3, 9, 11 and 15 acted as a monodentate manner which is supported by the appearance of two new bands in the ranges 1579-1593 cm^{-1} and 1363-1384 cm^{-1}, attributable to $\nu_{asym.}(COO^-)$ and $\nu_{sym.}(COO^-)$, respectively. [29] Further, the complex exhibits $\delta(COO^-)$ at 750 cm^{-1} which is considered diagnostic for monodentate acetates. [30] The separation value (Δ) between $\nu_{asym.}(COO^-)$ and $\nu_{sym.}(COO^-)$ in these complexes were more than 200 cm^{-1} (204-229 cm^{-1}) suggesting the coordination of carboxylate group in a monodentate fashion. [27]

The IR spectrum of the VO(IV) complex, complex 10, display a band at 971 cm^{-1} assigned to the stretching frequency of the ν(V=O). [31]

The broad bands in the 3530-3475 cm^{-1} region are due to coordinated water or water of crystallization. The bands for water of crystallization are different from those of coordinated water; the latter has bands in the 970-930 cm^{-1} and 660-600 cm^{-1} regions. The presence of water molecules within the coordination sphere in the hydrated complexes 2-3, 11 and 15 were supported by the presence of bands at 3530-3475 cm^{-1}, 1590-1600 cm^{-1}, 930-950 cm^{-1} and 615-635 cm^{-1} due to OH stretching, HOH deformation, H_2O rocking and H_2O wagging, respectively. [32, 33]

The sulphate ion has a regular tetrahedral structure belonging to the point group T_d. [34] In its ionic state, SO_4 has nine vibrational degrees of freedom, distributed in four normal modes of vibration. Out of these, only two are infrared active. [34] When SO_4 functions as a unidentate ligand, the oxygen coordinating to a metal atom is no longer symmetrically equivalent to the other three oxygen's and the effective symmetry of SO_4 is lowered to C_3, C_{3v}. [34] In C_3, $C_{3v,}$ symmetry, six infrared absorption bands are observed. When SO_4 functions as a bidentate group, its effective symmetry is further lowered to C_{2v}. In C_{2v} symmetry, eight modes of vibration, out of the total of nine, are infrared active. [35] The sulphato complex 10 showed bands at 1135, 1040, 968, 650, 600 cm^{-1} regions indicating a unidentate coordinating sulphato group. [36]

The spectrum of nitrato complexes 2, 8 and 14 show bands in 1455-1458 (υ1), 1028-1035 (υ2), 1367-1370 (υ4) and 699-709 (υ5) regions with υ1–υ4 separation of 88 cm^{-1}, characteristic of monodentate nitrato group. [37, 38]

Electronic Spectra and Magnetic Moments

The spectra of the diamagnetic Ag(I) complexes exhibit three bands in the 530-556, 460-488 and 370-394 nm ranges; the latter two may arise from charge transfer of the type ligand(π)→ $b_{1g}(Ag^+)$ and ligand (σ)→ $b_{1g}(Ag^+)$, respectively, in a typically distorted square planar environment around the metal ion. [39, 40]

The electronic spectra of the copper complexes **3** and **15** showed a band in 735-748 nm range assignable to $^2E_g \rightarrow {}^2T_g$ transition, which is the expected band for d^9 ion in an octahedral configuration with low crystal field splitting. [41] The magnetic moments of the copper complex **3** at room temperature was 1.83 B.M., Table 3, corresponding to one unpaired electron. [42] Complex **9** showed a band at 670 nm, ascribed to the d-d transition (dxz; dyz → dx^2-y^2). These results are typical of square pyramidal geometry. [43]

The electronic spectrum of complex **10** showed two bands in the visible region at 715 and 525 nm, which were assigned to $^2B_2 \rightarrow {}^2E$ and $^2E_2 \rightarrow {}^2B_1$ transitions, respectively, as expected for a square pyramidal vanadyl complex in accordance with the Ballhausen-Gray scheme. [44, 45]

The electronic spectrum of the ferric Complex **4**, showed bands at 744 nm, that may be assigned to $^6A_1 \rightarrow {}^4T_1(G)$, indicating distorted octahedral geometry around Fe(III) ion. [46, 47] The magnetic moment of this complex was found to be 5.8 B.M. and fall within the range observed for octahedral Fe(III) complexes. [48]

The electronic spectrum of Nickel(II) complex, complex **11**, showed bands at 805 and 510 nm that may be arising from $^3A_{2g} \rightarrow {}^3T_{1g}(F)$ and $^3A_{2g} \rightarrow {}^3T_{1g}(P)$ transitions, respectively in octahedral geometry. [49, 50]

The ruthenium complexes **5** and **12** showed two bands in the ranges 680-650 and 580-560 nm. The ground state of ruthenium(III) in octahedral environment is $^2T_{2g}$, arising from the $t^5{}_{2g}$ configuration, and the first excited doublet levels in the order of increasing energy are $^2A_{2g}$ and $^2T_{1g}$, arising from the $t^4{}_{2g}e^1{}_g$ configuration. Hence, these two bands correspond to $^2T_{2g} \rightarrow {}^2A_{2g}$ and $^2T_{2g} \rightarrow {}^2T_{1g}$ transitions, respectively. [37, 51]

The complexes **9-15** exhibits magnetic moment which were lower than the expected values indicating antiferromagnetic exchange existing between metal ions in these complexes (Table 3). [20, 21]

Table 3. Electronic absorption spectral bands (nm) and magnetic moment (B.M) for the ligands H_3L^1, H_3L^2, H_3L^4 and their complexes

No.	Ligands/Complexes	λ_{max} (nm)	μ_{eff} in B.M.
1	H_3L^1	396, 373, 322, 284	-
2	$H_3L^1Ag_2(NO_3)_2.H_2O$	556, 475 , 380, 334, 296	-
3	$H_3L^1Cu(OC(O)CH_3)_2.H_2O$	735, 445, 345, 290	1.83
4	$H_3L^1FeCl_3$	744, 430, 335, 295	5.8
5	$H_3L^1RuCl_3$	680, 580, 500, 409, 343, 300	1.89
6	$[H_3L^1PtCl].Cl$	415, 375, 345, 305	-
7	H_3L^2	433, 345, 284, 275	-
8	$H_3L^2Ag_2(NO_3)_2$	545, 460, 394, 340, 316, 290	-
9	$H_3L^2Cu_2(OC(O)CH_3)_4$	670, 460, 375, 285	1.54
10	$H_3L^2(VO)_2(OSO_3)_2$	715, 525, 338, 287	1.63
11	$H_3L^2Ni_2(OC(O)CH_3)_4.(H_2O)_2$	805, 590, 455, 342, 300	2.5
12	$H_3L^2Ru_2Cl_6$	650, 560, 339, 285	1.60
13	H_4L^3	375, 330, 280	-
14	$H_4L^3Ag_2(NO_3)_2$	530, 488, 460, 370, 312	-
15	$H_4L^3Cu_2(OC(O)CH_3)_4.(H_2O)_2$	748, 470, 370, 318	1.49

NMR Studies of the Diamagnetic Complexes

The signal of $NH_{benzimidazole}$ appeared at 13.75 in ligand H_3L^2 but could not be found in the other two ligands, this may be due to hydrogen bonding. This signal appeared in case of complex 6 at 14.03 indicating a change in the hydrogen bonding surrounding the ligand. The signal due to the hydroxyl groups were found at 12.58, 12.59 and 11.16 and 12.49 for the ligands H_3L^1, H_3L^2 and H_4L^3, respectively. Complex 6 showed two signals for the hydroxyl hydrogen indicating they are no longer equivalent since only one of them is involved in coordination (Figure 1). The comparison of the ^{1}HNMR and ^{13}C NMR spectrum of the complexes and ligands lead to a similar conclusion and indicate changes in the charge redistribution in the whole molecule induced by the complexation (Table 4(a-e)).

Suggested Structural Formulae of the Complexes

From the spectral data and the elemental, the structure of the prepared complexes may be formulated as shown in Figures 1 and 2.

Table 4(a). ^{1}H-NMR spectral data of H_3L^1 and Some of its metal complexes

Compounds	H(25)	H(26), H(27)	H(15)	H(3), H(4)	H(1), H(2)	H(18)	H(28), H(29)	CH_3(21)	CH_3(14)
H_3L^1	-	12.58 (s, 2H)	8.23(s, 1H)	7.56(psd, 2H)	7.19(psd, 2H)	5.99(s, 1H)	5.14(s, 2H)	2.64(s, 3H)	2.60(s, 3H)
2	-	12.47	8.41(s, 1H)	7.63(psd, 2H)	7.24(psd, 2H)	5.95(s, 1H)	5.22(s, 2H)	2.54(s, 3H)	2.51(s, 3H)
6	14.03br	12.73(s, 1H), 12.64(s, 1H)	8.42(s, 1H)	7.68(psd, 2H)	7.27(psd, 2H)	6.15(s, 1H)	5.15(s, 2H)	2.66(s, 3H)	2.51(s, 3H)

Table 4(b). ^{13}C-NMR spectral data of H_3L^1 and Some of its metal complexes

Compounds	(C20)	(C12)	(C17), (C19)	(C6)	(C15)	(C1), (C2)	(C16)	(C13)	(C3, C4)	(C10)	(C21)	(C14)
H_3L^1	202.78	176.54	166.18	151.79	137.70	137.5	122.37	112.8	105.38	44.96	26.74	15.38
2	205.38	178.46	169.64	154.88	140.1	138.76	125.14	115.99	106.07	45.09	29.02	17.96
6	205.27	178.50	169.59	155.01	139.98	139.10	126.38	117.27	106.10	45.28	30.08	19.10

Table 4(c). ^{1}H-NMR spectral data of H_3L^2 and Some of its metal complexes

Compound	H(31)	H(30)	H(29)	H(23)	H(11), H(12)	H(9), H(10)	H(26)	H(33), H(34)	H(35), H(36)	CH_3(32)	CH_3(22)
H_3L^2	13.75br	12.59 (S, 1H)	11.16 (S, 2H)	8.87 (s, 1H)	7.54 (psd, 2H)	7.18 (psd, 2H)	6.36 (s, 1H)	5.04 (s, 2H)	3.75 (s, 2H)	2.72 (s, 3H)	2.63 (s, 3H)
8	14.09	12.63	11.20	8.52	7.75	7.37	6.36	4.66	3.63	2.85	2.63

Table 4(d). ^{13}C-NMR spectral data of H_3L^2

Compounds	(C1)	(C3)	(C20), C(28)	(C27)	(C25)	(C14)	C(23)	C(9), C(10)	C(24)	C(21)	C(11), C(12)	C(18)	C(7)	C(32)	C(22)
H_3L^2	203.65	170.42	167.82	164.72	163.14	152.32	138.85	138.19	115.54	114.92	113.86	53.09	43.62	31.57	27.33

Table 4(e). ^{1}H-NMR spectral data of H_4L^3

Compound	H(25), H(41)	H(26), H(27)	H(15)	H(3), H(4), H(32), H(33)	H(1), H(2), H(30), H(31)	H(18)	H(28), H(29), H(42), H(43)	$C\underline{H_3}$(14), $C\underline{H_3}$(21)
H_4L^3	-	12.49 (s, 2H)	7.97 (s, 1H)	7.50(psd, 4H)	7.15(psd, 4H)	5.90 (s, 1H)	5.04(s, 2H)	2.55(s, 6H)

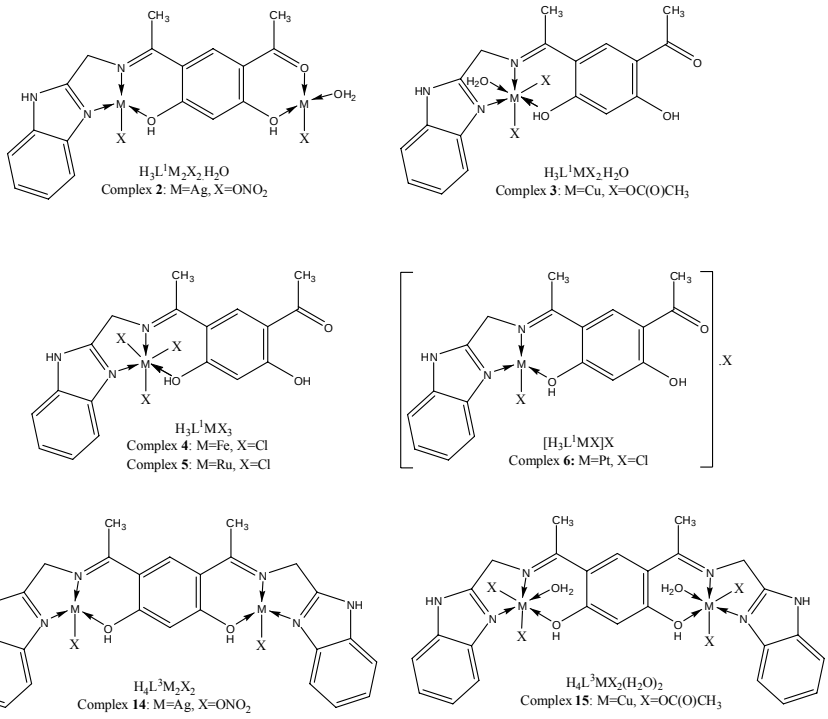

Figure 1. The proposed structures of H3L1 and H4L3 metal complexes.

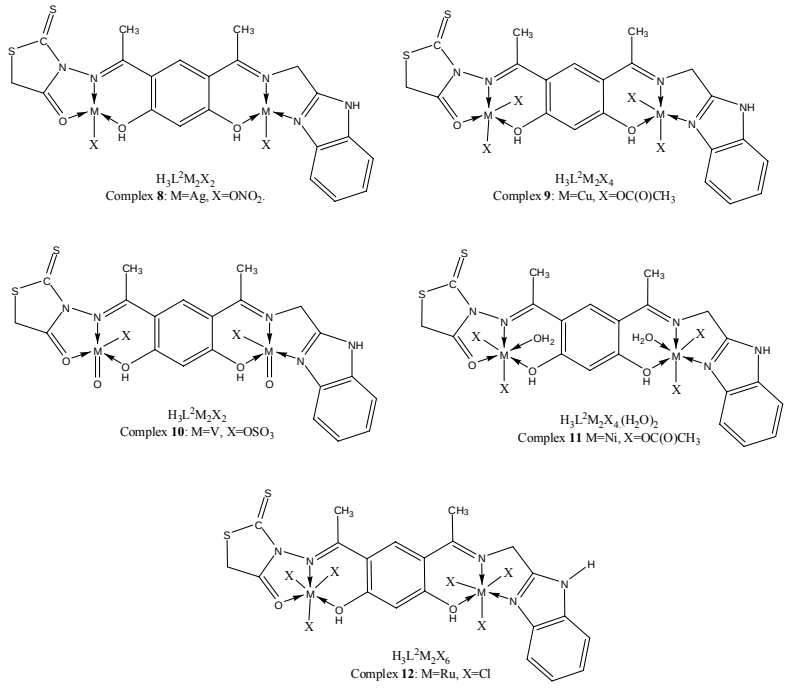

Figure 2. The proposed structures of H3L2 metal complexes.

BIOLOGICAL ACTIVITY

The cytotoxic activities of the three ligands and their complexes (compounds 1-15) were evaluated against the human breast cancer cell line (MCF-7). The Schiff base ligands H_3L^1, H_3L^2 and H_4L^3 were found to be biologically active and their metal complexes enhanced their cytotoxic activity.

All the tested compounds showed biological activity. The metal complexes of the three ligands have higher antitumor activity than their ligands except iron(III) and ruthenium(III) complexes of ligand H_3L^1. This may be due to the lipophilic character of the central metal atom explained by Tweedy's chelation. [52] The IC50 value of Cu(II) complexes 3 and 15 on MCF-7 cytotoxicity were significantly smaller than that of the all tested compounds, which means that Cu(II) complexes are more effective than the other complexes and their ligands. [53] It's to be noted that the copper is a redox active metal and the copper based metallo-complexes reacts with DNA leading to the production of reactive oxygen species (ROS). [54] The remarkable smaller value of IC50 of complexes 3 and 15 than that of the Tamoxifen would provide new potential antitumor drug that deserves more attention. The IC50 values were summarized as shown in Figure 3.

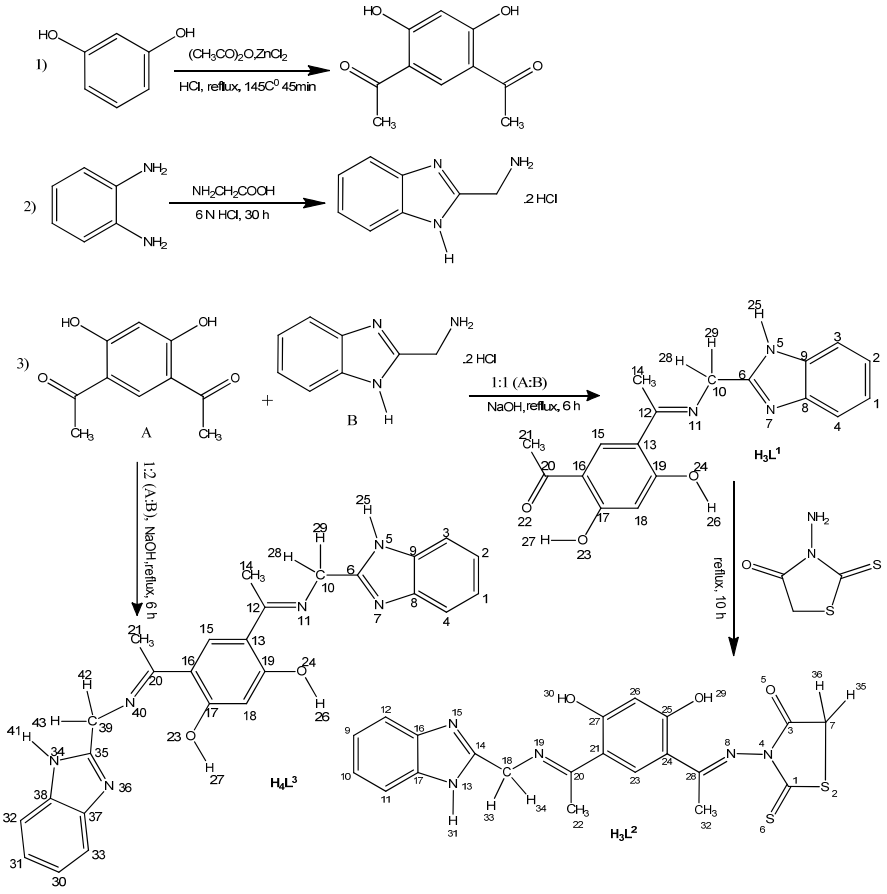

Figure 3. Cytotoxic activities of ligands and their complexes against human breast cancer cell line (MCF-7).

CONCLUSION

We report here a study of the coordination capability of three new Schiff bases derived from 2-Aminomethylbenzimidazole H_3L^1, H_3L^2 and H_4L^3 toward $Ag^{(I)}$, $Cu^{(II)}$, $Fe^{(III)}$, $Ru^{(III)}$, $Pt^{(II)}$, VO^{II}, $Ni^{(II)}$. Their metal complexes with transition metals have been prepared and characterized. The spectral data indicated that the ligand H_3L^1 behaved either as neutral tridentate or neutral pentadentate ligand while both H_3L^2 and H_4L^3 behaved as neutral hexadentate ligands. The compounds 1-15 were tested in vitro against the human breast cancer cell line (MCF-7) and the copper complexes 3 and 15 showed a remarkable smaller value of IC50 than that of the Tamoxifen which would provide a new potential antitumor drugs that deserves more attention.

REFERENCES

[1] You, Z.L.; Shi, D.H.; Xu, C.; Zhang, Q.; Zhu, H.L., "Schiff base transition metal complexes as novel inhibitors of xanthine oxidase" *European Journal of Medicinal Chemistry*, 43(4), (2008). 862-871.

[2] Bekhit, A.A.; El-Sayed, O.A.; Al-Allaf, T.A.K.; Aboul-Enein, H.Y.; Kunhi, M.; Pulicat, S.M.; Al-Hussain, K.; Al-Khodairy, F.; Arif, J., "Synthesis, characterization and cytotoxicity evaluation of some new platinum(II) complexes of tetrazolo[1,5-a]quinolones" *European Journal of Medicinal Chemistry*, 39(6), (2004). 499-505.

[3] Golcu, A.; Tumer, M.; Demirelli, H.; Wheatley, R.A., "*Cd(II) and Cu(II) complexes of polydentate Schiff base ligands: synthesis, characterization, properties and biological activity" Inorganica Chimica Acta*, 358(6), (2005). 1785-1797.

[4] Singh, K.; Barwa, M.S.; Tyagi, P., "Synthesis, characterization and biological studies of Co(II), Ni(II), Cu(II) and Zn(II) complexes with bidentate Schiff bases derived by heterocyclic ketone" *European Journal of Medicinal Chemistry*, 41(1), (2006). 147-153.

[5] Chohan, Z.H.; Praveen, M.; Ghaffar, M., "Structural and biological behaviour of Co(II), Cu(II) and Ni(II) metal complexes of some amino acid derived Schiff-bases" *Metal-Based Drugs*, 4(5), (1997). 267–272.

[6] Merck and Co., The Merck Index, An Encyclopedia of Chemical Drugs and Biologicals, 12th ed, Whitehouse Station NY, USA, 1996.

[7] Nawrocka, W., "Syntheses and pharmacological properties of new 2-aminobenzimidazole derivatives" *Bollettino chimico farmaceutico*, 135(1), (1996). 18-23.

[8] Iriepa, I.; Gil-Alberdi, B.; Gálvez, E.; Villasante, F.J.; Bellanato, J.; Carmona, P., "Synthesis, structural, conformational and pharmacological study of some carbamates derived from 3-methyl-2,4-diphenyl-3-azabicyclo[3.3.1]nonan-9b-ol" *Journal of Molecular Structure,* 482-483, (1999). 437-442.

[9] Vigorita, M.G.; Previtera, T.; Zappalà, C,.;Trovato, A.; Monforte ,MT.; Barbera, R.; Pizzimenti, F., "N-trifluoroacetyl derivatives as pharmacological agents. V. Evaluation of antiinflammatory and antimicrobial activities of some N-heterocyclic trifluoroacetamides" *Farmaco*, 45, (1990). 223-235.

[10] Nikolova, D.; Ivanov, R.; Buyukliev, S.; Konstantinov, M.; Karaivanova, M., "Preparation, physicochemical characterization and pharmacological study of novel ruthenium (III) complexes with imidazole and benzimidazole derivatives" *Arzneimittel-Forschung Drug Research*, 51(II), (2001). 758-762.

[11] El-Deeb, I.M.; Lee, S.H., "Design and synthesis of new anticancer pyrimidines with multiple-kinase inhibitory effect" *Bioorganic and Medicinal Chemistry*, 18, (2010). 3860-3874.

[12] Lin, Y.L.; Su, Y.T.; Chen, B.H., "A study on inhibition mechanism of breast cancer cells by bis-type triaziquone", *European Journal of Pharmacology*, 637(1-3), (2010). 1-10.

[13] Emara, A.A.A.; Abou-Hussen, A.A.A., "Spectroscopic studies of bimetallic complexes derived from tridentate or tetradentate Schiff bases of some di- and tri-valent transition metals" *Spectrochimica Acta Part A: Molecular and Biomolecular Spectroscopy*, 64(4), (2006). 1010-1024.

[14] Kovala-Demertzi, D.; Yadav, P.N.; Demertzis M.A.; Coluccia, M., "Synthesis, crystal structure, spectral properties and cytotoxic activity of platinum(II) complexes of 2-acetyl pyridine and pyridine-2-carbaldehyde N(4)-ethyl-thiosemicarbazones" *Journal of Inorganic Biochemistry*, 78(4), (2000). 347-354.

[15] F. J. Welcher, *The Analytical Use of EDTA*, Van Norstrand, USA, 1958.

[16] Vogel, A Text Book of Quantitative Inorganic Analysis, 4th ed., Longmans, London, 1978.

[17] Z. Holzbecher, L. Divis, M. Kral, L. Sucha, F. Vracil, Handbook of Organic Reagents in Inorganic Analysis, Wiley, Chichester, 1976.

[18] Skehan, P.; Storeng, R.; Scudiero, D.; Monks, A.; Mahon, J.; Vistica, D.; Warren, J.T.; Bokesch, H.; Kenney, S.; Boyd, M.R., "New colorimetric cytotoxic assay for anticancer drug screening" *Journal of the National Cancer Institute*, 13, (1990). 1107-1112.

[19] El-Bindary, A.A., "N-picolinamido-N-benzoylthiocarbamide transition metal complexes" *Transition Metal Chemistry*, 22, (1997). 381-384.

[20] Youssef, N.S.; El-Zahany, E.; El-Seidy, A.M.A.; Caselli, A.; Cenini, S., "Synthesis and characterization of some transition metal complexes with a novel Schiff base ligand and their use as catalysts for olefin cyclopropanation" *Journal of Molecular Catalysis A: Chemical*, 308(1-2), (2009). 159-168.

[21] Youssef, N.S.; El-Zahany, E.; El-Seidy, A.M.A.; Caselli, A.; Fantauzzi, S.; Cenini, S., "Synthesis and characterisation of new Schiff base metal complexes and their use as catalysts for olefin cyclopropanation" *Inorganica Chimica Acta*, 362, (2009). 2006-2014.

[22] Nakatamato, K. (1967). Infrared Spectra of Inorganic and Coordination Compounds. New York: Wiley Interscience.

[23] El-Wahab, Z.H.A.; Mashaly, M.M.; Salman, A.A.; El-Shetary, B.A.; Faheim, A.A., "Co(II), Ce(III) and UO_2(VI) bis-salicylatothiosemicarbazide complexes: Binary and ternary complexes, thermal studies and antimicrobial activity" *Spectrochimica Acta - Part A: Molecular and Biomolecular Spectroscopy*, 60 (12), (2004). 2861-2873.

[24] Patel, R.N.; Gundla, V.L.N.; Patel, D.K., "Synthesis, structure and properties of some copper(II) complexes containing an ONO donor Schiff base and substituted imidazole ligands" *Polyhedron*, 27(3), (2008). 1054-1060.

[25] Cukuravali, A.; Yilmaz, I.; Kirbag, S., "Spectroscopic Characterization and Biological Activity of Salicylaldehyde Thiazolyl Hydrazone Ligands and their Metal Complexes" *Transition Metal Chemistry*, 31(2), (2006). 207-213.

[26] K. Nakamoto, "Infrared Spectra of Inorganic and coordination compounds", Wiley Interscience, New York (1965).

[27] Boghaei, D.M.; Gharagozlou, M., "Synthesis and spectral characterization of novel ternary zinc(II) complexes containing 1,10-phenanthroline and Schiff bases derived from amino acids and salicylaldehyde-5-sulfonates" *Spectrochimica Acta Part A: Molecular and Biomolecular Spectroscopy*, 67, (2007). 944-949.

[28] Robinson, S.D.; Uttley, M.F. J., "Complexes of the platinum metals. Part II. Carboxylato(triphenylphosphine) derivatives of ruthenium, osmium, rhodium, and iridium" *Journal of the Chemical Society, Dalton Transactions*, (18), (1973). 1912-1920.

[29] El-Shazly, R.M.; Al-Hazmi, G.A.A.; Ghazy, S.E.; El-Shahawi, M.S.; El-Asmy, A.A., "Spectroscopic, thermal and electrochemical studies on some nickel(II) thiosemicarbazone complexes" *Spectrochimica Acta Part A: Molecular and Biomolecular Spectroscopy*, 61, (2005). 243-252.

[30] K. Nakarnota, "Infrared and Raman Spectra of Inorganic and coordination compounds", Wiley Interscience, New York, 1986.

[31] Emara, A.A.A.; Saleh, A.A.; Adly, O.M.I., "Spectroscopic investigations of new binuclear transition metal complexes of Schiff bases derived from 4,6-diacetylresorcinol and 3-amino-1-propanol or 1,3-diamino-propane" *Spectrochimica Acta Part A: Molecular and Biomolecular Spectroscopy*, 68(3), (2007). 592-604.

[32] Teotia, M.P.; Gurtu, J.N.; Rana, V.B., "Dimeric 5-and 6-coordinate complexes of tri and tetradentate ligands." *Journal of Inorganic and Nuclear Chemistry*, 42(6), (1980). 821-831.

[33] El-Dissouky, A.; Fahmy, A.; Amer, A., "Complexing ability of some γ-lactone derivatives. Thermal, magnetic and spectral studies on cobalt(II), nickel(II) and copper(II) complexes and their base adducts" *Inorganica Chimica Acta*, 133(2), (1987). 311-316.

[34] Rivera, J.M.; Guzmán, D.; Rodriguez, M.; Lamère, J.F.; Nakatani, K.; Santillan, R.; Lacroix, P.G.; Farfan, N., "Synthesis, characterization and nonlinear optical properties in a series of new chiral organotin(IV) Schiff base complexes" *Journal of Organometallic Chemistry*, 691(8), (2006). 1722-1732.

[35] Salama, T.M.; Ahmed, A.H.; El-Bahy, Z.M., "Y-type zeolite-encapsulated copper(II) salicylidene-p-aminobenzoic Schiff base complex: Synthesis, characterization and carbon monoxide adsorption" *Microporous and Mesoporous Materials*, 89(1-3), (2006). 251-259.

[36] Chandra, S.; Gupta, L.K., "Oxidation of phenol, styrene and methyl phenyl sulfide with H2O2 catalysed by dioxovanadium(V) and copper(II) complexes of 2-aminomethylbenzimidazole-based ligand encapsulated in zeolite-Y" *Journal of Molecular Catalysis A: Chemical*, 263(1-2), (2007). 227-237.

[37] Kannan, S.; Ramesh, R., "Synthesis, characterization, catalytic oxidation and biological activity of ruthenium(III) Schiff base complexes derived from 3-acetyl-6-methyl-2H-pyran-2,4(3H)-dione" *Polyhedron*, 25(16), (2006). 3095-3103.

[38] Kumara, K.N.; Ramesh, R., "Synthesis, luminescent, redox and catalytic properties of Ru(II) carbonyl complexes containing 2N2O donors" *Polyhedron*, 24(14), (2005). 1885-1892.

[39] Mostafa, S.I.; Bekheit, M.M., "Synthesis and structure studies of complexes of some second row transition metals with 1-(phenylacetyl and phenoxyacetyl)-4-phenyl-3-thiosemicarbazide" *Chemical and Pharmaceutical Bulletin*, 48(2), (2000). 266-271.

[40] Mostafa, S.I.; Ikeda, S.; Ohtani, B., "Transition metal Schiff-base complexes chemically anchored on Y-zeolite: their preparation and catalytic epoxidation of 1-octene in the suspension and phase boundary systems" *Journal of Molecular Catalysis A: Chemical*, 225(2), (2005). 181-188.

[41] Sanmartín, J.; Novio, F.; García-Deibe, A.M; Fondo, M.; Ocampo, N.; Bermejo, M.R., "Dinuclear neutral complexes of a symmetric N_2; N_2-donor diimine ligand". *Polyhedron*, 25(8), (2006). 1714-1722.

[42] Mohamed, G.G.; El-Gamel, N.E.A., "Synthesis, investigation and spectroscopic characterization of piroxicam ternary complexes of Fe(II), Fe(III), Co(II), Ni(II), Cu(II) and Zn(II) with glycine and DL-phenylalanine" *Spectrochimica Acta Part A: Molecular and Biomolecular Spectroscopy*, 60, (2004). 3141-3154.

[43] Matsumoto, K.; Sekine, N.; Arimura, K.; Ohba, M.; Ohba, H.; Sakiyama, H.; Ōkawa, H., "μ-Acetato-di-μ-phenolato-metal(II)cobalt(II) (Metal = Fe, Co, Ni, Cu, Zn) Complexes with Low-Spin Co(II): Synthesis, Structures, and Magnetism" *Bulletin of the Chemical Society of Japan*, 77(7), (2004). 1343-1351.

[44] Gangadharmath, U.B.; Annigeri, S.M.; Naik, A.D.; Revankar, V.K.; Mahale, V.B., "Synthesis, characterisation and evaluation of molecular-orbital parameters, spin-orbit, dipolar and fermi-contact terms of VO^{2+} ion in thiosemicarbazone complexes" *Journal of Molecular Structure: THEOCHEM*, 572, (2001). 61-71.

[45] Boghaei, D.M.; Bezaatpour, A.; Behzad, M., "Synthesis, characterization and catalytic activity of novel monomeric and polymeric vanadyl Schiff base complexes" *Journal of Molecular Catalysis A: Chemical*, 245(1-2), (2006). 12-16.

[46] Sallam, S.A.; Orabi, A.S.; El-Shetary, B.A.; Lentz, A., "Copper, nickel and cobalt complexes of Schiff-bases derived from □-diketones" *Transition Metal Chemistry*, 27, (2002). 447-453.

[47] Singh, N.K.; Singh, S.B., "Complexes of 1-isonicotinoyl-4-benzoyl-3-thiosemicarbazide with manganese(II), iron(III), chromium(III), cobalt(II), nickel(II), copper(II) and zinc(II)" *Transition Metal Chemistry*, 26(4-5), (2001). 487-495.

[48] García-Friaza, G.; Fernandez-Botello, A.; Pérez, J.M.; Prieto, M.J.; Moreno, V., "Synthesis and characterization of palladium(II) and platinum(II) complexes with Schiff bases derivatives of 2-pyridincarboxyaldehyde. Study of their interaction with DNA" *Journal of Inorganic Biochemistry*, 100(8), (2006). 1368-1377.

[49] Ali, M.A.; Mirza, A.H.; Bujang, F.H.; Hamid, M.H.S.A.; Bernhardt, P.V., "Synthesis, characterization and X-ray crystallographic structural study of copper(II) and nickel(II) complexes of the 2-quinoline carboxaldehyde Schiff base of S-methyldithiocarbazate (Hqaldsme)" *Polyhedron*, 25(17), (2006). 3245-3252.

[50] Krishnapriya, K.R.; Kandaswamy, M., "Coordination properties of a dicompartmental ligand with tetra- and hexadentate coordination sites towards copper (II) and nickel (II) ions" *Polyhedron*, 24(1), (2005). 113-120.

[51] Balasubramanian, K.P.; Parameswari, K.; Chinnusamy, V.; Prabhakaran, R.l; Natarajan, K., "Synthesis, characterization, electro chemistry, catalytic and biological activities of ruthenium(III) complexes with bidentate N, O/S donor ligands" *Spectrochimica Acta Part A: Molecular and Biomolecular Spectroscopy*, 65(3-4), (2006). 678-683.

[52] Tümer, M.; Ekinci, D.; Tümer, F.; Bulut, A., "Synthesis, characterization and properties of some divalent metal(II) complexes: Their electrochemical, catalytic, thermal and antimicrobial activity studies" *Spectrochimica Acta Part A: Molecular and Biomolecular Spectroscopy*, 67(3-4), (2007). 916-929.

[53] Chen, J.; Huang, Y-w.; Liu, G.; Afrasiabi, Z.; Sinn, E.; Padhye, S.; Maa, Y, "The anticancer activity and the mechanism study of 1,2 naphthoquinone thiosemicarbazone and its metal derivatives against MCF-7 human breast cancer cells" *Toxicology and Applied Pharmacology*, 197, (2004). 40-48.

[54] Chakraborty, A.; Kumar, P.; Ghosh, K.; Roy, P., "Evaluation of a Schiff base copper complex compound as potent anticancer molecule with multiple targets of action" *European Journal of Pharmacology*, 647(1-3), (2010). 1-12.

Smart Nanocomposites
Volume 2, Number 2
ISSN: 1949-4823

INVESTIGATING PROPERTIES OF GAS-SENSITIVE NANOCOMPOSITES OBTAINED VIA HIERARCHICAL SELF-ASSEMBLY

V. A. Moshnikov[1], I. E.Gracheva[1], N. S. Pshchelko[2], M. G. Anchkov[1] and K. L. Levine[2]

[1]Saint-Petersburg State Electrotechnical University "LETI",
197376, Russia, St. Petersburg, prof. Popova, 5
[2]General and Technical Physics, The St. Petersburg State Mining University,
199106, Russia, St. Petersburg, 21 linia VO bld 2.

ABSTRACT

Gas-sensitive nanocomposites based on silicon dioxide and tin dioxide were obtained via self-assembly by sol-gel method. Surface morphology of nanomaterials synthesized from sol solutions in medium of precursor based on tetraethoxysilane was characterized by atomic force microscopy. Formation approach of metal contacts adhered to hierarchical porous structure based on electroadhesion technology was proposed. The advantages of this technique were discussed, and the theoretical concepts of processes taking place during formation of adhesive contacts were considered. Electrical properties of nanomaterials based on porous silicon with the introduced metal oxide nanocomposites were studied by impedance spectroscopy. Gas-sensitive properties of synthesized samples were measured.

Keywords: hierarchical nanocomposites, self-assembly, sol-gel method, gas-sensitivity, impedance spectroscopy

INTRODUCTION

One of the most dynamically developing trends in nanotechnology is related to engineering of new structural and functional materials such as functional hierarchical materials [1], which have a special architecture of element packing. These materials are composed of different-scale elements organized in a way that elements of a smaller scale are placed into elements of larger. Hierarchical architecture of functional material allows using a single technologic platform to create materials with greater diversity of useful characteristics, by controlling the composition of substructures on one or several levels of hierarchical

architecture. Nowadays there are many examples of artificial functional hierarchical materials, both film- and bulk-type. The share of materials obtained via “bottom-up” technologies is growing, which indicates that in due course materials of such architecture will replace modern synthetic functional materials [5].The main mechanism of hierarchical nanomaterials generation is self-assembly [6,7].

The product of hierarchical self-assembly is a material with hierarchical porous structure. The simplest example of such self-assembly is a Julien fractal [8]. A regular Julien fractal (see Figure 1) has a constant value of Hausdorff–Besicovitch dimension ($D = \ln 17 / \ln 3$). (In the monograph [9] is described a 3D Julien fractal analogue with the dimension D=ln13/ln3). This object is easier to handle than multileveled fractal nanostructures [10], where fractal dimensions vary with scaling allowing in some cases observation of transitions between mass and surface fractals. With the help of Julien fractal we can describe preparation of materials with a set of determined pore sizes. Pores of different sizes are utilized in different types of devices, such as nanoreactors with a different capillary sizes, channels for product delivery and withtake, adsorption centers etc. It should be noted that the existing pore classification by IUPAC (micropores, mesopores, macropores) is based on specific nature of adsorption, desorption of water vapors depending on pore size. In micropores volume condensation is observed, in mesopores – condensation with capillary effects, in macropores – effects of adsorption, desorption, as seen in macro objects.

According to the modular principle, the composite consists of modules (fragments) that serve as “bricks” for more complex structures. This is of fundamental significance for all “bottom-up” nanotechnologies. Dimensional properties of nanoparticles and the whole macro object can be adjusted through control of the initial modules’ sizes and their integration.

This is of interest for nanoelectronics to generate nanoparticles with hierarchical structure [10,12]. Due to large surface areas of the obtained nanostructured materials they can be effectively utilized in miniature and reliable sensors for gases [13,14,15,16] and multisensor “electronic nose” systems which possess high sensitivity and selectivity for ultra-small quantities of explosives, drugs and dangerous substances. The purpose of this publication is to study the properties of nanomaterials with a hierarchical structure, obtained from fluid phase via self-assembly, and to develop new process designs for obtaining and diagnostics of gas-sensitive layers.

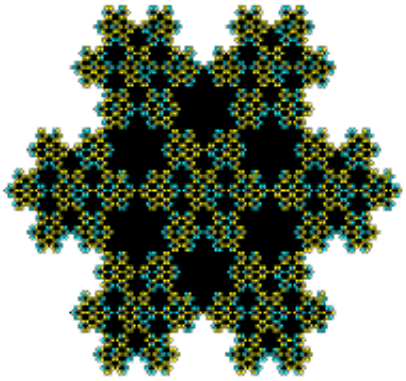

Figure 1. 3D projection of a determinate Julien fractal aggregate.

EXPERIMENTAL

Methods

Self-assembly from fluid phase by sol-gel method [17,18,19] is frequently chosen for large scale production In this paper this method was chosen to obtain samples with a hierarchical structure. The prepared solution-sol is deposited on a rotating glass substrate surface. The synthetic route consisted of alkoxide hydrolysis followed by polycondensation in a thin layer of sol. As a result of the deposition gel spatial structures was formed on a substrate surface.

Chemicals

Solutions-sols were obtained on the basis of binary heterochain inorganic polymers. The initial pre-cursors used for preparation of solutions-sols were easily hydrolyzed components. Such components formed poly-molecules due to interaction with water. Tetraethoxysilane (TEOS, $Si(OC_2H_5)_4$) was chosen to obtain nanostructured films of silicon dioxide. To obtain the two-component oxide materials based on silicon dioxide the hydrolysis and polycondensation of TEOS in the presence of inorganic salt of tin was carried out.

The optimum ratio of basic components in an initial solution provides fast partial or full hydrolysis of alkoxides and forming sol. This reaction is catalyzed by acid and is very sensitive to the ratio of acid and alcohol in the solution.

Apparatus

Cross sections were created by focused Ga ion beam using Strata FIB 205 (FIE) to determine the thickness of semiconductor nanostructured layers. Local ion-beam preparation of complex heterogeneous objects with resolution of 0.1 micron is provided by this analytical and technological system.

AFM was used to measure the surface morphology of thin-film nanostructures synthesized from sol solutions. Tapping mode AFM experiments were performed using NTEGRA-Therma nanolaboratory (NT-MDT, Zelenograd, Russia). Commercial etched silicon tips NSG 01 (NT-MDT, Zelenograd, Russia) with typical resonance frequency of 150 kHz were used as AFM probes. The radius of curvature of the probes was ≥10 nm. AFM images of 256x256 elements were recorded. Electronic microphotographs were obtained by scanning electron microscope Quanta Ispect.

Study of the electrical properties of nanomaterials based on porous silicon with the introduced metal oxide nanoparticles was performed by using impedance spectroscopy [20,21,22,23] in a frequency range from 1 Hz to 0.5 MHz at 300 ºC using impedance meter «Z-500 P» (LTD «Elins»). This equipment allows to study nanostructures by impedance spectroscopy in a changing gas environment and temperature of gas detection.

RESULTS AND DISCUSSION

The ageing of sol-gel leads to the formation of primary linear structures followed by their transformation into nanoglobules. The density of nanoglobules is closely related to pH. Primary globules appear statistically in all parts of sol. Experiencing the Brownian motion, they form the fractal aggregates, that at the initial stage of growth are close to the model conceptions of Witten-Sander diffusion limited aggregation (DLA-model) [24]. The Brownian motion speed of such aggregates lowers significantly with the growth of mass. Along with that the space is approximately divided into new macro volumes, where the fractal aggregates (clusters) can consolidate (see Figure 2). This picture is close to the model of cluster-cluster aggregation. There may be several consolidation stages of increasingly large clusters. At the final stage either a percolation cluster forms or spinodal decomposition of the system takes place, as in Florry-Huggins model, widely known in the polymer physics [25,26,27].

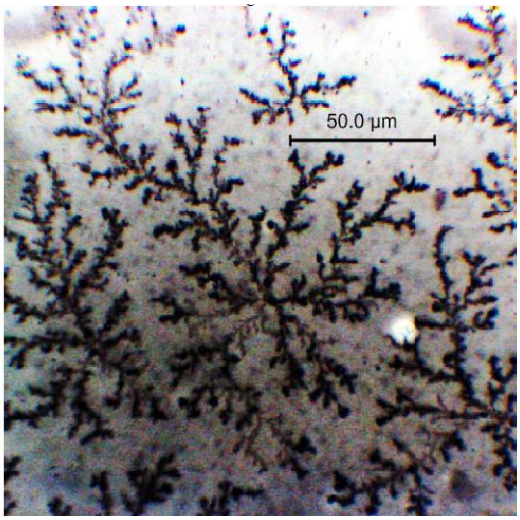

Figure 2. Optical image of fractal aggregates.

Figure 3 presents microphotographs of self-assembled structures. Fractal aggregates based on silicon dioxide were generated by sol-gel method.

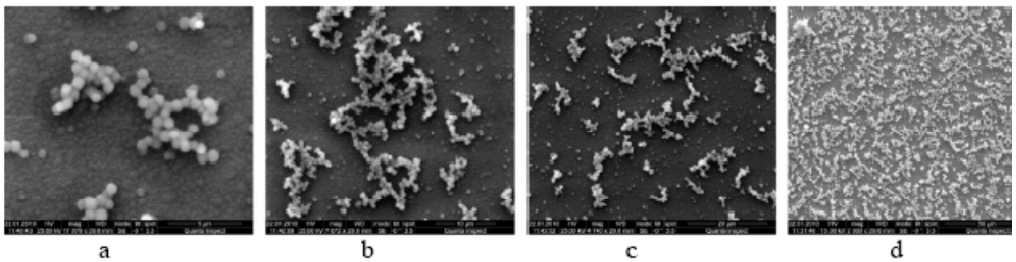

Figure 3. Microphotogaphs of fractal aggregates based on silicon dioxide, illustrating the self-assembly in sol-gel processes.

Image analysis shows that the film structure is a consolidated domain formed of clusters sized in the range between units and tens of micrometers, consisting of spherical particles. The growth of such fractals in sol-gel processes according to DLA-model proceeds together with a sporadic cluster-cluster aggregation. Due to random contacts between fractal aggregates and particles, curing reactions between branched structures takes place, and large percolation cluster forms.

It should be noted, that for new generation gas-sensitive sensors there is great interest in the techniques of creating porous layers with controllable and repeatable pore sizes, the formation nature of which is much more complex than can be described by modified DLA model.

Nanocomposites need to contain a layer for adhesion improvement and one or more layers of semiconductor metal oxides of the n-type conduction to provide gas-sensitivity.

Systems based on metal oxide nanocomposites with conductivity of n-type (such as SnO_2, ZnO, Fe_2O_3, NiO, V_2O_3, WO_3, Co_3O_4) are selective and highly sensitive to the condition of surface in high temperatures region. They are promising for application in devices for detection and identification of ultra-small quantities of explosives, drugs and dangerous substances. Among all listed materials tin dioxide meets all the complex requirements for creating sensoric systems. Its conductivity is quite susceptible to high temperatures due to redox reactions on the surface of oxide. Among other properties worth mentioning here is high adsorptive capacity due to free electron presence in semiconductor's conduction band, surface and oxygen vacancies, and an active chemisorbed oxygen.

To estimate the thickness of semiconductor nanostructured layers cross sections were made by a fine-focused Gallium ion beam. To study the sample's section the object table was rotated through 45º, the observation was carried out in secondary electrons, excited by an ion beam with a diameter of 7 nm. As a result of etching grooves sized ~ (5 ^{x} 5) μm were formed, the depth of the section was ~ 2 μm. It was discovered that the thickness of semiconductor layers is 200 nm.

As a result of AFM research was it was shown, that by changing thermodynamic and kinetic conditions of sol-gel nanotechnologies (with the structure of nanocomposites, precursors, quantity of solvents, cure time of the polymer sol solutions, annealing temperature) it is possible to control the evolution of fractal aggregates based on metal oxides. For example, an increased curing time of sol solution leads to changes in layer microstructure, moreover, the formation of fractally aggregated systems based on silicon dioxide and tin dioxide corresponds to different evolution stages: spherical structure formation by nucleophilic growth (see Figure 4A, nanocomposite $20SiO_2$-$80SnO_2$ (mole %)); labyrinth structure formation by spinodal decomposition (see Figure 4B, nanocomposite $10SiO_2$-$90SnO_2$ (mole %)); percolation mesh structure formation (see Figure 4C, nanocomposite $20SiO_2$-$80SnO_2$ (mole %)).

In the phase contrast regime with "tapping mode", hierarchical systems of grains with distinctive "level" sizes were registered. Pore size was around 10 nm (see Figure 5). According to IUPAC classification such pores are called mesopores. The surface fractality estimated and the area calculation was done taking into account AFM data. The calculations were carried out with a software product in LabVIEW environment. The share of open pores of lower hierarchical levels sized under 10 nm was estimated by thermal desorption of nitrogen under the BET theory. It was determined that the main share of total developed area belongs to the hierarchical levels of open pores.

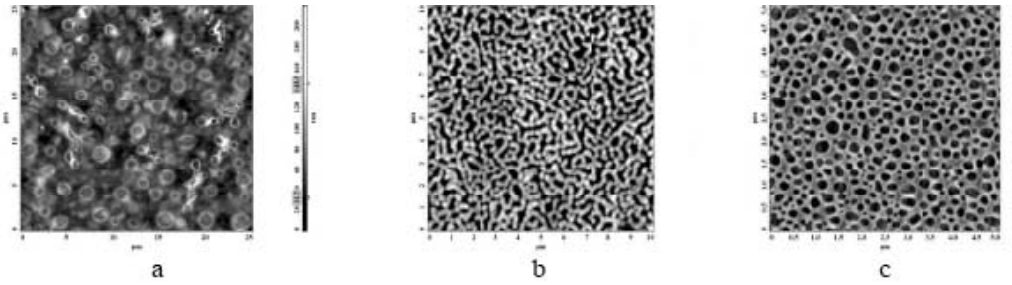

Figure 4. Atomic force microscopy images of different evolution stages of fractally aggregated systems based on tin dioxide and silicon dioxide: a) spherical structures formation by nucleophilic growth (scan range 25μm x 25μm); b) labyrinth structures formation by spinodal decomposition (scan range 10μm x 10μm); c) percolation mesh structures formation (scan range 5μm x 5μm) of semiconductor layer based on tin dioxide, obtained via sol-gel method.

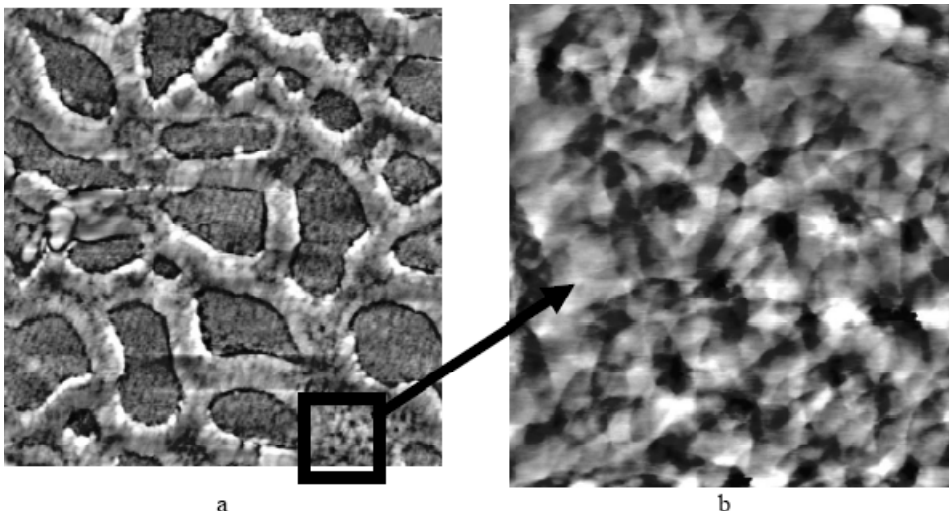

Figure 5. The image of percolation nanocomposite surface in phase contrast regime: a) scan range 2μm x 2μm; b) scan range 400 nm x 400 nm.

The advantages of structure with a pore hierarchy dramatically decreases by damages caused by creating contacts. That is why a challenging task is to find ways of forming metal contacts without destruction of porous structure. New engineering solutions come with the application of electroadhesion technology. There are two possible ways to do this: the first one is to create system of contacts with a further formation of gas-sensitive porous layers; the second way is based on application of nanocomposites' structure and properties, by other words, the presence of dielectric silicon dioxide inclusions. The electroadhesive attraction of an ion dielectric and conductor (semiconductor) is caused by forces of electrostatic attraction that emerge between joint parts when electric potential is applied to them. If the mode is chosen correctly, the strength of the juncture is of the diffusion welding level. The described technology has a number of advantages: materials can be joined in solid state by applying temperature considerably lower than melting one without intermediate layers (glue, solder etc), sweeping electric field affects the details "from the inside" of the joint (which allows to

join fragile details), to implement the technique no special expensive equipment is needed [28]. Physical processes, leading to the emerging of great attraction forces between objects, are associated with the generation of strong electric fields at the interface [29]. Electroadhesion is a result of electrostatic (ponderomotive) attraction of electrified objects, when opposite charges are separated by gap between contacting surfaces or a thin layer of one of the attracted objects, depleted by the charge carriers and having thus increased impedance, adjoining the interface surface. For that reason the major part of applied potential drops on that thin layer, which explains the emerging of strong electrostatic fields and forces.

The presence of the overlap span, explained by a fractal roughness of joined surfaces, plays an ambiguous role: on one hand, due to this span the emerging of strong attraction forces between joined parts is possible because the electric resistance of the overlap span is much higher than the resistance of the joined details, that is why the major part of the applied electric voltage falls on this thin span, leading to the emerging of strong electric fields and, consequently, electrostatic forces of attraction. On the other hand, the presence of this span prevents irreversible processes at the interface, leading to durable contact establishment, lasting even after in the absence of applied potential. At the same time, if we manage to obtain high ponderomotive pressure not only in the overlap span, but in the points of actual contact, the formation of a strong electroadhesive joint can be expected. The contact lasts even in the absence of electric field, due to mutual diffusion and electrochemical processes at the interface, leading to the "gluing" of the details. Such connection is what electroadhesive joint stands for. To obtain greater attraction in the points of actual contact interlayer polarization can be used. The essence of the interlayer polarization phenomenon is that under electrostatic forces free charges of dielectric drift to corresponding electrode. In the case of ionic dielectric charge carriers are positive ions, in the presence of electric field they start moving towards the cathode. In the space, previously occupied by positive ions before the voltage was applied, near the anode, an uncompensated negative charge appears. Therefore, negative charge increases near the anode and, consequently, the potential drop between the layer and the cathode decreases. In a while (usually tens of minutes) the potential drop almost reaches zero, so the intensity of electric field is distributed irregularly through the depth of dielectric – between the anode and the observed layer it is quite strong (~10^8 V/m), in other parts of the dielectric it is close to zero. As a result a thin (units of micrometers) negatively-charged subsurface layer forms near anode. The layer possess a strong electric field that was formed under an external electric field. Therefore loosely-bound ions leave their places (e.g. in glass it can be ions of Na, K, etc.), and anode layer clears from charge carriers. Consequently its resistance increases. For this reason in points of actual contact applied voltage will fall not on the whole depth of dielectric, but on a thin anode layer, which provides great ponderomotive pressure not only in the overlap span, but also in points of actual contact. Under a simultaneous effect of a high temperature an electroadhesive joint ("gluing" under electrostatic forces) of the materials happens. Electroadhesive technology can be effectively applied to permanent leak-proof fastening manufacture for such materials as ceramics, vitroceramics, glass, quartz and other ionic dielectrics with different metal conductors and semiconductor crystals in different combinations.

So far experiments have been carried out for a number of metal pairs, based on Al and Cu films on glass C47-1. Due to electroadhesive technology the Cu film adhesion increased four times, Al – 12 times compared to the initial one. Film adhesion of control samples (no voltage was applied to them) stayed practically the same. Experimental data was collected and

analised on how technological parameters (electric voltage, temperature, curing time, fractality of surface) and nanocomposites' properties (structure, tin dioxide – silicon dioxide ratio, degree of percolation mesh development, permittivity, density, etc.) influence the process. The key design variable of model is electrostatic force pressure. In the simplified model the charge gathering in the anode region and the intricate contact section are taken into account. The calculated value of the variable can reach tens of MPa. The calculated curves of pressure in the simplified model correlate well with experimental data on joint efficiency [30]. The size and shape of obtained particles depends on terms of sol-gel and hydropyrolytic synthesis. Special characteristics of micro- and nanocrystals of metal oxides are linked to their chemical properties, but they're also closely connected to the size and shape of the crystallites. Thus control over the shape and size of nano- and microsized semiconductor materials is of great interest for new functional devices.

Functioning for semiconductor gas sensors is based on metal oxide layers. They exhibiting porous nanostructured composites, is in changing electrical conductivity as a result of gas chemisorption. The first and essential stage of gas detection is oxygen adsorption on the surface of a semiconductor film. Electrons from the semiconductor drift to surface oxygen, which leads to energy band distortion (see Figure 6), where E_{vac} and E_{vacs} – vacuum levels in bulk and on the surface respectively; E_C and E_{CS} – bottom location of conduction band in relation to vacuum level in bulk and on the surface respectively; E_F – Fermi level; E_V and E_{VS} – top location of valence band in relation to vacuum level in bulk and on the surface respectively; χ and χ_S – electron affinity in bulk and on the surface respectively; $q\varphi$ и $q\varphi_S$ – electron work function in bulk and on the surface respectively; qU_S – value of surface barrier, due to the charging of surface; E_t – surface level position, corresponding to the chemisorbed particles) in the subsurface area to the depth, defined by Debye shielding distance (L_D).

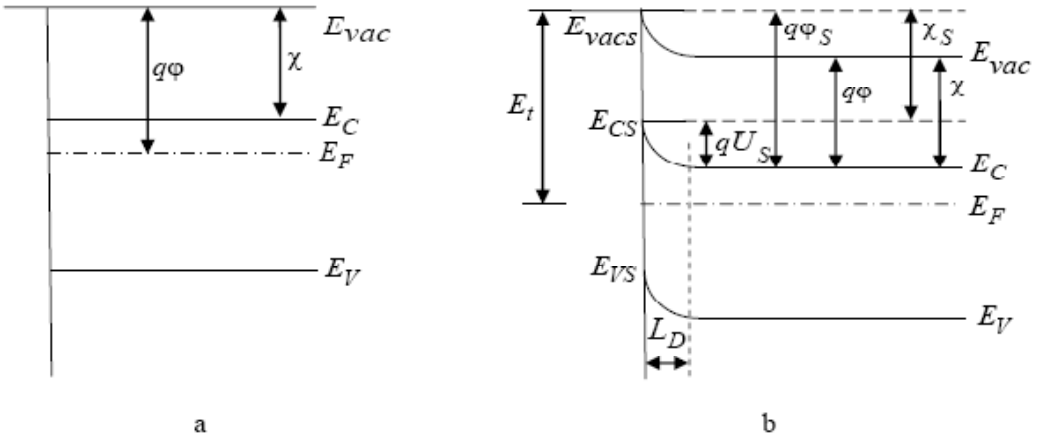

Figure 6. Band diagram of metal oxide semiconductor film: a) without oxygen adsorpted on the surface; b). with oxygen adsorbed on the surface (polarization not taken into account).

As the reducing gas interacts with oxygen ions, on the surface of semiconductor film electrons return to the bulk of the semiconductor, and the reaction products leave the surface neutrally, resistance of semiconductor structure therefore decreases (see Figure 7).

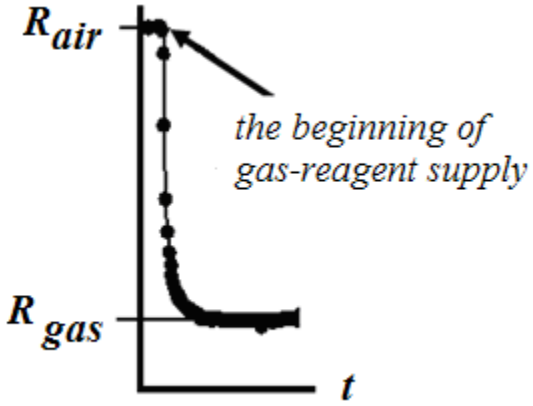

Figure 7. Typical time dependence of resistance for a mesh nanocomposite during pulsing of a gas-reagent.

In this work gas-sensitivity was measured using reducing acetone and ethanol vapors, the value of sensitivity was calculated as

$$S = \left(R_{air} - R_{gas}\right) / R_{gas} , \quad (1)$$

where R_{air} – sample's air resistance , a R_{gas} – sample's resistance in the presence of gas-reagent. An automatic cycle of gas-sensitivity calculation [31] was carried out in several stages: the heating of sensor (nanocomposite film) in a fixed atmospheric air flow to required temperature, the measurement of active layer resistance at this temperature and the pulsing of the observed substance (with 1000 ppm concentration) untill the moment of stabilization of active layer resistance in the vapors of the substance.

The study of gas-sensitive properties of film nanostructures based on tin dioxide led to the following results: nanostructures formed by nucleophilic growth (see Figure 3A) and labyrinth structures belonging to spinodal decomposition (Figure 3B) had a very low sensitivity to reducing ethanol and acetone vapors ($S \leq 0{,}5$), for mesh percolation structures (Figure 3C) sensitivity to gas-reagents rose to $S > 20$.

Impedance Measurements

Study of porous semiconductor nanomaterials based on metal oxides under a alternating electric field is of considerable interest for engineering of gas-sensitive layers for adsorptive semiconductor sensors of new generation. To process impedance experimental data the complex plane method was used, where impedance, as well as any other complex number, is presented as the connections of its real (Re(Z)) and imaginary parts (Im(Z)).

In Figure 8 (where A is bias potential) typical impedance spectra for silicon dioxide samples are presented, in Figure 9 for silicon and tin dioxide samples (20 SiO_2 – 80 SnO_2, mole %) in atmospheric air and in the presence of acetone vapors at the temperature of 350 ºC. It was discovered, that after semiconductor phase of tin dioxide had been injected into one-component system based on silicon dioxide, components of impedance decreased by three orders of magnitude, and the impedance charts changed.

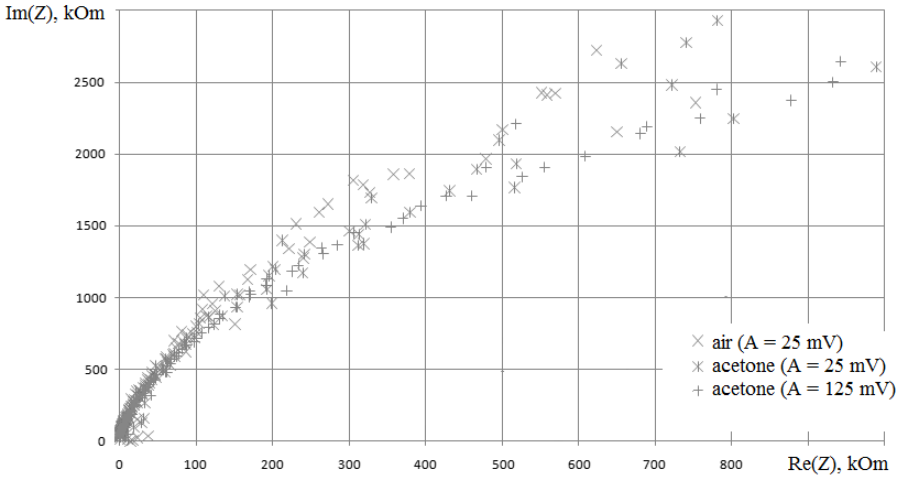

Figure 8. Relationship between the imaginary and real components of impedance for a sample based on SiO_2. Plot obtained in a frequency range 1 Hz – 0,5 MHz.

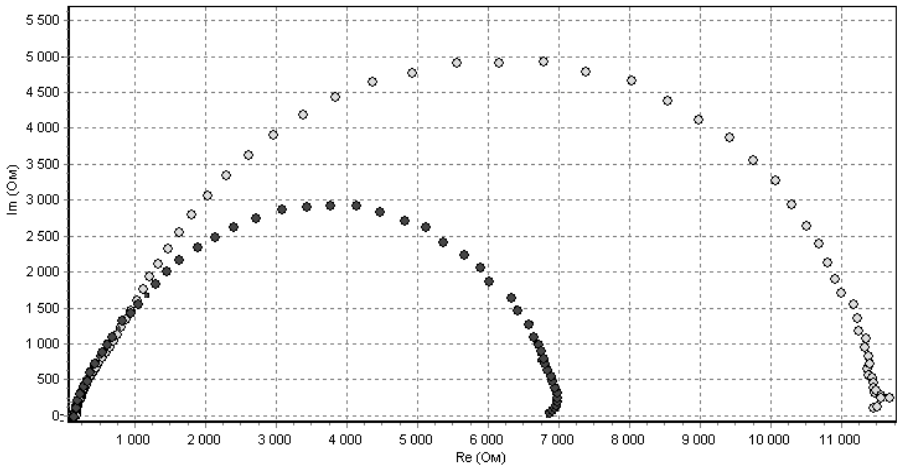

Figure 9. Nyquist plot for a sample based on silicon dioxide and tin dioxide, obtained frequency range 1 Hz – 0,5 MH z. ○ Dry air; ● Air with acetone vapors.

For the sample based on silicon dioxide the Nyquist plot has a shape of an exponential-looking curve starting from the origin of coordinates, which proves that there is a double electric layer on the phase boundary electrode – dielectric film structure. For the nanocomposite based on silicon and tin dioxide the Nyquist plot has a shape of a semicircle.

It is important to note, that frequency dependence of phase shift between current and voltage (φ) of alternating signal for a nanocomposite of the two-component system, plotted in semi-logarithmic scale (Bode plot) (see Figure 10), shows two relaxation maximums, with two relaxation times, close in value. Two peaks, changing with the change of gas environment and detection temperature, presumably show that nanomaterials have several types of pores (see Figure 6) with different construction, which offers new possibilities for diagnostics of systems with hierarchical structure. There are examples of impedance spectroscopy application to register nanoeffects [32], and nanosized pores [33].

In the work research has been made on how external electric field influences impedance of samples (their structure in Figure 11, where 1 – general electrode, towards which the voltages were applied and measured).

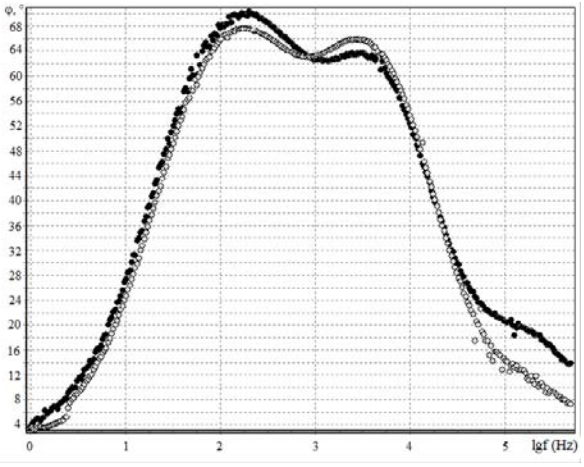

Figure 10. Relationship between impedance and frequency logarithm. ◯ Dry air; ● Air with acetone vapors.

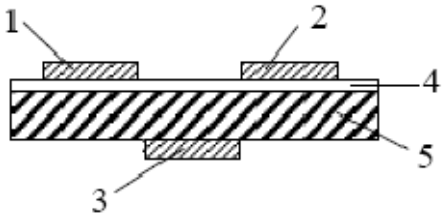

Figure 11. Structure of a gas-sensitive sample: 1,2,3 – 1st, 2nd and 3rd electric contacts, 4 – film of sensitive material; 5 – insulating glass base.

The measurements of impedance and phase shift between current and voltage (φ) of alternating signal were carried out with electric contacts 1 and 2 (see Figure 11). It was discovered, that with an increase of DC voltage between contacts 1 and 3 (see Figure 11) in high-frequency region there is a decrease in the imaginary part of impedance, while its real part stays constant (see Figure 12).

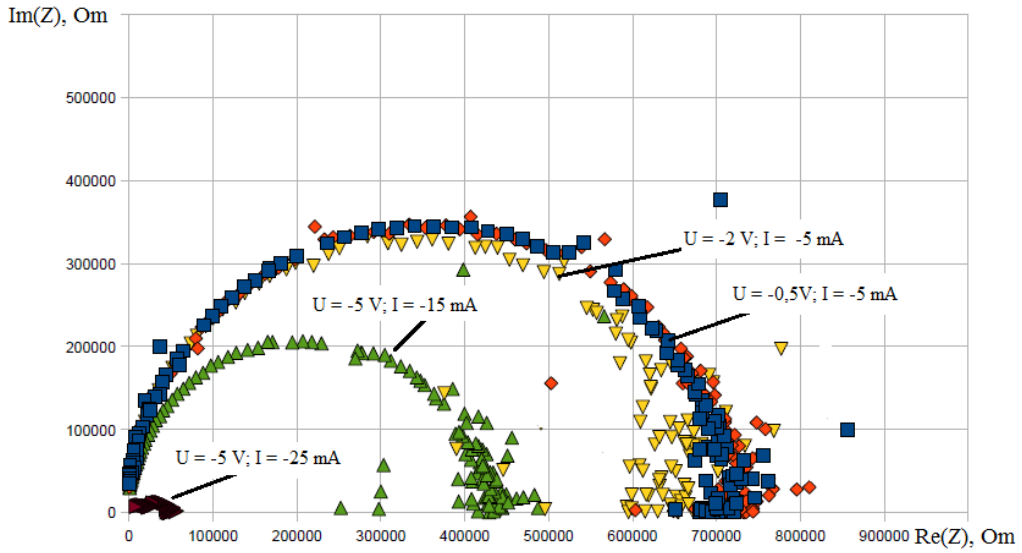

Figure 12. Typical Nyquist plot for a sample based on tin dioxide under changing external electric field (voltage and current are changed (from I = -5 mA to I = -25 mA) between 1st and 3rd electrical contacts).

It was shown, that the absolute value of stabilization current, supplied by a constant-voltage regulator, contributes significantly to semicircle shifting in the Nyquist plot. When the absolute value of stabilization current increases by less than two times (from 15 to 25 mA) and the absolute value of stabilizing voltage stays constant (5 V), the real part of impedance decreases by more than 7 times, and the imaginary part decreases by more than 10 times, which can presumably be connected with the decrease of depleted charge region on the boundaries of sample grains.

It was discovered, that under DC stabilized voltage and some absolute value of bias current a second semicircle appears in the Nyquist plot (see Figure 13), and with the growth of bias current parameters of segment, belonging to high-frequency region, stay almost the same, while the y-coordinate of the circle center in a high-frequency region increases.

Simplified equivalent circuit models can be presented as two series of parallel circuits. For a high-frequency region this is a R_V-CPE_V chain, linked to grains bulk properties (index V) and for a low-frequency region this is a R_{GB}-CPE_{GB} chain, describing grain boundaries (index GB) of crystallites (see insertion in Figure 13). Here R – resistor, CPE – constant phase element, which impedance can be described as

$$Z = 1/\left(A(j\omega)^n\right), \tag{2}$$

where pre-exponential frequency-independent factor A illustrates physical meaning and dimension. If stabilizing voltage is constant and absolute value of bias current is increasing A_V changes very slightly, while A_{GB} sufficiently increases, which can be explained by a combined effect of depleted charge region reduction on grain boundaries and surface states charge exchange.

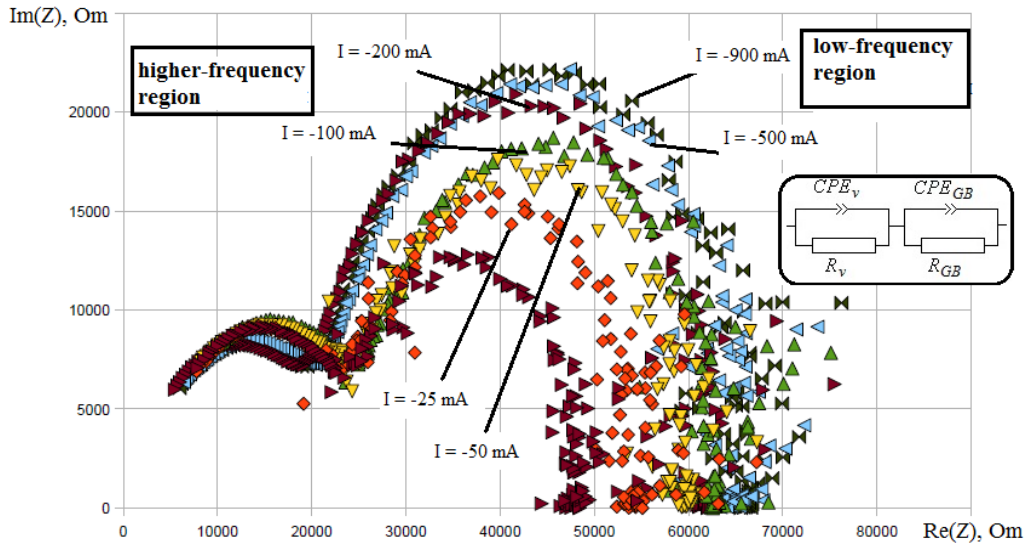

Figure 13. Typical Nyquist plot for a sample based on tin dioxide under changing external electric field (voltage and current are changed
(from I = -25 mA to I = -900 mA) between 1st and 3rd electrical contacts).

CONCLUSION

It was shown, that control over self-assembly in sol-gel processes allows controlling the structure of fractal clusters and their gas-sensitive properties. The study of gas-sensitive properties of film nanostructures based on tin dioxide and silicon dioxide led to following results: nanostructures, formed by nucleophilic growth, and labyrinth structures, belonging to spinodal decomposition, had very low sensitivity to reducing ethanol and acetone vapors, for mesh percolation structures the value of sensitivity to gas-reagents rose to S > 20. It was discovered that conducting branches of porous materials obtained via sol-gel method were not solid, but represented a mesoporous material. A diagnostic method for hierarchical structures based on metal oxides was suggested, the essence of which was in application of perturbation action with variable frequency, gas environment and detection temperature. The analysis of experimental data lead to the conclusion that variable gas environment and external electric field distorted energy bands in the subsurface region of semiconductor sensoric nanomaterials. It was possible to control admittance via application of signal changing in frequency domain to the system of nanosensors. The approach described above provides new possibilities to increase sensitivity and selectivity in multisensoric “electronic nose” systems.

The work has been carried out in the framework of Federal Target Program realization “Academic and teaching staff of innovative Russia” in 2009-2013, government contract P1249, 07.06.2010.

REFERENCES

[1] Patent KR20100025401,Gas sensor using nano-porous indium oxide spherical structure and fabrication method thereof, published 09.03.2010.

[2] Patent KR20090073350, Highly sensitive and fast responding oxide semiconductor-type gas sensor using hierarchical structure and fabrication method thereof, published 03.07.2009.

[3] Patent JP2005290032, Method for producing hierarchical porous body containing meso pore having long range order, published 20.10.2005.

[4] Patent US2010010513, Porous material having hierarchical porous structure and preparation method thereof, МПК: A61B17/08; C01B25/10; A61B17/03; C01B25/00, published. 14.01.2010.

[5] M. Alfimov. Functional hierarchical materials// *Russian nanotechnologies*. –Т. 5. – №5 – 6. – 2010. – WWW.nanorf.ru.

[6] Carlos Csar Bof Bufon, Jos David Cojal Gonzlez, Dominic J. Thurmer, Daniel Grimm, Martin Bauer and Oliver G. Schmidt. Self-Assembled Ultra-Compact Energy Storage Elements Based on Hybrid Nanomembranes // *Nano Lett.* – 2010. – 10 (7). – P. 2506–2510.

[7] Honggang Cui, E. Thomas Pashuck, Yuri S. Velichko, Steven J. Weigand, Andrew G. Cheetham, Christina J. Newcomb, Samuel I. Stupp. Spontaneous and X-ray–Triggered Crystallization at Long Range in Self-Assembling Filament Networks // *Science*. –2010. – Vol. 327. – No. 5965. P. 555-559.

[8] Julien R. Fractal aggregates*// Success of physical science*. 1989. T. 157. № 2. P. 339 – 357.

[9] Shabanova N.A., Sarkisov P.D. The basics of sol-gel technologies for nanodispersed silicon dioxide. Moscow*: Academkniga,* 2004. 208 p.

[10] Shilov V.V., Shilova O.A., Gomza Y.P. Modern conceptions of fractal nanocomposite structures, obtained via sol-gel method // Chemical nanotechnologies and funcyional nanomaterials. St.Petersburg.: *RESTEK*. 2003. P. 18–20.

[11] Moshnikov V.A., Gracheva I.E., Kuznezov V.V., Maximov A.I., Karpova S.S., Ponomareva A.A., Hierarchical nanostructured semiconductor porous materials for gas sensors // *Journal of Non-Crystalline Solids*. 2010. T. 356. № 37-40. C. 2020-2025.

[12] Gracheva I.E., Moshnikov V.A., Karpova S.S., Maraeva E.V. Net-like structured materials for gas sensors. *Journal of Physics: Conference Series* 291 (2011) 012017 (http://iopscience.iop.org/1742-6596/291/1/012017).

[13] Madou M. J., Morison S. R. Chemical sensing with solid state devices. London: Academic Press, 1991.

[14] Metal Oxides: *Chemistry and Applications by* J.L.G. Fierro. Taylor and Francis, 2005. – 808 p.

[15] Davidov S.Y., Moshnikov V.A., Tomaev V.V.Давыдов Adsorptive processes in polycrystal semiconductor sensors. – St.Petersburg: SPSEU, 1998.

[16] Semiconductor sensors in physico-chemical studies // Ed. L. Yu. Kupriyanov. Amsterdam: Elsevier, 1996.

[17] Brinker C. J., Scherer G. W. Sol-Gel Science. The Physics and Chemistry of Sol-Gel Processing.–San Diego*: Academic Press*, 1990., 908 p.

[18] Corriu R., Nguyên T. A. Molecular Chemistry of Sol-Gel Derived Nanomaterials. John Wiley and Sons, 2009
[19] Handbook of sol-gel science and technology: processing, characterization, and applications / Ed. Sumio Sakka.–New York, 2004.–V.1-3.
[20] Orazem Mark E., Tribollet Bernard. Electrochemical Impedance Spectroscopy. The Electrochemical Society Series.–Wiley*: Interscience*, 2008. 524 p.
[21] Barsoukov E., Macdonald J. Ross. Impedance Spectroscopy. Theory, Experiment, and Applications. Second Edition.–Willey*: Interscience*, 2005. 595 p.
[22] Gracheva I.E., Moshnikov V.A. Analysis of surface processes in gas-sensitive nanostructures via impedance spectroscopy// News of the State Electrotechniacal University. *Solid State Physics and Electronics*. 2008, Issue 6, P. 19-24.
[23] Kremer F. Dielectric spectroscopy - yesterday, today and tomorrow // J. *Non-Cryst. Solids*.–2002.–Vol. 305.–P. 1–9.
[24] Juliae R. Fractal aggregates // *Success of physical science*. 1989. T. 157. № 2. P. 339–357.
[25] Huggins M. // Journ. Phys. Chem. 1942. V. 46. P. 151.
[26] Flory P. J. Principles of Polymer Chemistry. New York, Ithaca: *Cornell University Press,* 1971.
[27] Grosberg A.Y., Khokhlov A.R. Statistical physics of macro molecules: study guide, Moscow: Science, *Main Office of Physico-Mathematical Literature*, 1989. 344 p.
[28] Pshchelko N.S. Polarization of dielectric subsurface layers on the boundary of electroadhesive contact with the conductor// Base metals. Moscow, 2005. - №9. – *Nanostructured metals and materials*. – P.44-50.
[29] Deryagin B.V., Krotova N.A., Smilga V.P. Solid body adhesion. – Moscow: *Science*, 1973. – 280 p.
[30] Ozols A.R., Pshchelko N.S., Tairov V.N. Physical bases, calculation and application of irreversible electroadhesive joint of solid bodies. – Riga: *University of organic synthesis of Latvian Academy of Sciences*, 1989. – 165 p.
[31] Gracheva I.E., Maximov A.I., Moshnikov V.A., Plekh M.E. A Computer-Aided Setup for Gas-Sensing Measurements of Sensors Based on Semiconductor Nanocomposites // *Instruments and Experimental Techniques*. – 2008. – Vol. 51. – No. 3. – P. 462–465.
[32] Dennis E. Tallman, Kirill L. Levine, Chavanin Siripirom, Victoria J. Gelling, Gordon P. Bierwagen, and Stuart G. Croll, *Applied Surface Science*, 254 (2008) 5452 – 5459.
[33] K. L. Levin and N. S. Pshchelko*, Polymer Science,* Ser. A, 2011, Vol. 53, No. 6, pp. 510–520.